UNIVERSIDADE DE LISBOA

FACULDADE DE CIÊNCIAS

DEPARTAMENTO DE QUÍMICA E BIOQUÍMICA

EXPLORING PLASMA MEMBRANE HETEROGENEITY IN *SACCHAROMYCES CEREVISIAE* WITH A FOCUS ON SPHINGOLIPID HYDROXYLATION

Helena Monteirinho Leitão

Mestrado em Bioquímica e Biomedicina

Dissertação orientada por:
Professor Doutor Rodrigo F. M. de Almeida
Doutor Joaquim Trigo Marquês

2023

This work was supported by Fundação para a Ciência e a Tecnologia (FCT), Portugal through CEECIND/03247/2018 to JTM, EXPL/BIA-BFS/1034/2021, Centro de Química Estrutural (UIDB/00100/2020 and UIDP/00100/2020) and I.M.S. - LA/P/0056/2020

Resumo

O principal objetivo desta dissertação de mestrado foi aprofundar o conhecimento atual sobre as propriedades biofísicas e a organização da membrana plasmática de um fungo-modelo, *Saccharomyces cerevisiae*. Ao pesquisar novas abordagens experimentais para estudar regiões específicas da membrana plasmática fúngica, através do uso de sondas de membrana fluorescentes, espera-se identificar novos alvos para o desenvolvimento de estratégias terapêuticas mais eficazes.

Nos últimos anos tem-se observado um aumento significativo nos casos de infeções fúngicas em todo o mundo, juntamente com uma diminuição na eficácia dos medicamentos antifúngicos atualmente disponíveis. Essa situação tem gerado grandes desafios no tratamento de doenças causadas por fungos. Os fungos, enquanto agentes patogénicos, representam uma ameaça relevante tanto para indivíduos com sistemas imunológicos enfraquecidos como para pessoas saudáveis. A complexidade das infeções fúngicas é ainda mais agravada pela falta de opções terapêuticas disponíveis, destacando-se a necessidade urgente de desenvolver novas estratégias de tratamento. Para superar as limitações das terapias antifúngicas atuais, há um foco crescente no desenvolvimento de medicamentos antifúngicos direcionados à membrana plasmática. O foco no desenvolvimento de medicamentos antifúngicos que atingem diretamente a membrana plasmática pode ser uma estratégia para prevenir a sua resistência, pois existem menos mecanismos de resistência conhecidos a medicamentos que atuam diretamente na membrana.

A membrana plasmática do fungo fornece suporte estrutural, agindo como uma barreira protetora que protege o fungo do ambiente hostil envolvente. Esta singularidade torna a membrana um alvo atraente para o desenvolvimento de medicamentos destinados a combater espécies fúngicas patogénicas. A membrana celular dos fungos é uma bicamada lipídica enriquecida com diversos lípidos pertencentes às classes glicerofosfolípidos, esfingolípidos e esteróis. Os esfingolípidos constituem cerca de 30% dos fosfolípidos da membrana plasmática do fungo *Saccharomyces cerevisiae*. A inositolfosforilceramida (IPC) é o esfingolípido complexo mais abundante em *S. cerevisiae*, representando cerca de ~65% dos esfingolípidos totais, enquanto a manosilinositolfosforilceramida (MIPC) e a manosildiinositolfosforilceramida ($M(IP)_2C$) correspondem a ~15% e ~20% dos esfingolípidos totais, respetivamente. A nível estrutural, estes esfingolípidos incluem uma ceramida e um grupo inositol unidos por uma ligação fosfodiéster. Cada um difere não apenas no tamanho do grupo polar, mas também na carga líquida geral, sendo esta -1 em IPC e MIPC, e −2 em $M(IP)_2C$. O IPC destaca-se como um importante grupo de esfingolípidos complexos em fungos e estão ausentes em mamíferos. A deleção de certos genes pode provocar alterações nas percentagens de esfingolípidos na membrana plasmática. A deleção dos genes *SUR2* e *SCS7* previnem a hidroxilação do C4 da base esfingóide e do C2 da cadeia acilo do esfingolípido, respetivamente; enquanto a deleção do gene *IPT1* leva à acumulação do esfingolípido complexo MIPC mas evita a formação de $M(IP)_2C$. Esta classe de lípidos é objeto de interesse neste projeto, dado que os esfingolípidos podem apresentar diversas hidroxilações, seja no base esfingóide ou na cadeia acilo, o que pode influenciar certas propriedades biofísicas e a organização da membrana plasmática. É hipotetizado que o grau de hidroxilação tenha um grande impacto, nomeadamente na estabilização de domínios gel (SLEDs, Domínios ricos em esfingolípidos) que estão presentes na membrana plasmática dos fungos em condições fisiológicas, mas não de mamífero.

Os fungos, particularmente a levedura *S. cerevisiae*, possuem um esfingolipidoma menos complexo em comparação com as células de mamíferos e um número significativamente reduzido de genes envolvidos no metabolismo lipídico, o que permite atribuir mais facilmente propriedades biofísicas ou interações estruturais em determinadas classes de lípidos de membrana. Durante a década de 1970, os pesquisadores reconheceram o potencial da *S. cerevisiae* como sendo o organismo modelo para o estudo de sistemas eucarióticos. Notavelmente, *S. cerevisiae* foi o primeiro organismo eucariota a ter o genoma completo sequenciado, publicado em 1996 por Goffeau. Além disso, *S. cerevisiae* tem a distinção de ter a única coleção completa de cepas mutantes de deleção, fornecendo um recurso valioso para vários rastreios experimentais.

Neste projeto, o estudo das propriedades biofísicas e a heterogeneidade da membrana plasmática de células de *S. cerevisiae* foi realizado principalmente recorrendo a métodos de espetroscopia e microscopia de fluorescência. Um dos objetivos deste estudo foi avaliar a distribuição de sondas de membrana fluorescentes por diferentes domínios, fornecendo informação complementar sobre a organização e as propriedades biofísicas da membrana plasmática de *S. cerevisiae*. A membrana plasmática foi marcada com 1,6-difenil-1,3,5-hexatrieno (DPH), trimetilamina-difenilhexatrieno (TMA-DPH) e com ácido propanóico derivado do DPH (PA-DPH). Estas últimas duas sondas são catiónicas e aniónicas, respetivamente. O DPH é uma das sondas fluorescentes mais comumente usadas para estudar propriedades dinâmicas e estruturais de bicamadas lipídicas e membranas celulares por meio da medição da anisotropia de fluorescência em estado estacionário ou resolvida no tempo. Distribui-se uniformemente entre os vários domínios laterais presentes na bicamada lipídica, fornecendo informações relativas sobre a sua ordem global. O TMA-DPH é uma sonda de membrana fluorescente que marca o folheto externo da membrana plasmática das células. Devido à sua porção catiónica, o TMA-DPH fica ancorado ao grupo carregado na interface lípido-água. Neste trabalho, colocou-se a hipótese de que o TMA-DPH interage preferencialmente com SLEDs devido à carga negativa de esfingolípidos complexos em leveduras pelo facto de que em estudos anteriores, a anisotropia de fluorescência desta sonda inserida na membrana plasmática de diferentes estirpes de *S. cerevisiae* era próxima de 0.3, sendo este um valor típico da fase gel. Por outro lado, o PA-DPH aniónico está a ser utilizado pela primeira vez para a caracterização biofísica da membrana plasmática de leveduras e deve comportar-se de forma distinta do TMA-DPH. A viabilidade celular foi avaliada nas células de levedura e não foi afetada por nenhuma das sondas fluorescentes.

Neste projeto, a análise de imagens de microscopia de fluorescência corroborou a hipótese de que os derivados do DPH marcam essencialmente a membrana plasmática, pois sugere que o DPH se distribui uniformemente entre a membrana plasmática e as membranas internas, enquanto o TMA-DPH e o PA-DPH se localizaram apenas, ou pelo menos maioritariamente, na membrana plasmática da célula com uma distribuição aparentemente quase uniforme em toda a sua extensão, devendo os domínios preferencialmente marcados, ser de dimensão inferior ao limite de resolução da microscopia de fluorescência "*wide-field*". Para avaliar os parâmetros que caracterizam a fluidez da membrana plasmática marcada pelas sondas, foram realizados ensaios de anisotropia de fluorescência em estado estacionário, com medições a tempos fixos de incubação, ou em função do tempo de incubação. Tanto nas células *wild-type* (*wt*) quanto nas células com deleção do gene *SUR2*, o DPH marcou regiões mais fluidas, incorporando primeiro na membrana plasmática, espalhando-se posteriormente para as membranas internas devido às suas propriedades apolares. Após os primeiros momentos de incubação das células com DPH, os valores de anisotropia permaneceram estáveis ao longo do tempo, o que pode indicar que ele se espalha rapidamente pelas membranas. Por outro lado, o TMA-DPH e o PA-DPH aparentavam incorporar-se em domínios de membrana com características diferentes nos momentos iniciais de incubação. No entanto, os derivados de DPH tiveram a tendência para se espalhar para os

mesmos domínios de membrana após ~24 minutos de tempo de incubação. Os resultados do estudo revelam que a membrana plasmática de *S. cerevisiae* aparenta ter um alto grau de organização, conforme refletido pelos baixos valores de anisotropia de DPH. O valor dos derivados de DPH são iguais ou superiores ao valor do DPH em membrana plasmática isolada o que abrange uma presença notável de domínios ordenados em fase líquido ordenado e em fase gel.

O segundo objetivo deste projeto foi identificar as propriedades biofísicas da membrana plasmática da levedura em células mutadas de *S. cerevisiae sur2*Δ, e comparar com estudos anteriores realizados no laboratório com as estirpes *scs7*Δ, *ipt1*Δ e *erg6*Δ. A deleção do gene *ERG6* altera a via de biossíntese do ergoesterol, pelo que previne a formação do mesmo resultando na acumulação de zimosterol e colesta-5,7,24-trienol. A componente longa do decaimento da intensidade de fluorescência da sonda *t*-PnA foi também estudada nas células mutadas, uma vez que esta sonda pode servir como um marcador distintivo para domínios de gel, especialmente quando excede 30 nanossegundos. A presença da fase gel foi confirmada nas células *wt* e detetada pela primeira vez em *sur2*Δ, tendo sido previamente identificada também em *scs7*Δ, *ipt1*Δ e *erg6*Δ. A ausência das enzimas Sur2p, Scs7p, Ipt1p e Erg6p afetou a fluidez da membrana plasmática, levando a valores aumentados de anisotropia para todas as sondas de membrana em comparação com as células *wt*. Este estudo comparativo demonstrou que as propriedades biofísicas e a ordem global da membrana plasmática das células de *S. cerevisiae* são afetadas pelo padrão de hidroxilação dos esfingolípidos em C4 da cadeia esfingóide e C2 da cadeia acilo; além disso, é fluenciado pela substituição de $M(IP)_2C$ por MIPC em células *ipt1*Δ; e também pela ausência de ergosterol na membrana plasmática.

Em estudos futuros, é importante dar continuidade aos testes das propriedades de ordem global das sondas fluorescentes DPH, TMA-DPH e PA-DPH, uma vez que os resultados de anisotropia confirmam que, em tempos curtos de incubação, estas sondas são uma estratégia promissora para revelar com maior detalhe a heterogeneidade da membrana plasmática da levedura e, talvez, na membrana plasmática de outros organismos.

PALAVRAS-CHAVE: Membrana plasmática fúngica, *Saccharomyces cerevisiae*, Domínios ricos em esfingolípidos (SLEDs), Hidroxilação de esfingolípidos, Sonda fluorescente de membrana.

Abstract

Amidst a growing global trend of fungal infections and diminishing antifungal drug efficacy, the fungal plasma membrane emerges as a potential target for enhanced antifungal treatments. By employing innovative experimental approaches, the concomitant use of fluorescent membrane probes 1,6-diphenyl-1,3,5-hexatriene (DPH) and its derivatives, cationic TMA-DPH and anionic PA-DPH, this study aimed to i) develop a new methodology to study sphingolipid-enrich domains (SLEDs) in gel phase in *Saccharomyces cerevisiae* plasma membrane and ii) further characterize the biophysical properties and organization of the plasma membrane of *Saccharomyces cerevisiae* cells. All probes were shown to not compromise cellular viability. In terms of cellular distribution, DPH was confirmed to distribute across both the plasma and internal membranes, while TMA-DPH and PA-DPH localized predominantly in the plasma membrane. Notably, fluorescence anisotropy assays over time revealed that, at short incubation times, TMA-DPH and PA-DPH label different regions of the membrane, most likely due to their opposite charges. It is hypothesized that TMA-DPH, owing to its positive charge, will firstly incorporate into SLEDs due to electrostatic interactions with negative charges present in sphingolipids polar head group. This trend was observed in both *wild-type* and *sur2*Δ cells lacking C4 -OH group in the sphingoid base.

Trans-parinaric acid (*t*-PnA) was also employed to assess the properties of gel SLEDs, which were identified in *sur2*Δ cells for the first time. Considering the long lifetime component of *t*-PnA in these cells (~44 ns), SLEDs are more compact compared to *wt* cells. This is in line with previous results obtained in other yeast strains with altered sphingolipid profile, namely *scs7*Δ and *ipt1*Δ, where SLEDs also exhibited alterations in their compactness. This study reinforces that lipid composition, especially the hydroxylation pattern of sphingolipids, plays a pivotal role in defining membrane properties, thus SLEDs may constitute an explored target for antifungal therapies.

KEY WORDS: Fungal plasma membrane, *Saccharomyces cerevisiae*, Sphingolipid-enriched domains (SLEDs), Sphingolipid hydroxylation, Fluorescent membrane probe.

Table of Contents

List of Figures

List of Tables

List of abbreviations and symbols

Abbreviations

ANEPPS – Aminonaphthylethenylpyridinium potential sensitive

ANOVA – Analysis of variance

CHOL – Cholesterol

CPS – Counts per second

DAG – Diacylglycerol

DHS – Dihydrosphingosine

DMEM – Dulbecco's modified Eagle medium

DMSO – Dimethylsulfoxide

DPH – 1,6-diphenyl-1,3,5-hexatriene

ERG – Ergosterol

FLIM – Fluorescence Lifetime Imaging Microscopy

FRET – Förster Resonance Energy Transfer

G3P – Glycerol-3-phosphate

GDB – Global disease burden

HEPES – 4-(2-hydroxyethyl)-1-piperazineethanesulfonic acid

IC – Internal conversion

IPC – Inositolphosphorylceramide

ISC – Intersystem crossing

LCB – Long chain base

M(IP)$_2$C – Mannosyldiinositolphosphorylceramide

MCC – Membrane compartment containing protein Can1

MCP – Membrane compartment containing protein Pma1

MCW – Membrane compartment containing Wsc1

MIPC – Mannosylinositolphosphorylceramide

NaCl – Sodium chloride

NaH_2PO_4 – Sodium dihydrogenphosphate

Nys – Nystatin

PBS – Phosphate Buffered Saline

PA – Phosphatidic acid

PA-DPH – Propanoic acid DPH derivative

PC – Phosphatidylcholine

PE – Phosphatidylethanolamine

PG – Phosphatidylglycerol

PI – Phosphatidylinositol

PM – Plasma membrane

PS – Phosphatidylcholine

S.D. – Standard Deviation

SC – Synthetic Complete Medium

SL(s) – Sphingolipid(s)

SLEDs – Sphingolipid-enriched domains

SM – Sphingomyelin

SPT – Single-photon timing

TCSPC – Time-correlated single-photon counting

***T*m** – Main-phase transition temperature

TMA-DPH – Trimethylamine diphenylhexatriene

***t*-PnA** – Trans-parinaric acid

wt – Wild-type

YPD – Yeast extract peptone dextrose medium

Symbols

A – Absorvance

$\bar{\tau}$ – Amplitude-weighted mean fluorescence lifetime

Rc – Corrected noise

Sc – Corrected signal

log – Exponential phase

S_0 – Fundamental electronic state

$\langle\tau\rangle$ – Intensity-weighted mean fluorescence lifetime

lag – Latency phase

τ_i – Lifetime of decay component *i*

ld – Liquid disordered

lo – Liquid ordered

τ_{long} – Long component lifetime

S_1 – Lowest excited state energy level

ε - Molar absorption coefficient

α_i – Normalized pre-exponential factor or amplitude

α_{long} – Normalized amplitude of long component lifetime

I_{VV} – Parallel component of fluorescence intensity

I_{VH} – Perpendicular component of fluorescence intensity

rpm – Rotation per minute

$\langle r\rangle$ – Steady-state fluorescence anisotropy

R^2 – Squared linear correlation coefficient

so – Solid ordered

t – Time, s

Chapter 1. State of the art

1.1. Motivation

For the last few decades, the increasing occurrence of fungal infections worldwide and the declining effectiveness of current antifungal drugs have raised significant challenges in the treatment of fungal diseases. As opportunistic pathogens, fungi pose a significant threat to both immunocompromised individuals and healthy populations. The challenges associated with fungal infections are further aggravated by the limited repertoire of antifungal therapies, leading to the urgent need for the development of novel treatment strategies (Vitiello *et al.* 2023).

Fungal infections, known as mycoses, can manifest as superficial, subcutaneous, or systemic invasive mycoses, affecting various anatomical sites such as the skin, mucous membranes, nails, and internal organs (Brown *et al.* 2012; Vitiello *et al.* 2023). Superficial infections of the skin and nails are the most common fungal diseases in humans, e.g. the global prevalence of fungal skin disease in 2017 from the Global Disease Burden (GDB) data set was, approximately, 750 million people (Urban *et al.* 2021). Candida species, such as *Candida albicans* and *Candida glabrata*, are among the most prevalent fungal pathogens responsible for severe systemic mycoses (Vitiello *et al.* 2023). Additionally, Aspergillus species, such as *Aspergillus fumigatus*, are responsible for invasive pulmonary infections with high mortality rates, particularly in immunocompromised individuals (Denning *et al.* 2011). It is important to highlight that certain disinfectants frequently employed in hospital settings may not be effective against fungal pathogens. For instance, ethanol 70% exhibited no efficacy as an antifungal agent against prevalent airborne fungal genera (Rogawansamy *et al.* 2015), but it was found suitable for cleaning minor spills caused by *Candida auris* (Ahmad and Asadzadeh, 2016).

The fungal cell wall, being located externally, serves as a vital component in the life of fungi. It provides structural support, acting as a protective barrier that shields the fungus from its surrounding hostile environment. Comprised of various polysaccharides, the chemical composition of the cell wall is distinct. This uniqueness, along with the associated plasma membrane, makes the fungal cell envelope an attractive target for the development of drugs aimed at combating pathogenic fungal species (Tada *et al.* 2013). The influence of fungi on human health is magnified by the limited selection of antifungal drugs available for the treatment of systemic fungal infections. These drugs fall into three main classes: azoles, which target the biosynthesis of ergosterol; echinocandins inhibit the biosynthesis of the fungal cell wall, acting as non-competitive inhibitors of (1,3)-β-D-glucan synthase; and polyenes, which according to the classical model bind to ergosterol in the fungal cell membrane, forming pores and causing cell lysis. Unfortunately, the repertoire of antifungal medications is confronted with additional challenges, including the rise of multidrug-resistant fungal strains and the emergence of inherently resistant pathogens (Castelli *et al.* 2014; Revie *et al.* 2018).

Despite the significant advancements in antifungal therapies for invasive fungal infections over the past decade, the outcomes for patients receiving these treatments have been consistently unsatisfactory. In contrast to other pathogens, namely bacteria, fungi share a closer evolutionary relationship with humans, resulting in limitations in the discovery and development of effective antifungal drugs (Brown *et al.* 2012). The treatment of fungal infections is challenging due to several factors, one of them being that the limited arsenal of antifungal drugs restricts the options for clinicians, making effective treatment outcomes difficult to achieve (Brown *et al.* 2012; Revie *et al.* 2018).

To overcome the limitations of current antifungal therapies, there is a growing focus on the development of membrane-targeting antifungal drugs. The plasma membrane of fungal cells play a crucial role in endocytosis, secretion, nutrient uptake, ion homeostasis, signal transduction, morphogenesis, and cell wall or extracellular matrix synthesis (Lanze *et al.* 2020). The focus on the development of antifungal drugs that directly target the plasma membrane can even be a strategy to prevent resistance, as there are fewer known resistance mechanisms to drugs that act directly on the membrane, such as polyenes, than to azoles or echinocandins (Cowen *et al.* 2015).

In this project, we aim to deepen the current knowledge on the biophysical properties and membrane organization of the plasma membrane of a fungus, *Saccharomyces cerevisiae*, to better understand how it can be used as a target in antifungal therapies. By researching for new experimental approaches to study specific regions of the fungal plasma membrane, through the use of fluorescent probes, we strive to identify novel targets for the development of more effective therapeutic strategies. This research holds significant implications for the clinical management of fungal infections and the future design of antifungal agents.

Since the plasma membrane holds an important role in understanding the issues previously stated, the following topics will explain in greater detail the biological membranes and their composition and structure; the plasma membrane of the yeast *Saccharomyces cerevisiae,* its unique characteristics and biophysical properties; and an explanation of the methods employed in this project.

1.2. *Saccharomyces cerevisiae* as a model fungus

In order to explore the intricate mechanisms within eukaryotic cells, focusing on a species that is unicellular and relatively simple presents a logical approach, as it eliminates the complexities associated with multicellular development (Alberts *et al.* 2008).

Saccharomyces cerevisiae, also known as baker's yeast, has emerged as a valuable model organism for investigating a broad range of biological processes (Alberts *et al.* 2008). The scientific term "*Saccharomyces*" originates from the Greek word denoting "sugar fungus" while "*cerevisiae*" is derived from "Ceres," the Roman God associated with crops (Feldmann 2012). Yeast cells hold a prominent place in scientific history as the first organism to be domesticated. Notably, *S. cerevisiae* played a pivotal role in the field of genomics by becoming the first eukaryote to have its complete genome sequenced, published in 1996 by Goffeau in the article “Life with 6000 genes” (Goffeau *et al.* 1996; Feldmann 2012). During the 1970s, researchers recognized the potential of *S. cerevisiae* as a model organism for studying eukaryotic systems (Giaever and Nislow 2014). Additionally, *S. cerevisiae* has the distinction of having the only complete collection of deletion mutant strains, providing a valuable resource for various experimental screenings. The availability and application of this strain collection have significantly advanced our understanding of gene function, genetic interactions, and gene-environment dynamics in both *S. cerevisiae* and other biological systems (Giaever and Nislow 2014). Currently, the Saccharomyces Genome Database (SGD; http://www.yeastgenome.org/) serves as a comprehensive resource offering information on every gene in *S. cerevisiae* yeast. This valuable database not only relies on published literature but also incorporates systematic investigations of each *S. cerevisiae* gene for which knowledge has been acquired. This dissertation will focus on *S. cerevisiae* cells and its plasma membrane biophysical properties.

Yeast is a unicellular fungus belonging to the kingdom of fungi (Alberts *et al.* 2008). According to current scientific understanding, it shares a closer evolutionary relationship with animals than with plants (Brown *et al.* 2012). *S. cerevisiae* exhibits robustness and simplicity in growth, thriving effortlessly in a nutrient-rich medium. Similarly to other fungi, it possesses a sturdy cell wall and lacks mobility, and it possesses mitochondria but not chloroplasts (Alberts *et al.* 2008). Under favourable nutrient conditions, *S. cerevisiae* proliferates and undergoes cell division at a remarkable pace, similar to bacterial replication. Reproduction in yeast cells occurs through either vegetative means, involving simple cell division, or sexually through the fusion of two haploid yeast cells, resulting in a diploid cell harbouring two sets of genetic material. The diploid cell can subsequently undergo meiosis, a reduction division, to generate haploid cells once again. *S. cerevisiae* possesses the unique ability to indefinitely divide in both the haploid and diploid states, and the transition between the two can be deliberately induced by modifying the growth conditions (Lodish *et al.* 2005; Alberts *et al.* 2008).

Its extensive utilization in scientific research arises from several key advantages it offers. These include its compact size, rapid growth, well-characterized genetics, and ease of genetic manipulation, all of which make it an invaluable tool for studying fundamental cellular mechanisms. Also, yeast is commercially available and can provide a cheap source for biochemical studies (Sherman 2002; Alberts *et al.* 2008). This organism is a unicellular organism that, unlike more complex eukaryotes, can be grown on defined media, giving complete control over its chemical and physical environment. (Goffeau *et al.* 1996).

S. cerevisiae cells showcase characteristic ultrastructural attributes similar to other eukaryotic cells, characterized by the presence of membrane-bound organelles (Figure 1.1). This yeast cells exhibit notable diversity in terms of cell size, shape, and coloration. Their sizes can vary, ranging from approximately 2–3 µm in length to as much as 20–50 µm, with a diameter spanning 1–10 µm (Tofalo and Suzzi 2015). The yeast cell wall maintains the structure and the rigidity of the cell but is freely permeable for solutes smaller than 600 Da (Van Der Rest *et al.* 1995). The yeast cell wall measures around 100–200 nm in thickness and contributes to approximately 25% of the cell's total dry mass. The cell membrane of fungi is a lipid bilayer that is enriched with diverse lipids belonging to the classes glycerophospholipids, sphingolipids and sterols (Sant *et al.* 2016). The statement "the plasma membrane separates the other membranes and cell components from the external medium" is clearly an insufficient description of the many functions of the plasma membrane, since many processes that are vital for the organism take place at the plasma membrane (Van Der Rest *et al.* 1995).

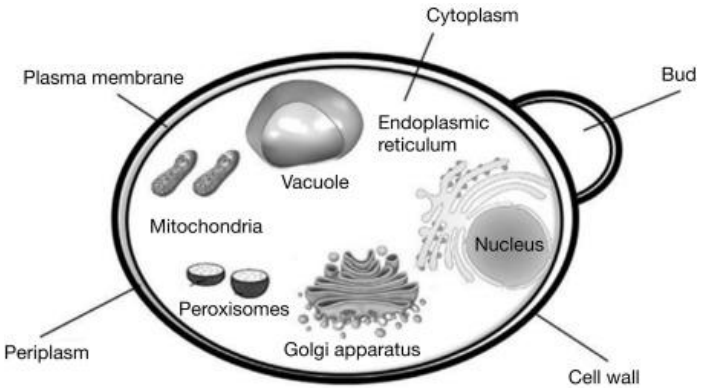

Figure 1.1. *S*chematic illustration of *S. cerevisiae* cell structure. The major components of yeast cells are the cell wall, plasma membrane, cytoplasm, nucleus, mitochondria, endoplasmic reticulum, and golgi apparatus (Van Der Rest *et al.* 1995).

Investigating the plasma membrane of *S. cerevisiae* cells has been of great significance due to the parallels it shares with other eukaryotic organisms. This research has enhanced our comprehension of the roles of specific membrane lipids and the significance of cellular compartmentalization in eukaryotic cells in general. Additionally, the study of the S. *cerevisiae* plasma membrane enables to identify differences between yeast and human cell membranes, offers insights into the mechanisms of action of antifungal agents, uncovering potential novel targets, and, thus, contributing to the development of more efficacious therapies.

1.2.1. Growth profile of yeast

Due to the rapid adaptability of fungi to changing environmental conditions, it is crucial to meticulously standardize and characterize cultivation conditions. This step is vital to ensure the generation of results that are not only meaningful but also replicable. Batch cultures are frequently described using the classical growth curve found in textbooks, which typically consists of distinct phases, as represented in Figure 1.2, including the latency phase, exponential phase, stationary phase, and declining phase (Vrabl *et al.* 2019).

S. cerevisiae cultures grown on glucose-based media exhibit various growth phases. One of the most well-studied growth arrest phases in *S. cerevisiae* occurs after growth on glucose-containing media. The latency (lag) phase represents one of the initial stages in the fungal growth cycle, during which fungi tends to adapt to their growth environment. In the initial exponential growth phase, also known as logarithmical or log phase, this yeast primarily ferments the available glucose for energy. However, when glucose becomes scarce, the cells briefly halt their growth and switch to a respiratory mode of energy generation. This transition period is referred to as the "diauxic shift". During the subsequent post-diauxic growth phase, cell growth slows down, and the cells utilize the ethanol produced during the earlier fermentation phase. Once this ethanol is completely used up, the cells enter the true stationary phase, where the cell population no longer increases (Werner-Washburne *et al.* 1996).

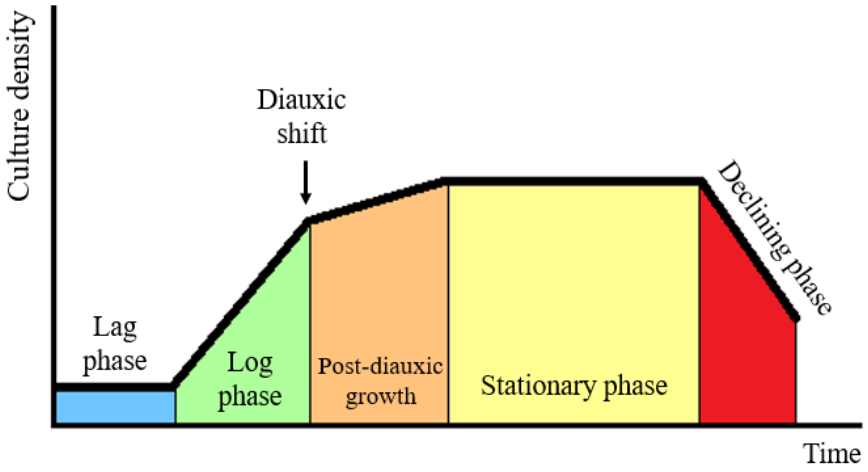

Figure 1.2. Representation of the typical growth phases of yeast cells throughout time. Adapted from (Werner-Washburne *et al.* 1996; Vrabl *et al.* 2019).

1.3. The composition of biological membranes

Prokaryotes, which are the simplest and smallest cells, are surrounded by a plasma membrane but lack internal membrane limited subcompartments. In contrast, eukaryotic cells, which are larger in size, have a more complex organization. Each organelle is enclosed by one or more biological membranes and contains a unique set of proteins. Some proteins are embedded within the organelle's membranes, while others reside in the aqueous interior space. These proteins enable each organelle to carry out specific cellular functions. The cytoplasm refers to the cellular region outside the nucleus, which is the largest organelle. Additionally, the cytosol, the aqueous part of the cytoplasm not occupied by organelles, possesses its own distinct proteins (Lodish *et al.* 2005)**.**

A biological membrane refers to a selective barrier or boundary that separates the internal contents of a cell or cellular compartment from its external environment (Figure 1.3). Biochemically, a wide range of fundamental cellular processes occur within or involve membranes to a significant extent (De Almeida and Loura 2004). Biological membranes are composed of a bilayer made up of lipid molecules, commonly referred to as the phospholipid bilayer. This bilayer structure consists of two sheets of lipids, creating a barrier that separates the internal and external cellular environments. Alongside lipids, membrane proteins and sugars are integral components of biological membranes. Membrane proteins are essential for preserving the structural integrity, organization, and transport processes across the membrane. Sugars, on the other hand, are present on a single side of the bilayer and are covalently bonded to specific lipids and proteins within the membrane structure (Watson 2015).

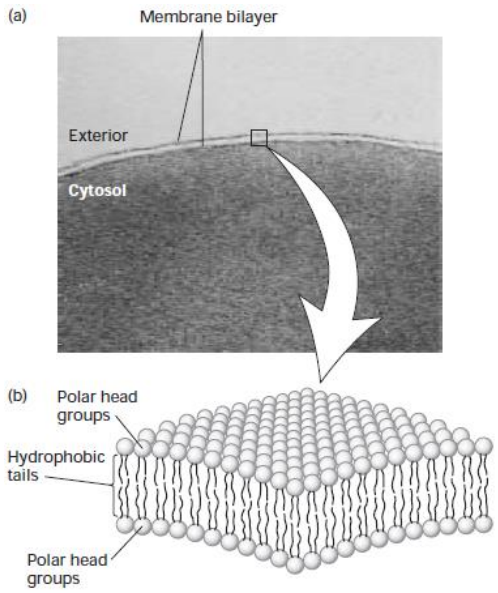

Figure 1.3. The bilayer structure of biological membranes. (a) The image indicates the presence of two polar layers, consistent with the bilayer structure for phospholipid membranes. (b) Schematic interpretation of the phospholipid bilayer in which polar groups face outward to shield the hydrophobic fatty acyl tails from water. Source: (Lodish *et al.* 2005).

1.3.1. Yeast and mammalian biological membrane composition

Biological membranes have two main components: proteins and lipids. However, in this dissertation, the main focus will be on membrane lipids. There are three major groups of membrane lipids regarding their structure and molecular composition: glycerophospholipids, sphingolipids and sterols (Nelson and Cox 2005). Each of these constituents contributes to the membrane's unique characteristics and functions, and their biosynthetic pathways are stringently regulated to ensure cellular integrity and operation (Dickson 2010).

All three classes of membrane lipids are amphipathic molecules having a hydrophilic (polar) head group and a hydrophobic (apolar) tail. Although the common membrane lipids have this amphipathic character in common, they differ in their chemical structures, abundance, and functions in the membrane (Lodish *et al.* 2005).

1.3.1.1. Glycerophospholipids

One of the major components of cellular membranes is a class of molecules known as glycerophospholipids (Hishikawa *et al.* 2014). Glycerophospholipids are a prominent group of molecules that play a crucial role in cellular membranes. Within mammalian cells, the composition of glycerophospholipids varies significantly between different cell types, organelles, and inner/outer membranes. These variations have been shown to have crucial implications in a wide range of cellular functions, such as signal transduction, vesicle trafficking, and membrane fluidity (Van Meer *et al.* 2008). Glycerophospholipids usually arrange themselves into bilayer structures, where the polar head groups of the lipids face the surrounding water molecules, while the hydrophobic hydrocarbon tails associate with each other, creating an inner hydrophobic layer. The hydrophobic part of these lipids is a diacylglycerol (DAG), which consists of saturated or cis-unsaturated fatty acyl chains of different lengths. Glycerophospholipids are derived from glycerol 3-phosphate and they are composed of glycerol, two fatty acid chains, and a phosphate group (Figure 1.4). The fatty acid chains may vary in the number of carbons (commonly 16 or 18) and their degree of saturation (0, 1, or up to 6 double bonds). A glycerophospholipid can be categorized based on the nature of its head group (Lodish *et al.* 2005; Watson 2015).

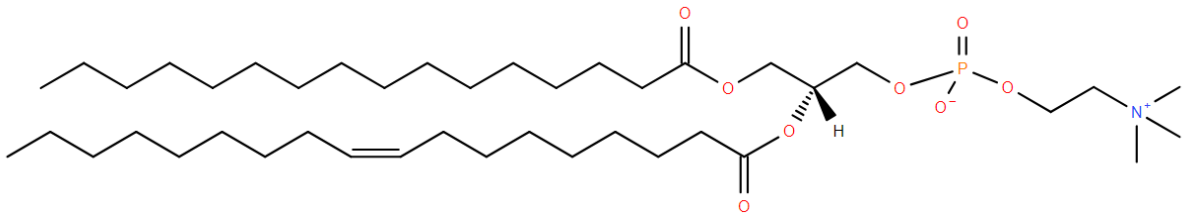

Figure 1.4. Chemical structure of a glycerophospholipid. The figure represents a 1-hexadecanoyl-2-(9Z-octadecenoyl)-sn-glycero-3-phosphocholine, commonly known as PC. Source: Lipid Maps.

The class of glycerophospholipids include phosphatidylcholine (PC), phosphatidylethanolamine (PE), phosphatidylserine (PS), phosphatidylinositol (PI), and phosphatidic acid (PA). PC and PE are the most abundant glycerophospholipids found in plasma membranes. PC is the most predominant phospholipid in animal membranes (Figure 1.5), accounting for over 50% of the glycerophospholipids in most eukaryotic membranes. Its exceptional adaptability makes it a perfect fit for membranes (Van Meer *et al.* 2008; Stilwell 2016). It forms a planar bilayer structure spontaneously, where each PC molecule has a nearly cylindrical shape. Most PC molecules have one cis-unsaturated fatty acyl chain, making them fluid at room temperature (Van Meer *et al.* 2008). These lipids play a significant role in shaping various membrane properties, notably membrane fluidity. While the fluidity of a membrane is largely influenced by the length and degree of unsaturation of the acyl chains, the composition of the polar head group also holds importance (Stilwell 2016).

PE is the second most abundant glycerophospholipid in humans but is the principal glycerophospholipid in bacteria. This distinction arises from the capacity of humans to convert PE into PC, whereas bacteria lack this capability, leading them to rely on PE as their primary membrane phospholipid (Stilwell 2016). PE has a conical molecular geometry due to its relatively small polar headgroup. PE also forms bilayers, however, unlike PCs, in the absence of other phospholipids, PEs prefer nonlamellar phase including reverse hexagonal phase, an unusual membrane structure that is discussed further in the Section: "Lamellar Phases" (Stilwell 2016). When incorporated into PC bilayers, PE introduces curvature stress to the membrane. This curvature stress is utilized in processes such as budding, fission, and fusion (Van Meer *et al.* 2008).

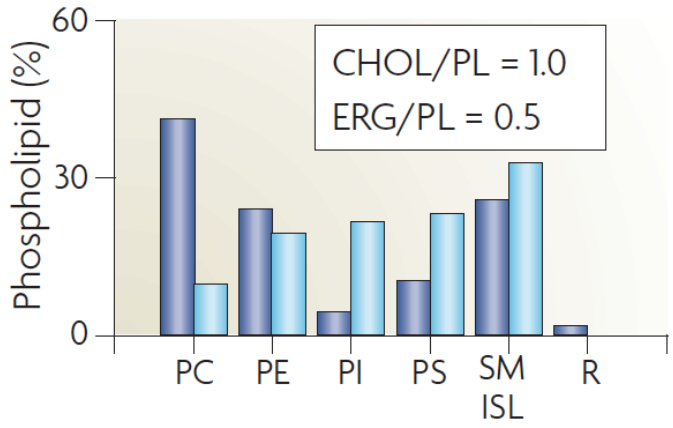

Figure 1.5. Mammalian and fungal plasma membrane lipid composition present important differences. The lipid compositional data are expressed as a percentage of the total phospholipid in mammals (blue) and yeast (light blue). CHOL, cholesterol; ERG, ergosterol; PC, Phosphatidylcholine; PE, phosphatidylethanolamine; PI, phosphatidylinositol; SM, sphingomyelin; ISL, yeast inositol sphingolipid; R, remaining lipids. Source: (Van Meer *et al.* 2008).

The abundance of the different glycerophospholipids in mammal cells' membrane is represented in Figure 1.6.

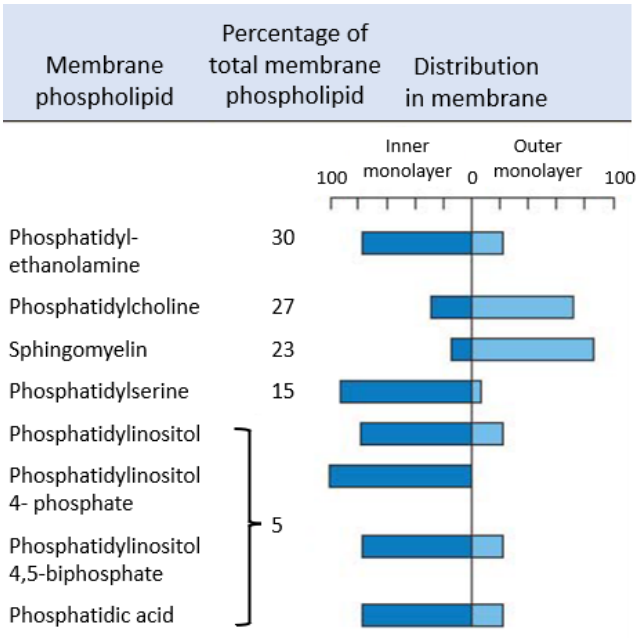

Figure 1.6. Distribution of glycerophospholipids between the inner and outer monolayers of erythrocyte plasma membrane and its percentage. Adapted from: (Nelson and Cox 2005; Martin 2011).

Glycerophospholipids are synthesized via *de novo* pathway (Figure 1.7) starting with glycerol-3-phosphate (G3P), leading to the initial production of PA and DAG or cytidine diphosphate-DAG (CDP-DAG) (Kennedy 1956; Hishikawa *et al.* 2014). Through the *de novo* pathway, a diverse array of glycerophospholipids with distinct polar heads at the sn-3 position of the glycerol backbone, including PC, PE, PS, PI, phosphatidylglycerol (PG), and mitochondrial cardiolipin (CL) are synthesized. Subsequently, the acyl chains of glycerophospholipids undergo remodeling through orchestrated reactions involving phospholipase As, acyl-CoA synthases, transacylases, and lysophospholipid acyltransferases (Hishikawa *et al.* 2014).

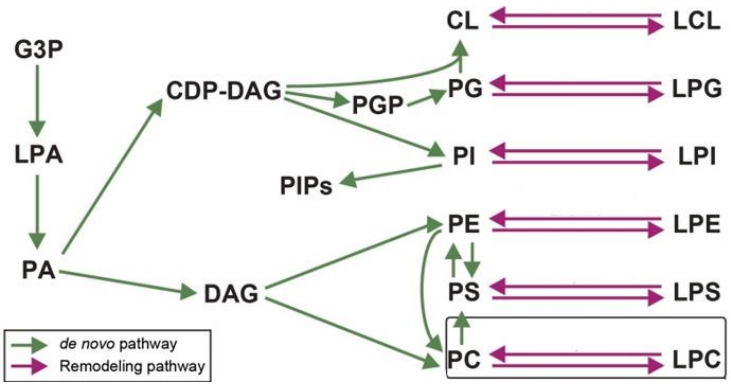

Figure 1.7. Biosynthetic pathways of glycerophospholipids. Upper panel shows the *de novo* synthesis (green lines) and the fatty acid remodeling (magenta lines) of glycerophospholipids. CDP-DAG, cytidine diphosphate-diacylglycerol; CL, cardiolipin; DAG, diacylglycerol; G3P, glycerol-3-phosphate; LCL, lysocardiolipin; LPA, lysophosphatidic acid; PA, phosphatidic acid; PG, phosphatidylglycerol; LPG, lysophosphatidylglycerol; PI, phosphatidylinositol; LPI, lysophosphatidylinositol; PE, phosphatidylethanolamine; LPC, lysophosphatidylcholine; LPE, lysophosphatidylethanolamine; LPS, lysophosphatidylserine; PC, phosphatidylcholine; PS, phosphatidylserine. From: (Hishikawa *et al.* 2014).

1.3.1.2. Sphingolipids and its backbone hydroxylation patterns

Sphingolipids are a major component of *S. cerevisiae* plasma membrane, representing about 7% of the mass of the plasma membrane and 30% of phospholipids (Patton and Lester 1991). *S. cerevisiae* has proven to be an exceptionally informative host in unravelling the mechanisms of sphingolipid biosynthesis and degradation, as well as their diverse cellular functions (Dickson 2010). Sphingolipids impact membrane biophysical properties such as fluidity and order, hydration, lateral diffusion and inter-leaflet coupling which are fundamental for understanding their cellular functions (Marquês *et al.* 2018). Also, sphingolipids play a crucial role in shaping and modulating membrane domains, alongside proteins, leading to membrane compartmentalization - an essential regulatory feature in numerous membrane-associated cellular events (Carquin *et al.* 2016).

The structure of a sphingolipid consists of a sphingosine backbone connected to a fatty acid through an amide bond. In recent years, there has been significant research and review focused on the diverse structural aspects of sphingolipids, particularly concerning their three essential building blocks: **headgroup, acyl chain or fatty acid chain, and long-chain (sphingoid) base (LCB)** (Figure 1.8). They are classified into ceramides, sphingomyelin, and glycosphingolipids based on the variation in their hydrophilic attachments, such as functional groups or substituents. The hydrocarbon chain length and degree of unsaturation of the latter two have been thoroughly explored. Nevertheless, an additional feature, contributing to the structural diversity across all sphingolipid classes, is the potential for different patterns of hydroxylation. The two most common variations in the sphingolipid backbone are the presence or not of a hydroxyl (-OH) group at the C2 of the acyl chain and/or of a hydroxyl group at the C4 of the LCB (Marquês *et al.* 2018; Mallela *et al.* 2022).

Nevertheless, there are some main differences between yeast and mammalian cells. In mammals, complex sphingolipids are categorized into two main types: sphingomyelins and glycosphingolipids. The structural diversity of complex sphingolipids is amplified by variations in the fatty acyl chain and the LCB within the ceramide backbone. Fungi, especially the budding yeast *S. cerevisiae*, possess a more straightforward sphingolipid composition compared to mammalian cells. They also have a notably smaller number of genes associated with lipid metabolism. Inositolphosphorylceramides (IPCs) stand out as an important group of complex sphingolipids in fungi, and they are notably absent in mammals (Santos *et al.* 2020). Regarding the chain length, in *S. cerevisiae*, the fatty acid chain length within ceramides and complex sphingolipids is primarily C26:0, primarily in the form of 2-hydroxyl-cerotic acid (2-OH-C26:0) (Marquês *et al.* 2018). Conversely, in mammals, the acyl chain length can vary between C14 and C26, and hydroxylation may also occur at the C2 position, albeit typically at lower levels compared to fungi. Fungi employ phytosphingosine as the LCB, whereas mammals utilize sphingosine. However, both mammals and yeast can contain dihydrosphingosine. In yeast, phytosphingosine usually consists of 18 or 20 carbon atoms, with C18 phytosphingosine being the more prevalent form (Santos *et al.* 2020).

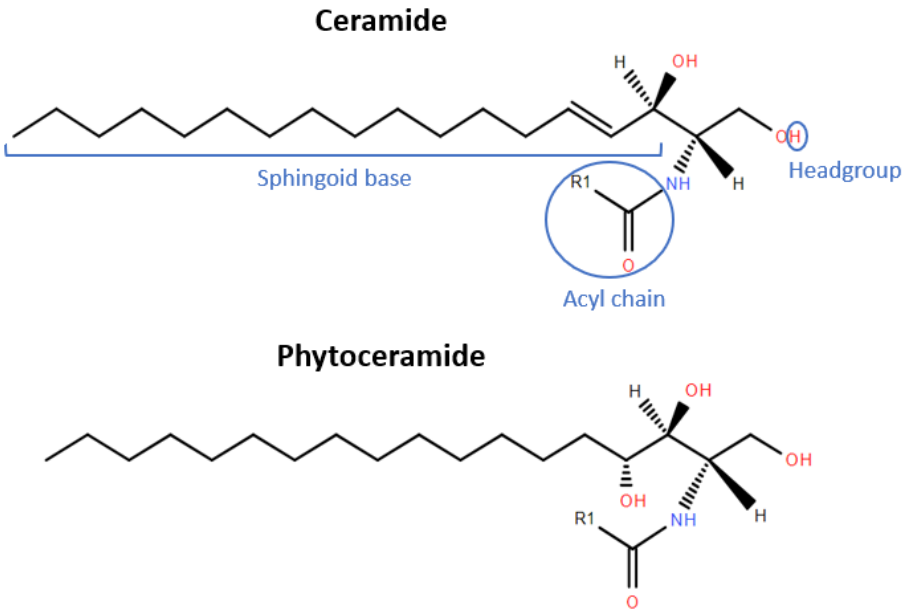

Figure 1.8. Representation of simple sphingolipids found in mammals and fungi cells, as well as its three building blocks: headgroup, acyl chain and sphingoid base. R_1 represents the hydrocarbon segment of a fatty acid. Phytoceramides differ from the typical mammalian ceramides by having a hydroxyl group attached to C4 of the sphingoid base, while the mammalian ceramides are desaturated at the sphingoid C4 (Plesofsky *et al.* 2008). The presence of phytoceramides in mammalian cells is significantly lower compared to yeast and plant cells (Rego *et al.* 2014). Image source from: Lipid Maps.

Sphingolipid metabolic pathways are conserved among fungi, plants, and mammals. The initial stages of sphingolipid biosynthesis, leading up to the formation of dihydroceramide, are shared by plants, fungi, and mammals. In mammals, complex sphingolipids are categorized into two types: sphingomyelins and glycosphingolipids. In mammals, glycosphingolipids are synthesized by adding one or more sugar residues, such as glucose and galactose, to the 1-hydroxy group (head group) of ceramides, including gangliosides. The primary complex sphingolipids found in animal membranes are sphingomyelins, formed by the transfer of the phosphatidylcholine head group to the 1-OH position of ceramides (Marquês *et al.* 2018). In fungi, particularly the budding yeast *S. cerevisiae*, possess a less complex sphingolipidome compared to mammalian cells, and a significantly reduced number of genes involved in lipid metabolism. An important group of complex sphingolipids in fungi is inositolphosphorylceramides, which are absent in mammals. In *S. cerevisiae*, one can find IPC, mannosylinositolphosphorylceramide (MIPC), and mannosyldiinositolphosphorylceramide ($M(IP)_2C$), each differing not only in the size of their polar headgroup but also in the overall net charge, which is −1 in IPC and MIPC, and −2 in $M(IP)_2C$ (Santos *et al.* 2020). *S. cerevisiae* exclusively synthesizes inositol-containing complex sphingolipids, whereas other fungi and plants not only produce inositol-containing complex sphingolipids but also glucosylceramides. Sphingolipidomics analysis of total lipids shows that IPCs are the most abundant sphingolipid species in *S. cerevisiae*, ~65% of total sphingolipids, while MIPCs and $M(IP)_2Cs$ are ~15% and ~20%, respectively (Marquês *et al.* 2018). The different complex sphingolipids of mammals and fungi are represented in Figure 1.9.

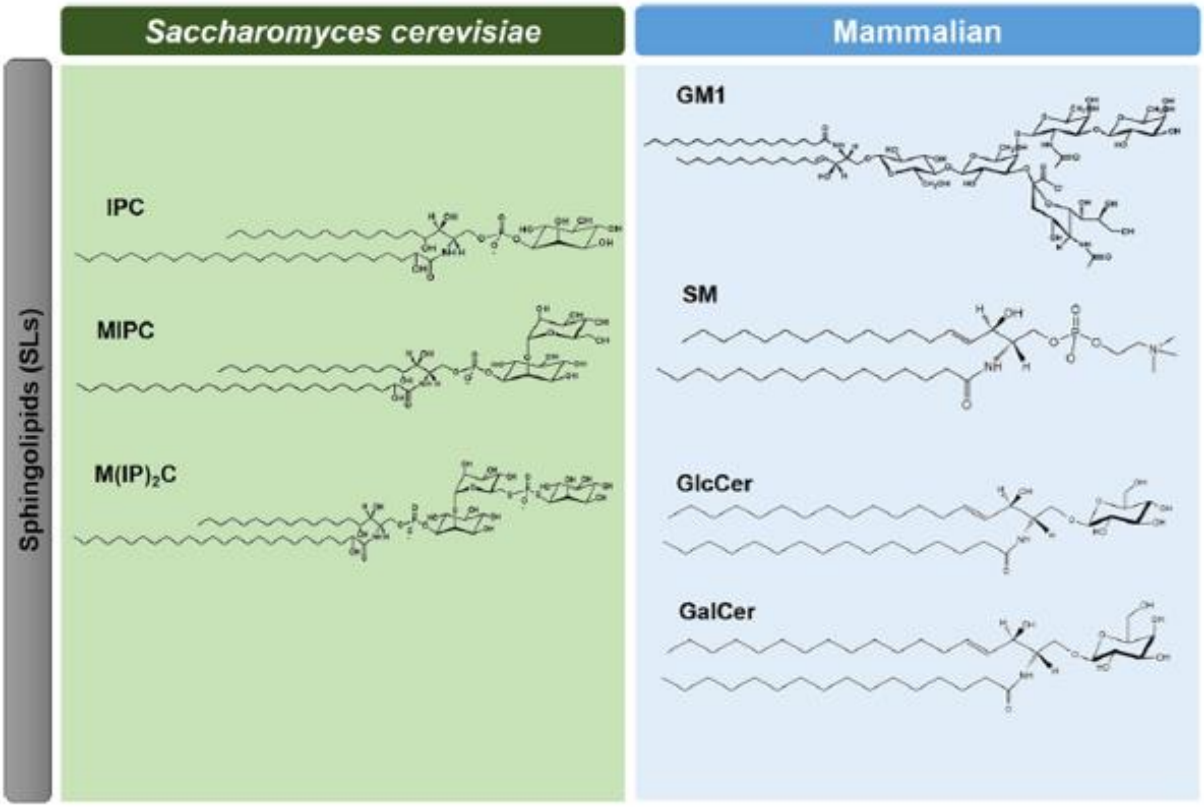

Figure 1.9. Structures of complex sphingolipids found in the plasma membrane of fungi and mammals. Green: budding yeast *S. cerevisiae*; blue: examples of different complex SLs found in mammalian cells PM. IPC, inositolphosphorylceramide; MIPC, mannosylinositolphosphorylceramide; $M(IP)_2C$, mannosyldiinositolphosphorylceramide; GM1, ganglioside GM1; SM, sphingomyelin; GlcCer, glucosylceramide; and GalCer, galactosylceramide. Source: (Santos *et al.* 2020).

Figure 1.10 represents the sphingolipds accumulated by certain gene mutations, such as *sur2*Δ, *scs7*Δ and *ipt1*Δ. To better understand which product is accumulated, it will be explained the biological function of the enzymes associated with each gene that is deleted. The enzymes are represented as the name of the gene and the surfix "p". ***Sur2*p**, a sphinganine C4-hydroxylase which catalyses the conversion of dihydrosphingosine (DHS) in phytosphingosine (PHS), encoded by the *SUR2* gene (Haak *et al.* 1997; Grilley *et al.* 1998; Bae *et al.* 2004; Marquês *et al.* 2018). The *SUR2*/*SYR2* gene is not essential for vegetative growth, but a deletion mutant has the interesting property of increased resistance to the antifungal compound syringomycin E (Grilley *et al.* 1998). ***Scs7*p** is a sphingolipid fatty acyl 2-hydroxylase that catalyses the C2 hydroxylation of the very long-chain fatty acids of dihydroceramides and phytoceramides, has hydroxylase/desaturase domains and it is not essential for growth (Mitchell and Martin 1997; Hama *et al.* 2000; Bae *et al.* 2004; Marquês *et al.* 2018). The final steps are the formation of three species of complex sphingolipids including IPC, MIPC and $M(IP)_2C$ (Dickson and Lester 1999). Firstly, the ceramides are converted to IPC by transfer of inositol phosphate from phosphatidylinositol to the 1-OH group of ceramide (Dickson and Lester 1999). IPC can be further mannosylated to form MIPC. The terminal step in *S. cerevisiae* sphingolipid synthesis is the transfer of inositol phosphate from phosphatidylinositol to MIPC to yield the most abundant complex sphingolipid in yeast, $M(IP)_2C$ (Structure shown in Figure 1.10) (Dickson and Lester 1999). The formation of $M(IP)_2C$ is catalysed by ***Ipt1*p**, an inositolphosphotransferase, which is involved in the synthesis of $M(IP)_2C$. $M(IP)_2C$ is simultaneously a phospholipid and a glycolipid (Dickson *et al.* 1997).

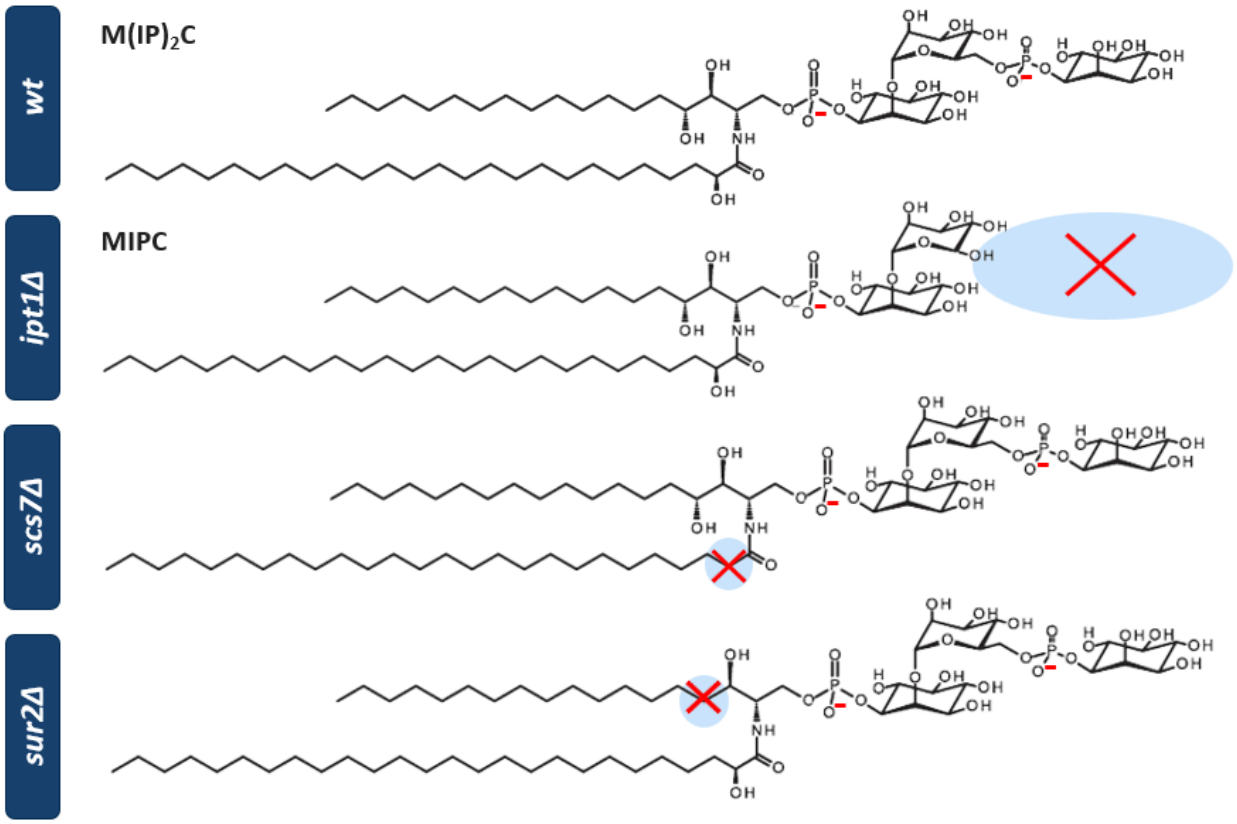

Figure 1.10. Sphingolipids accumulated in yeast *S. cerevisiae* as a consequence of mutations in the sphingolipid metabolic pathway caused by deleted genes. The *ipt1*Δ cells do not catalyse the formation of the complex sphingolipid $M(IP)_2C$, which will lead to MIPC accumulation, presenting a smaller head group and a charge of -1 instead of -2. In *scs7*Δ cells, there is no hydroxylation of the C2 at the acyl chain, furthermore, in *sur2*Δ cells, there is no hydroxylation of the C4 at the sphingoid base. IPC, inositolphosphorylceramide; MIPC, mannosylinositolphosphorylceramide; $M(IP)_2C$, mannosyldiinositol phosphorylceramide. Adapted from (Marquês et al. 2018).

1.3.1.3. Sterols

Sterols, such as cholesterol and ergosterol, constitute another major class of membrane lipids. Ergosterol is the predominant sterol in *S. cerevisiae*, representing 79% of the sterols in the plasma membrane (Figure 1.11). In the article Pedroso *et al.* 2009, the yeast sterol profile from the plasma membrane was determined, stating that there is an higher percentage of sterols in the plasma membrane than in the internal membranes. Sterols play a vital role as membrane constituents in eukaryotic cells, contributing significantly to membrane organization and function (Arora *et al.* 2004). The importance of sterols in the plasma membrane is underscored by the fact that disruptions in sterol biosynthesis can lead to severe cellular defects. For instance, mutations in the genes involved in ergosterol biosynthesis in *S. cerevisiae* can result in increased membrane permeability, impaired endocytosis, and increased sensitivity to antifungal drugs (Heese-Peck *et al.* 2002).

Sterols are characterized by a rigid, planar structure consisting of four fused carbon rings, with a hydroxyl group at one end and a hydrocarbon chain at the other (Figure 1.12) (Arora *et al.* 2004). This structure allows sterols to interact with the fatty acid chains of phospholipids, preventing them from

packing. This interaction helps to regulate membrane fluidity by preventing fatty acid chains of phospholipids from packing together, which would otherwise increase membrane rigidity. They also contribute to the formation of lipid rafts, which are microdomains in the membrane that are enriched in certain types of lipids and proteins (Lipid rafts will be further explained in Section "Membrane Compartments"). These lipid rafts play important roles in signal transduction, protein sorting, and membrane trafficking (Simons and Ikonen 1997).

There are several types of sterols, each one varies and it is more predominant among different organisms. In mammalian cells, the primary sterol is cholesterol, while in fungi, including *S. cerevisiae*, the predominant sterol is ergosterol (Figure 1.11) (Parks and Casey 1995). Structural disparities between the two include an extra double bond in the B ring and the aliphatic side chain of ergosterol, as well as an additional methyl group in its side chain (Dufourc 2008). Ergosterol is known as a "fungal hormone" with the capacity to stimulate growth and proliferation (Rodrigues 2018). In 2018, Solanko *et al.* deduced the distribution of sterols in a *S. cerevisiae* cell. Sterols found in the outer and inner leaflet of the plasma membrane make up about ~15% and ~55% of the cellular sterols, respectively. This is a result of an asymmetric distribution of ergosterol in the plasma membrane, with ~20% located in the outer leaflet and ~80% in the inner leaflet (Solanko *et al.* 2018). Recent findings have identified ergosterol as an immunoactive lipid that triggers host cell pyroptosis, a form of programmed cell death characterized by necrosis and inflammation (Rodrigues 2018). The presence of ergosterol is fungal cells, as opposed to cholesterol found in mammalian cells, is a distinguishing difference that can be exploited for selective toxicity (Odds *et al.* 2003). A multitude of antifungal medications operate by disrupting ergosterol biosynthesis or by directly binding to ergosterol, resulting in membrane instability and cellular death (Revie *et al.* 2018).

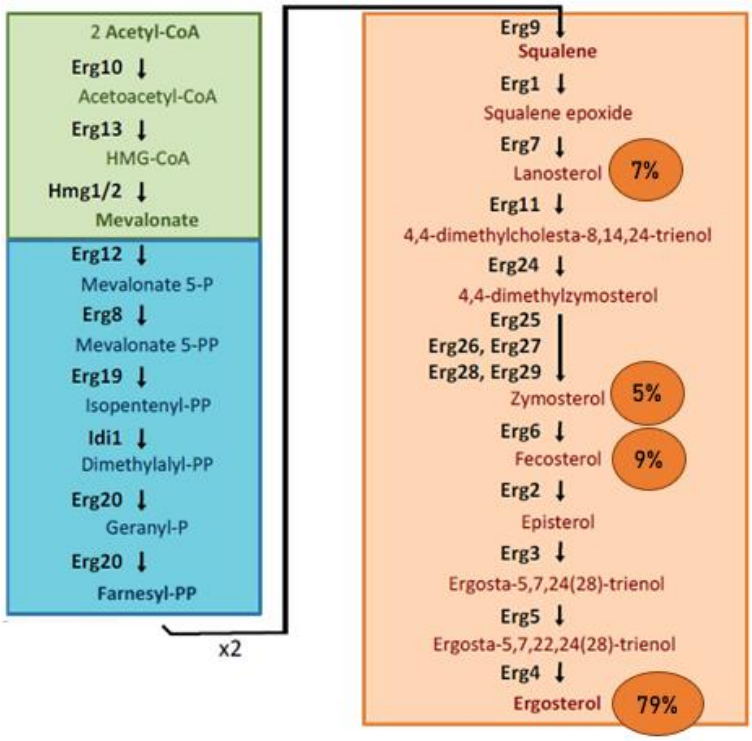

Figure 1.11. Ergosterol biosynthetic pathway in *S. cerevisiae* plasma membrane and the profile of some main sterols. There are three modules (boxes) into which the pathway can be divided: the green box is the mevalonate pathway, occurs in the vacuole and mitochondria; the blue box consists of farnesyl pyrophosphate (farnesyl-PP) biosynthesis and is carried out in the vacuole; and the orange box contains the late pathway, which ends with ergosterol biosynthesis, and mainly takes place in the ER. The sterol profile of *S. cerevisiae* is represented in the figure as percentages. These values are from the article: Pedroso *et al.* 2009. Adapted from (Jordá and Puig 2020).

Zymosterol (Figure 1.12) is a biosynthetic precursor for both cholesterol and ergosterol in the Blöch pathway. Remarkably, cholesterol, ergosterol and zymosterol exhibit minimal structural differences, however unlike cholesterol and ergosterol, zymosterol cannot form liquid ordered phase (a special type of lipid lamellar phase that will be discussed ahead). Nonetheless, zymosterol stands as the fourth most abundant sterol in the plasma membrane of *S. cerevisiae* (Pedroso *et al.* 2009; Khmelinskaia *et al.* 2020).

The budding yeast, *S. cerevisiae*, is a well-established model organism for investigating intracellular sterol homeostasis due to the shared basic steps in sterol metabolism and tracking across various eukaryotic organisms. Under aerobic conditions, yeast cells refrain from incorporating external sterols and instead fulfil their sterol requirements by internally synthesizing ergosterol. The synthesis of yeast ergosterol occurs via a highly conserved and intricate pathway, divided into three modules (Figure 1.11). The first module, present in all eukaryotes, leads to the formation of mevalonate from acetyl-coenzyme A (acetyl-CoA). The second module takes place within the vacuole and involves the creation of farnesyl pyrophosphate (farnesyl-PP). The third module, known as the late pathway, entails ergosterol synthesis through consecutive reactions, primarily occurring in the endoplasmic reticulum (ER) membrane. Initially, the squalene synthase Erg9 enzyme utilizes two molecules of farnesyl-PP to produce squalene, the precursor of all steroids. Subsequently, squalene is converted into lanosterol. In the following steps, lanosterol transforms into zymosterol via a complex process involving various demethylation, reduction, and desaturation reactions. Zymosterol serves as the first intermediate in the biosynthesis pathway and can be incorporated into cellular membranes. Next, the Erg6 enzyme converts zymosterol into fecosterol, leading to the formation of episterol, which is ultimately desaturated and reduced to ergosterol. While ergosterol is synthesized in the ER, it is predominantly transported to the plasma membrane.

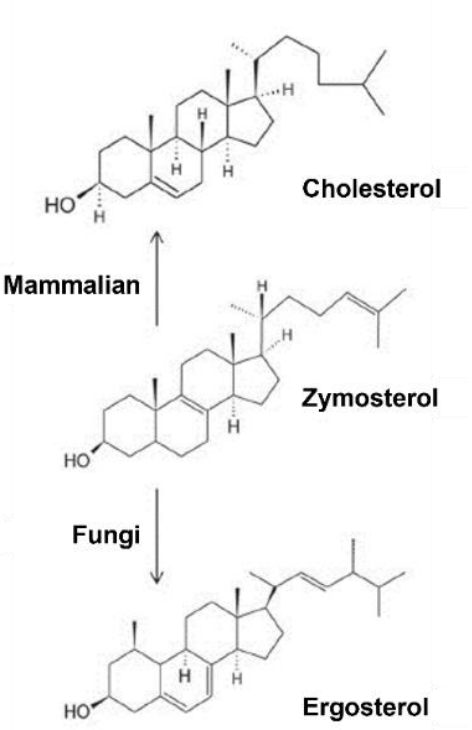

Figure 1.12. Structure of the main sterols in mammalian and fungi cells, and its last common biosynthetic precursor. Adapted from: (Khmelinskaia et al. 2020).

To sum up, sterols are essential components of the plasma membrane in eukaryotic cells. They regulate membrane fluidity, contribute to the formation of specialized membrane domains such as lipid rafts, and play crucial roles in various cellular processes. The distinct sterol composition of different organisms, such as cholesterol in mammals and ergosterol in fungi, highlights their importance in maintaining cellular integrity and function. Furthermore, the targeting of sterols in fungal pathogens has proven to be a successful strategy for antifungal treatments.

1.4. The structural organization of biological membranes

The previous section covered what is a biological membrane, as well as its main components in yeast and mammal cells. Now, how are these components organized in the plasma membrane? It greatly depends on the interactions that are established between its components. Lipids can be organized in different phases depending on their molecular structure and the physical conditions. In this section, a brief overview of the different possible lamellar phases will be provided along with lipid domains and membrane compartments present in the biological plasma membrane.

1.4.1. Membrane structure models throughout history

In 1665, Robert Hooke used a microscope to examine a piece of cork and observed hollow spaces that resembled honeycombs. He named these hollow spaces "cells," implying the presence of boundaries enclosing an empty region. However, it is important to note that the cell boundaries observed by Hooke and his contemporaries were actually the plant cell walls, visible with their microscopes (Lombard 2014).

In the early 20th century, it became evident that if cell membranes existed, they would likely contain lipids as a significant component. The molecular structure of membranes remained largely unexplored until a significant breakthrough occurred in 1925 by Gorter and Grendel. Gorter and Grendel's experiments concluded that cells were enveloped by a lipid membrane that consisted of two layers - a lipid bilayer - with the hydrophobic components located in the inner part of the membrane and the hydrophilic components in the outer part. This groundbreaking discovery shed light on the molecular structure of cell membranes (Gorter and Grendel 1925; Lombard 2014).

In the 1930s, while the presence of proteins in membranes was acknowledged, their specific location within cell membranes had received limited attention. In 1935, Danielli and Davson proposed a hypothesis suggesting that the lipid bilayer was flanked by two thin layers of proteins. They were mindful of the ongoing discussions surrounding membrane permeability and thus acknowledged the potential existence of proteins that could span across the membrane (Lombard 2014).

In 1972, S. J. Singer and Garth L. Nicolson introduced the **Fluid Mosaic Model** as a conceptual framework (Figure 1.13). According to this model, membranes are made up of lipids, proteins and carbohydrates. The "mosaic" term of this model refers to the mixture of lipids and intrinsic proteins in the membrane. These boundaries are also "fluid" because their components can move laterally, allowing both diffusion of components and local specific gatherings (Lombard 2014). This structure entails the presence of ionic and highly polar groups protruding from the membrane into the surrounding aqueous

environment, while nonpolar groups are predominantly embedded within the hydrophobic interior of the membrane. Although some lipid molecules may have specific interactions with membrane proteins, the overall structure of the membrane can be likened to a two-dimensional solution of oriented integral proteins (or lipoproteins) within the viscous phospholipid bilayer solvent. The authors suggest possible mechanisms for various membrane functions and membrane-mediated phenomena within the framework of this model (Singer and Nicolson 1972).

The fluid mosaic model continues to shape current research in membrane biology and remains a fundamental concept in understanding cellular membranes. Over the years, new information has emerged, shedding light on the significance and functions of distinct membrane domains, like lipid rafts and protein/glycoprotein complexes. These insights contribute to our understanding of the overall structure, dynamics, and functions of cellular membranes. Additionally, they underscore the roles of membrane-associated cytoskeletal barriers and extracellular matrix structures in constraining the lateral movement and mobility of membrane components. Updated versions of the model emphasize the mosaic nature of cellular membrane macrostructure. Many protein and lipid components exhibit limited rotational and lateral mobility within the membrane, especially in their natural states. This limited mobility is influenced by various interactions, including lipid-lipid, protein-protein, and lipid-protein interactions, as well as interactions involving cell-matrix, cell-cell, and intracellular membrane-associated proteins and cytoskeletal elements. Futhermore, smaller membrane nano- and submicro-sized domains, such as lipid rafts and protein complexes, are essential for preserving specialized membrane structures that are dynamically interrelated within a crowded membrane plane. While this new data adds complexity and hierarchy to the original model, the fundamental concepts presented in the original model remain relevant today (Nicolson 2013).

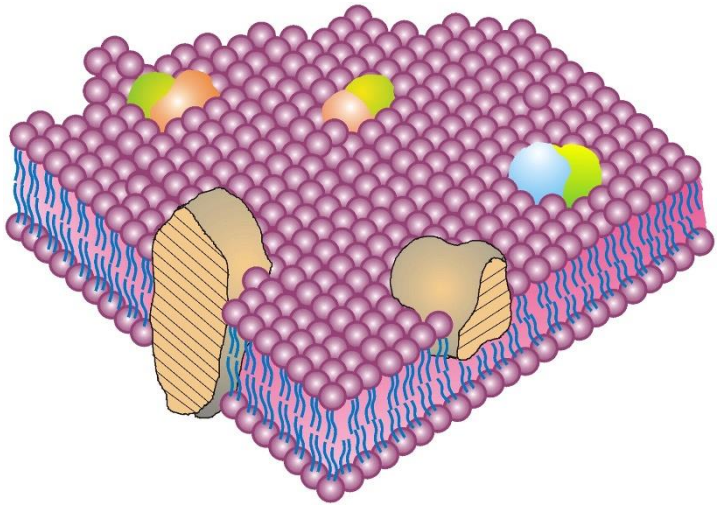

Figure 1.13. The fluid mosaic membrane of Singer and Nicholson. The image represents the structural view of cell membrane's section with integral proteins distributed randomly in a fluid lipid bilayer. Source: (Nicolson 2013).

1.4.2. Lamellar phases

In an aqueous environment, the lipid bilayer that forms biological membranes can assume various physical states. These states are defined by factors such as the arrangement of lipids, the orderliness of molecules, and the mobility of lipids within the bilayer. Therefore, physical and chemical variables like temperature, pH, ionic strength, the chemical composition of lipids, and the presence of cholesterol play a significant role in determining the properties of the bilayer (Eeman and Magali 2010).

The fluidity of a lipid bilayer is a consequence of its ability to facilitate lateral diffusion. If the movements in the membrane are rapid it means that the interior of the membrane is more fluid. This fluidity is influenced by various factors, including lipid composition, the structure of phospholipid hydrophobic tails, and temperature. Long, saturated fatty acyl chains have a strong tendency to pack tightly together, resulting in a rigid bilayer. In contrast, phospholipids with short fatty acyl chains or unsaturated chains form more fluid bilayers due to reduced surface area for interaction and less stable weaker van der Waals interactions, respectively. When a highly ordered bilayer is heated, the increased molecular motions of the fatty acyl tails cause it to undergo a transition to a more fluid, disordered state (Lodish *et al.* 2005). The temperature at which the phase transition (*T*m) of phospholipids occurs is influenced by both the osmotic pressure of the surrounding environment and the composition of the membrane. *T*m signifies the point at which the quantity of phospholipids in the fluid state equals the quantity in the rigid state (Laroche *et al.* 2001).

Studies that determine the properties of the lipid phases in the membrane are conducted using model systems. Biological membranes are then characterized by comparing their properties to the results obtained in model systems. Two primary lipid phases are observed in model systems: the gel and fluid phases (Figure 1.14). In the gel phase, also known as the solid-ordered (So) phase, lipids are organized in a two-dimensional triangular lattice within the membrane plane (Janiak et al. 1979). This phase is characterized by low water content, with the rotation along the molecule's long-axis occurring slowly due to the organization of hydrocarbon chains in an all-*trans* conformation. The So phase features closely packed lipids with strong van der Waals interactions between the hydrocarbon chains, establishing H-bonds among sphingolipids and between sphingolipids and the ester carbonyl group of glycerophospholipids. This strong H-bonding network increases the *T*m of the sphingolipid-enriched domains, also known as SLEDs (SLEDs will be explained further in the Section “Sphingolipid enriched domains (SLEDs) and sterol rich domains”) and plays a significant role in lateral segregation of sphingolipids and the formation of ordered domains in fungi (Marquês *et al.* 2018). The lateral diffusion in the gel phase is much slower than in any of the fluid phases (Santos *et al.* 2020).

In the fluid phase, also referred to as the liquid-disordered (Ld) phase, *trans*-gauche isomerization leads to less extended lipid chains. The fluid phase is more hydrated than the gel phase, since the lipid bilayer in a gel state becomes thinner with increasing water content. Furthermore, the two-dimensional triangular lattice is entirely disrupted. Consequently, both lateral diffusion and rotational diffusion of lipids are more favourable in fluid lipid bilayers (Eeman and Magali 2010).

When cholesterol is present, lipid bilayers can organize into another lamellar phase known as the liquid-ordered (Lo) phase. This phase combines characteristics of both the gel and fluid phases (Ipsen *et al.* 1987). The incorporation of cholesterol into a So phase disrupts the lateral triangular lattice, leading to a reduction in the ordering of the lipid chains. Conversely, in a Ld phase, the rigid hydrophobic moiety of cholesterol is intercalated between the lipid chains, favoring a *trans* chain conformation (Sankaram and Thompson 1990). The Lo phase exhibits both lateral and rotational diffusion patterns that are similar to those of the Ld phase, but it displays a conformational order similar to that of the So phase. As shown in Figure 1.14, Ld and Lo phases, as well as Lo and So phases, can coexist within the same lipid bilayer (Eeman and Magali 2010). For instance, a phase coexistence between a cholesterol-poor Ld phase and a cholesterol-rich Lo phase has been experimentally observed in lipid bilayers composed of phosphatidylcholine/cholesterol (Sankaram and Thompson 1991) and sphingomyelin/cholesterol mixtures (Ahmed *et al.* 1997).

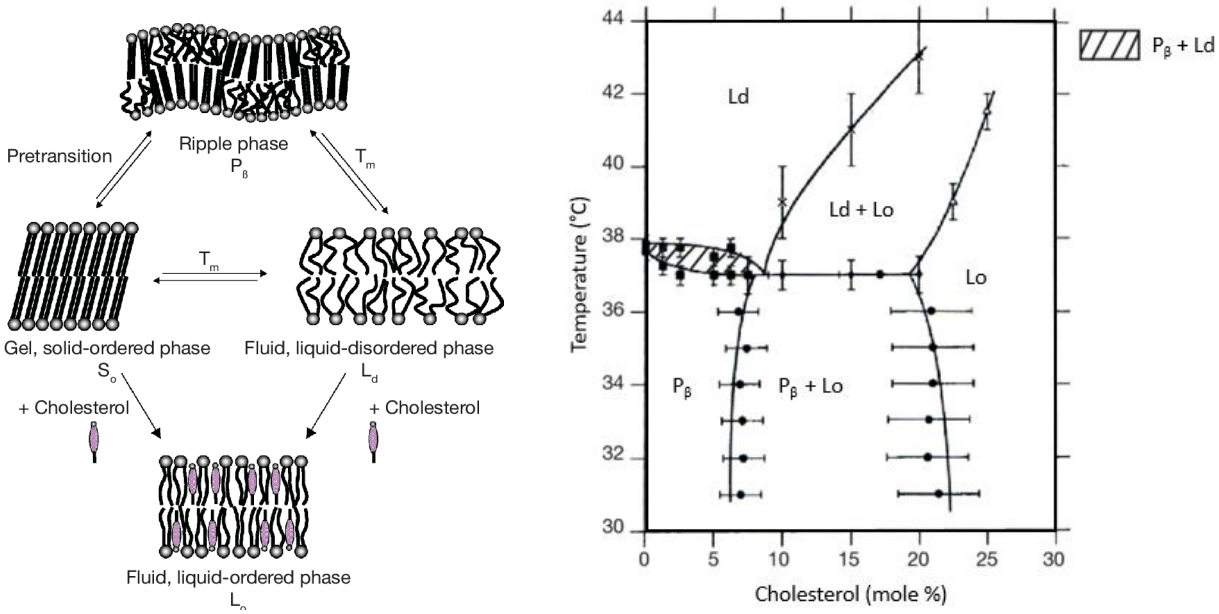

Figure 1.14. Characteristics of different physical states of a lipid bilayer. On the left, is a scheme illustrating the different physical states adopted by a lipid bilayer in aqueous medium. For the lipids that exhibit a pretransition temperature, exists an additional lamellar phase - the ripple phase. As this phase appears prior to the main chain melting, it must correspond to a partially disordered lipid phase. On the right, is represented a phase diagram for mixtures of cholesterol and chain-perdeuteriated dipalmitoylphosphatidylcholine (DPPC) in function of temperature. The phases are labelled as follows: P_β, rippled phase; Ld, liquid-disordered phase; Lo, liquid-ordered; So, gel phase; and T*m*, transition temperature. Adapted from: (Vist and Davis 1990; Eeman and Magali 2010).

1.4.3. Lipid domains and membrane compartments in the plasma membrane

The plasma membrane of *S. cerevisiae* is not a homogenous mixture of lipids and proteins but it is organized into distinct domains. These domains, characterized by their high concentrations of particular lipids and proteins, serve essential functions in numerous cellular processes (Malinsky *et al.* 2010), e.g. regulation of Na(+), K(+), and pH levels, which, in turn, impact a wide range of cellular processes, including cell growth and apoptosis. Also, lipid domains can have an impact on the susceptibility to drugs, and when drugs interact with the plasma membrane, they can modify the composition of the lipid domains and compromise membrane integrity, ultimately resulting in the demise of yeast cells (Mollinedo 2012).

As a consequence of the emphasis on membrane fluidity after the Singer and Nicolson's fluid mosaic model, the biological membrane was initially thought to be a uniform lipid bilayer, with proteins either embedded within or attached to it (Singer and Nicolson 1972; Malinsky *et al.* 2010). However, evidence accumulated over the past twenty years or more, has established that membranes display specific regions / are highly compartmentalized, indicating that they are laterally divided into compartments (Simons and Ikonen 1997; Malinsky *et al.* 2013).

.

1.4.3.1. Lipid domains

One of the models that explains the concept of diverse membranes relies on the physicochemical attributes of lipids. It is believed that membrane domains arise from the natural separation of lipid phases. Certain lipids, such as sterols and sphingolipids with long saturated fatty acids, aggregate to form what are known as **lipid rafts** (Figure 1.15) (Lingwood and Simons 2010; Malinsky *et al.* 2010). The concept of lipid rafts within the cell membrane was initially introduced in a 1988 review by Kai Simons and Gerrit van Meer. This hypothesis was developed to elucidate the unique trafficking of specific proteins from the Golgi to the apical plasma membrane in polarized simple epithelial cells (Simons and Van Meer 1988). The concept of lipid rafts facilitating compartmentalization suggests a specifically designed membrane structure that organizes functionality within the bilayer. Originally, this function was presumed to be associated with membrane trafficking. However, it is now understood that rafts could potentially impact the arrangement of any membrane bioactivity (Lingwood and Simons 2010).

In mammalian cells, lipid rafts represent specific membrane microdomains that are abundant in cholesterol and sphingolipids (Shah *et al.* 2015). Concerning the lipid composition percentage of lipid rafts, although the lipid proportions may differ among various cell types, the plasma membrane of mammalian cells typically consists of approximately 30-40% cholesterol, 10-20% sphingomyelin in terms of plasma membrane lipids and glycosphingolipids are usually present at lower levels (Langes *et al.* 1989; Van Meer 1989). In contrast, yeasts lack sphingomyelin and instead possess inositol phosphosphingolipids, which may serve as equivalents to mammalian sphingomyelin (Matmati and Hannun 2008). Lipid rafts are believed to compartmentalize the plasma membrane and play crucial roles in both survival and cell death signalling (Mollinedo 2012).

Recent research has provided the first direct evidence of the presence of gel domains in living cells, particularly in wild-type (*wt*) cells. These findings suggest that the plasma membrane predominantly consists of ordered domains, with gel domains mainly localized in the plasma membrane and primarily composed of lipids. This was evident from the observation of a notably extended lifetime component, exceeding 30 nanoseconds (Aresta-Branco *et al.* 2011) .Notably, these gel domains are

distinct from ergosterol-enriched lipid rafts, as they are primarily composed of sphingolipids, potentially IPC, and contain glycosylphosphatidylinositol-anchored proteins. This composition suggests an essential role in membrane traffic, signalling, and interactions with the cell wall. The abundance of sphingolipid-enriched gel domains appears to be inversely related to the overall order of the cellular membrane system, indicating their involvement in regulating membrane properties (Aresta-Branco *et al.* 2011). These domains were denominated as **Sphingolipid-enriched domains (SLEDs),** which are highly rigid lipid domains enriched in sphingolipids, however, they are depleted of sterols. Gel domains exist in the plasma membrane of yeast cells under physiological conditions, however, they are absent in the plasma membrane of mammalian cells under the same conditions. This distinction may play a role in the selective action of antifungal agents on fungal membranes as opposed to mammalian plasma membranes (Santos *et al.* 2020).

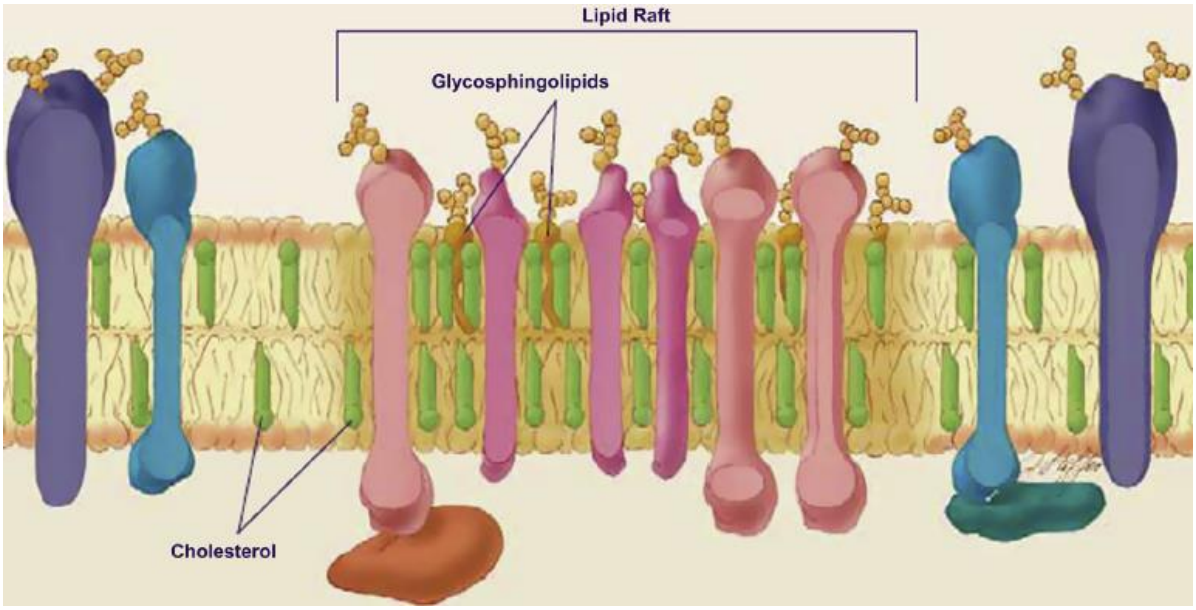

Figure 1.15. Representation of the lipid raft model and its components in the plasma membrane of mammal cells. Source: (Stilwell 2016).

1.4.3.2. Membrane compartments

Membrane compartments within the plasma membrane of fungi exhibit significant differences compared to mammalian lipid rafts. These compartments are larger, more temporally stable microdomains with well-defined localization, making them observable using conventional optical microscopy (Santos *et al.* 2020). Among these distinct membrane compartments, the two major ones are the **membrane compartment containing Pma1p (MCP) and the one containing Can1p (MCC)** (represented in Figure 1.16). Pma1p is the plasma membrane H^+-ATPase, responsible for establishing and maintaining the fungal plasma membrane transmembrane potential and regulating pH and intracellular ion concentration, with homologues found in all fungi (Kane 2016). MCP is a large and highly stable membrane compartment, appearing as a network under a confocal microscope, but super-resolution microscopy revealed that it consists of isolated foci. On the other hand, the MCC is linked to furrow-like invaginations, maintained by a large cytosolic protein complex known as the eisosome. There is a suggestion that the MCC/eisosome is enriched with ergosterol. This compartment harbors distinct ergosterol-dependent nutrient transporters, including Can1p (an arginine permease), Fur4p (an

uracil permease), and Tat2p (high-affinity tryptophan permease), and its integrity is compromised in mutants with deletions in certain steps of ergosterol biosynthesis. The nutrient uptake by MCC/eisosome H^+-symporters is dependent on the transmembrane potential created and sustained by the MCP protein Pma1p (Santos *et al.* 2020; Bento-Oliveira *et al.* 2020).

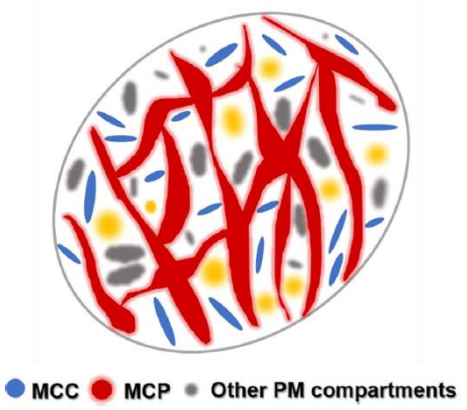

Figure 1.16. Representation of the top view of an area of the yeast plasma membrane and its major compartments. MCC, membrane compartment containing Can1p; MCP membrane compartment containing Pma1p. Source: (Santos *et al.* 2020).

The depletion of the complex sphingolipid $M(IP)_2C$ (*ipt1*Δ cells) results in an increase in the stiffness of gel domains, which, to a certain degree, may impede the incorporation of antifungals that target SLEDs into the membrane. The absence of $M(IP)_2C$ leads to a change in Pma1p distribution and consequently affects the organization of membrane compartmentalization (MCP). While certain sphingolipids in the plasma membrane of fungi could potentially serve as specific binding sites for certain antifungal agents, the significance of an intact MCP/SLED cannot be discounted as a critical factor in the initiation of their toxic effects (Santos *et al.* 2020).

As stated previously, the highly rigid SLEDs found in fungi, appear so far to be absent in mammalian cells, which qualifies sphingolipid domains at the plasma membrane as potential targets for antifungal drug therapies (Santos *et al.* 2020). E.g., in 2017, nystatin (Nys) was used in model systems with gel domains without sterols. Nys is a potent, broad-spectrum antifungal drug that operates by creating pores within the cellular membrane. In membranes containing gel domains, Nys-induced pore formation occurs through the destabilization of these gel phases. This research demonstrates that the formation of active Nys species relies on both the type of lipid and the presence of ordered gel domains. In summary, their findings suggest that moderate membrane permeabilization is observed in fluid membranes, while Nys-induced pore formation predominantly occurs at the boundaries between gel and fluid domains. Additionally, the properties and composition of gel domains impact Nys-mediated membrane stabilization and induced membrane permeabilization. These results indicate that Nys-membrane interactions depend on the specific membrane packing defects inherent to each gel/fluid system and Nys/lipid chain disparities, which increase Nys insertion into the membrane and promote stable pore formation (Dos Santos *et al.* 2017).

Understanding the differences between mammalian cells and fungal cells is crucial for the development of effective antifungal therapies. An in-depth understanding of these differences can guide the development of more potent and selective antifungal agents with reduced side effects, improving the efficacy of treatments and reducing the risk of drug resistance.

1.5. Fluorescence spectroscopy as an approach of election to study yeast cells' plasma membrane *in vivo*

Before exploring fluorescence spectroscopy, it is important to understand the concept of luminescence. The term "luminescence" originated from the Latin word "*lumen*" meaning light andwas first introduced as "*luminescenz*" by the physicist and science historian Eilhardt Wiedemann in 1888. It was used to describe all light phenomena not solely dependent on temperature, in contrast to incandescence, which produces hot light. Luminescence is often referred to as cold light. A more precise definition of luminescence is the spontaneous emission of radiation from an electronically excited or vibrationally excited species that is not in thermal equilibrium with its surroundings (Valeur and Berberan-Santos 2012).

Fluorescence and phosphorescence are particular cases of luminescence. (Valeur and Berberan-Santos 2012). The primary practical distinction between fluorescence and phosphorescence lies in the time elapsed between photon absorption and photon emission. Fluorescence refers to the process where a material absorbs a photon and almost instantly emits a lower energy photon. On the other hand, phosphorescence involves a more prolonged period as it necessitates a forbidden transition (Lakowicz 2006). However, this thesis will focus more on fluorescence, its technologies and applications.

Fluorescence technologies have revolutionized various fields of research, diagnostics, and imaging by providing valuable information about the behaviour and interactions of biomolecules and cellular structures.

Fluorescence spectroscopy is a powerful tool for studying the structure and dynamics of biological membranes *in vivo*. It involves the use of fluorescent probes that can integrate into the membrane and report on various properties such as membrane fluidity, polarity, and phase behaviour. Fluorescence imaging enables the visualization and quantification of intracellular molecules, even at the single-molecule level. Time-resolved fluorescence has gained popularity due to the enhanced information it provides compared to stationary or steady-state measurements (Lakowicz 2006). Fluorescence is emitted when a molecule returns from the excited state to the ground state (Klostermeier and Rudolph 2017), and usually occurs from aromatic molecules (Lakowicz 2006).

1.5.1. Steady-state and time-resolved fluorescence measurements

Fluorescence measurements can be divided into two main categories: steady-state and time-resolved measurements. Steady-state measurements, which are the most common, involve continuous illumination and observation of the sample. The sample is exposed to a continuous beam of light, and its emission spectrum or intensity is recorded. Since fluorescence events typically occur on the nanosecond timescale, most measurements fall into the steady-state category. Once the sample is exposed to light, it rapidly reaches a stable emission state.

The second type of measurement is time-resolved, specifically designed for capturing fluorescence intensity decays or fluorescence anisotropy decays. In this approach, the sample is exposed to a short pulse of light, with a pulse duration usually shorter than the sample's decay time. A high-speed detection system allows recording the intensity or anisotropy decay with (sub)nanosecond resolution, allowing for accurate time-resolved measurements (Lakowicz 2006).

In steady-state fluorescence studies, a commonly used light source is the high-pressure xenon arc lamp. It offers the advantage of providing continuous emission covering a wide range, from approximately 250 nm to the near-infrared region. To control the excitation wavelength, a monochromator is employed. During the experimental setup (represented in Figure 1.17), fluorescence is collected at a right angle with respect to the incident beam and then detected through a monochromator using a photomultiplier. The use of motorized monochromators allows for automatic scanning of wavelengths, with electronic devices and a computer controlling the process. The optical module comprises various components, including a sample holder, shutters, and, if necessary, polarizers. Additionally, it contains a beam splitter that consists of a quartz plate reflecting a small percentage of the exciting light towards a quantum counter or a photodiode usually called the reference channel, since it gives a signal proportional to the intensity of the incident light (Valeur and Berberan-Santos 2012).

In time-resolved fluorescence studies, the predominant technique for determining lifetimes or decay parameters is the time-correlated single-photon counting (TCSPC) method, more commonly referred to as single-photon timing (SPT). The fundamental principle hinges between the probability of detecting a single photon at time "*t*" following an exciting pulse and the concurrent fluorescence intensity. By systematically timing and recording individual photons emitted in response to numerous exciting pulses, the fluorescence intensity decay curve can be reconstructed. As illustrated in Figure 1.17, a standard single-photon counting instrument is depicted. The SPT technique offers several advantages, including its high sensitivity, exceptional dynamic range and linearity, often spanning three to four decades and potentially up to five, and well-defined statistics based on the Poisson distribution, allowing for proper weighting of each data point during analysis.

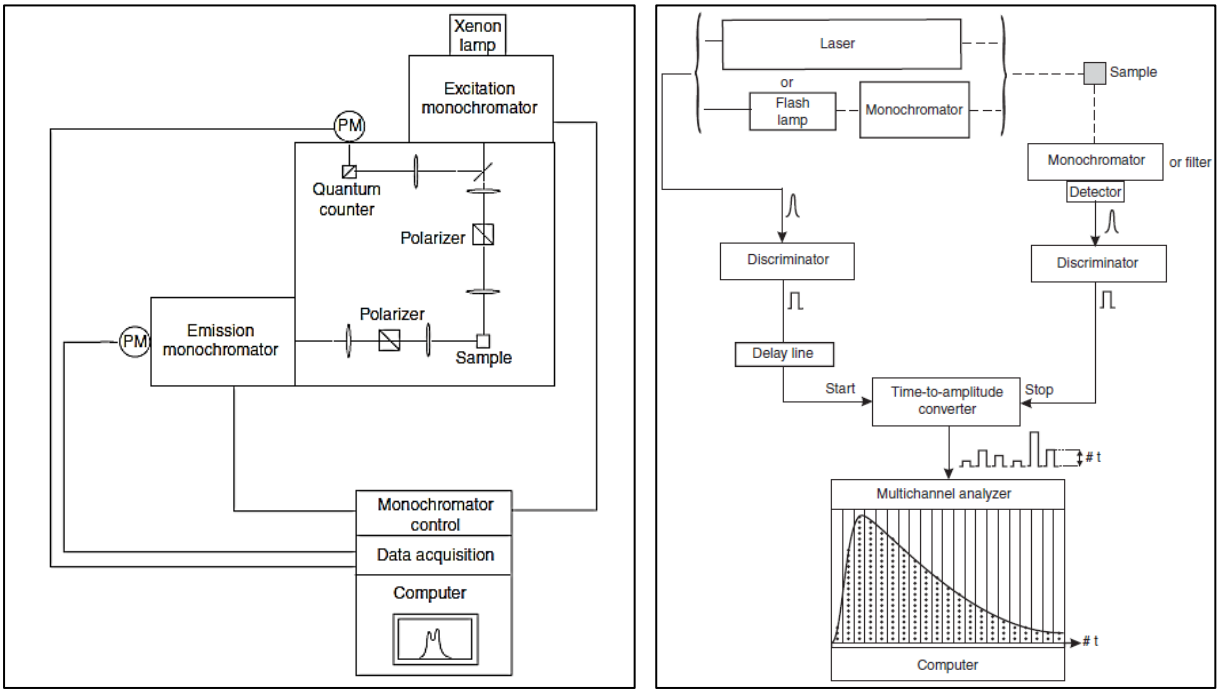

Figure 1.17. Schematic representation of a conventional fluorimeter (left) and diagram of a single-photon timing fluorimeter. Source: (Valeur and Berberan-Santos 2012).

1.5.2. Excitation and emission spectra

The study of excitation and emission spectra is fundamental to understanding the interactions between light and matter in various systems. To gain insights into the excitation and emission process, a helpful method is to represent the process using a diagram originally proposed in the 1930s (Lichtman and Conchello 2005). In 1933, Aleksander Jablonski, a Polish physicist, introduced a simplified three-energy-level diagram to explain luminescence phenomena observed in various organic compounds (Jabłoństski 1933). The more elaborate version of this diagram, which includes vibronic transitions, is widely known as the **Jablonski diagram** (Frackowiak 1988). The Jablonski diagram is a graphical representation used to illustrate the various electronic energy states of a molecule and the transitions between these states during fluorescence and phosphorescence processes. It is commonly used in the field of fluorescence spectroscopy and provides a visual representation of the electronic transitions that occur when a molecule absorbs and emits light (Lakowicz 2006).

The Jablonski diagram is represented in Figure 1.18 and consists of vertical energy levels representing different electronic states of the molecule. The lowest energy level, labeled as the ground state (S_0), represents the stable state of the molecule where the molecules are in their lowest energy configuration (Lichtman and Conchello 2005; Lakowicz 2006). Upon absorption of excitation light, the molecule undergoes transitions from the singlet ground state S_0 to the excited states S_1 (and possibly higher states like S_2), as well as different vibrational sub-states within S_1. Higher electronically excited states rapidly relax to S_1 within a very short time (ca. 10^{-12} s) - vibrational relaxation (VR). The S_1, v_0 state has a longer lifetime (1-10 ns), leading to fluorescence emission that is independent of the excitation light wavelength. After being excited, the molecule employs various pathways to dissipate the absorbed energy and return to the ground state. One of these pathways is known as internal conversion, which involves a transition between electron orbital states (e.g., S_2 to S_1). Another process called vibrational relaxation occurs, where the vibrational energy within the fluorophore is transferred to nearby molecules through direct interactions. It is important to note that vibrational relaxation does not result in the emission of any photons. Both internal conversion and vibrational relaxation occur rapidly and effectively bring the molecule back to the lowest energy level of S_1. While internal conversion can occasionally lead excited molecules all the way to the ground state S_0, most fluorophores prefer a different path due to the large energy difference between the ground state vibrational modes and the first singlet excited state. In efficient fluorophores, the favoured final energy pathway to return to the ground state involves the emission of a photon. This emitted photon's energy bridges the gap between the lowest vibrational state of S_1 and any one of the vibrational or rotational states of S_0. The emission spectrum of a fluorophore encompasses the range of wavelengths that this emitted photon can have (Lichtman and Conchello 2005). Additionally, molecules can enter the triplet state T_1 from S_1 through inter-system crossing (ISC), involving an inversion of electron spin, which is a spin-forbidden transition. The molecule then may emit phosphorescence when returning from T_1 to S_0 through another spin-forbidden transition, but for organic compounds under most physiological conditions it will relax electronically through nonradiative processes (Klostermeier and Rudolph 2017).

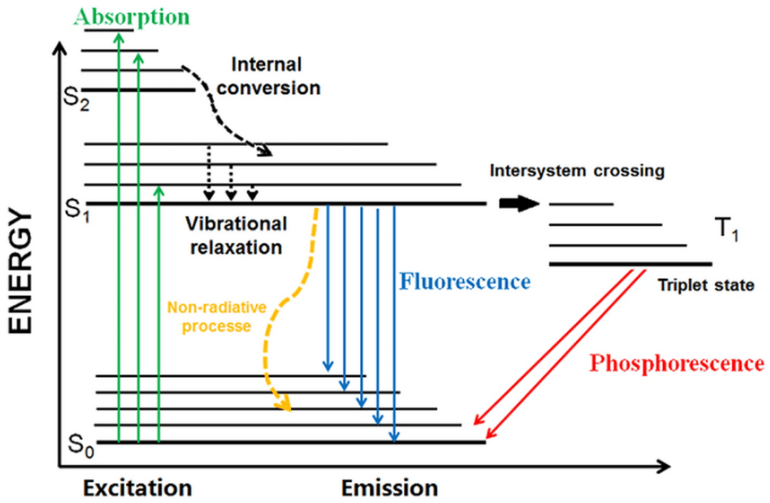

Figure 1.18. Perrin Jablonski diagram of fluorescence and phosphorescence. Source: (Schweizer *et al.* 2021).

1.5.3. Fluorescence anisotropy

Fluorescence anisotropy measures the rotational mobility of the fluorophores that are excited with polarized light (Sinha *et al.* 2010). Anisotropy measurements play a significant role in the biochemical applications of fluorescence. They provide information about the size and shape of macromolecules, such as proteins and the rigidity of molecular environments(Lakowicz 2006).

The foundation of fluorescence anisotropy measurements lies in the principle of photoselective excitation, where polarized light is used to selectively excite fluorophores. These fluorophores preferentially absorb photons with electric vectors aligned parallel to their transition moment, which has a specific orientation with respect to the molecular axis. In solution, the fluorophores have a random orientation, and the linearly polarized light will preferentially excite those that have their transition dipole aligned at the time of excitation, leading to partial orientation (photoselection) of the excited fluorophore population and partially polarized fluorescence emission (Figure 1.19). Additionally, fluorescence emission occurs with light polarized along a fixed axis within the fluorophore given by the orientation of the emission transition moment. The maximum measured anisotropy is determined by the relative angle between these moments.

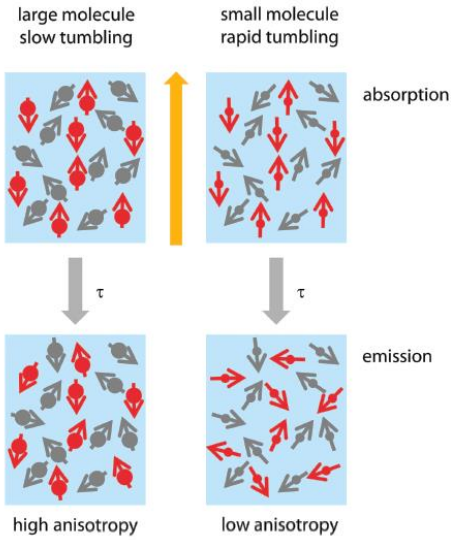

Figure 1.19. Photoselection and randomization of the orientation. During the lifetime τ of the excited state, large molecules (left) have rotated very little, resulting in mostly vertically oriented transition dipoles of the excited fluorophores. Consequently, the emitted light's polarization direction remains the same. The polarization direction of the emitted light is therefore the same as that of the incident light. Small molecules (right) rotate much faster, leading to a randomization of the orientation of the transition dipoles of the excited fluorophores during fluorescence. Source: (Klostermeier and Rudolph 2017).

1.5.4. Intensity decay

In time-resolved fluorescence spectroscopy, it is possible to gather more information than in steady-state conditions, especially related to membrane dynamics, domain sizes, and lipid-protein interactions (De Almeida *et al.* 2009). Using this technique, measurements of fluorescence intensity decay curves of a fluorophore in a sample are conducted.

Due to technical limitations, directly measuring fluorescence on the nanosecond time scale is not feasible. Instead, a method called *time-correlated single photon* counting (TCSPC) is employed. TCSPC involves recording the time of arrival of the first photon emitted from the sample after the excitation pulse. These photon arrival times are collected over numerous excitation-emission cycles and organized into histograms. The fluorescence decay can then be derived from the envelope of these arrival time histograms (Valeur and Berberan-Santos 2012). The obtained fluorescence lifetime values after analysing an intensity decay have several applications in membrane biophysics, such as determining the preference of a fluorophore (partition coefficient) between lipid phases and for determining lipid phase diagrams through the variation of lifetimes with composition (De Almeida *et al.* 2009).

1.5.5. Fluorescent membrane probes

The study of lipid domains within a living system demands highly sensitive techniques that introduce minimal interference. Specifically, this involves utilizing fluorescence spectroscopy in conjunction with high-intensity membrane probes possessing photophysical characteristics that are responsive to the nature of lipid domains and changes in membrane biophysical properties (Bastos *et al.* 2012). Fluorescent probes can disturb the system under study. Due to the high sensitivity of fluorescence measurements, the probes can be used at very low concentrations, minimizing disturbance. Also, membrane probes that are analogous to lipids or have a cylindrical shape and that are intercalated between the acyl chains can cause a small and very localized disturbance as well (Bastos *et al.* 2012). The following probes were used in this thesis to label the plasma membrane of *S. cerevisiae* cells: 1,6-Diphenyl-1,3,5-hexatriene (DPH), Trimethylamine-diphenylhexatriene (TMA-DPH), Anionic propanoic acid derivative (PA-DPH) and *Trans*-parinaric acid (*t*-PnA), as shown in Figure 1.20. Each of these probes is expected to label different regions of the plasma membrane.

DPH is one of the most commonly used fluorescent probes to study dynamical and structural properties of lipid bilayers and cellular membranes via measuring steady-state or time-resolved fluorescence anisotropy (Poojari *et al.* 2019). A rather unique characteristic of DPH, compared to other membrane probes, is its tendency to distribute evenly among various lateral domains within a membrane. This property has been illustrated in scenarios involving membranes of varying phases, those with differing cholesterol content, and membranes that include a transmembrane protein (Loew 1988). DPH is the most commonly used technique for assessing macroscopic membrane rigidity, since it evaluates both the fluid and less-fluid regions of the membrane with equal precision (Abe and Hiraki 2009), uniformly distributed in most areas of the membrane, giving relative information about global order of the lipid bilayer (Aresta-Branco *et al.* 2011; Poojari *et al.* 2019). The lipid–water partition coefficient (Kp) for DPH is Kp = 1.3×10^6 (Huang and Haugland 1991).

TMA-DPH is a cationic derivative of the fluorescence polarization probe DPH. TMA-DPH serves as a fluorescent membrane probe, traditionally employed to label the outer leaflet of a membrane bilayer and the plasma membrane in cells. Due to its cationic moiety, it becomes anchored to the charged headgroup at the lipid-water interface and thereby reports on the acyl chain order closer to the interfacial region of the membrane (Abe and Hiraki 2009).Unlike DPH, TMA-DPH exhibited remarkably swift incorporation into the plasma membranes of treated cells and remained specifically localized on the cell surface for at least 25 minutes. Due to these characteristics, TMA-DPH emerges as a favorable choice for conducting specific plasma membrane fluidity measurements in living cells (Kuhry *et al.* 1983). This cationic DPH derivative provides information on membrane dynamics through fluorescence polarization and/or fluorescence lifetime techniques. Moreover, TMA-DPH finds applications in studying exocytosis and endocytosis processes involving labeled plasma membranes. Researchers have also explored its use in investigating the interaction of the aqueous environment with mitochondrial inner membrane dynamics (Chazotte 2011). The lipid–water partition coefficient for TMA-DPH, Kp = 2.4×10^5, is lower than for DPH (Kp = 1.3×10^6), reflecting the increased water solubility due to the polar substituents (Huang and Haugland 1991).

Physical techniques have extensively explored the role of lipid molecules in the function and structure of biological membranes. Among these techniques, fluorescence depolarization methods are notably well-suited for this purpose. DPH and TMA-DPH, are frequently employed in these experiments (Abe and Hiraki 2009).

As stated previously, in this study, the yeast membrane was labelled with DPH and two DPH derivatives, namely TMA-DPH and **PA-DPH**, which have the potential to label different regions of the yeast plasma membrane as a consequence of their charge. Moreover, it is hypothesized that the cationic TMA-DPH interacts preferentially with SLEDs due to the negative charge of complex sphingolipids in yeast (inositolphosphorylceramide based). On the other hand, PA-DPH is being used for the biophysical characterization of yeast plasma membrane for the first time and should behave distinctly from TMA-DPH. The lipid–water partition coefficient for PA-DPH is Kp = 6.5×10^5.

***t*-PnA** stands out as a unique probe with a distinctive affinity for gel domains within lipid bilayers where these domains coexist with either Ld or Lo domains. Within these domains, *t*-PnA exhibits a highly enhanced fluorescence quantum yield, making it particularly responsive to alterations in the quantity and composition of these organized regions. Both in the case of *t*-PnA and DPH, the chromophore is securely ensconced within the hydrophobic core of the lipid bilayer, therefore their fluorescence properties can be used to assess the packing arrangement of acyl chains (Aresta-Branco *et al.* 2011). The lipid–water partition coefficient for *t*-PnA is Kp is ~2 x 10^6 (Sklar 1980).

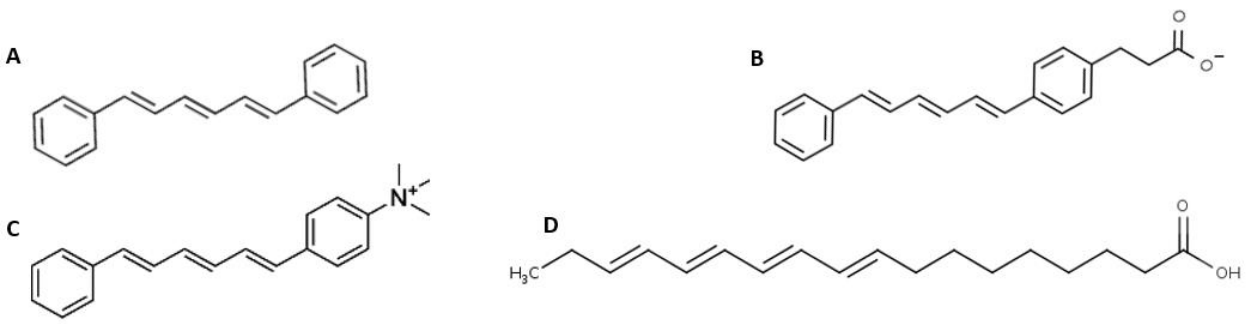

Figure 1.20. Chemical structure of the membrane fluorescent probes used in this work to label the plasma membrane of *S. cerevisiae cells*. DPH (A) and its derivatives, PA-DPH (B), TMA-DPH (C) and t-PnA (D). Adapted from: (Huang and Haugland 1991).

Chapter 2. Methods

2.1. Reagents and materials

Peptone for microbiology was obtained from PanReac AppliChem (Chicago, IL, USA), yeast extract from Fisher Bioreagents (Waltham, MA, USA), agar agar BAC from Labbox (Barcelona, Spain), glucose from D(+)-Glucose anhydrous BAC from (Dublin, Ireland). The organics solvents methanol HPLC gradient grade was purchased from Thermo Fisher Scientific (Waltham, MA, USA) and ethanol absolute spectroscopy grade from Scharlau (Barcelona, Spain). The fluorescent probes DPH 97.5–100% purity was purchased from Thermo Fisher Scientific (Waltham, MA, USA), TMA-DPH 95–100% purity from Invitrogen (Carlsbad, CA, USA), PA-DPH 99–100% purity was obtained from Avanti Polar Lipids (Alabaster, AL, USA) and *t*-PnA was purchased from Santa Cruz Biotech. (Santa Cruz, CA, USA).

2.2. Yeast strains

In this project, five different strains of *S. cerevisiae* were used as listed in Table 2.1.

Table 2.1. *S. cerevisiae* strains used in this work, background, genotype description, source and growth media.

Yeast strains	Background	Genotype	Source	Growth media
wild-type (*wt*)	BY4741/Y00000	MATa; his3△1; leu2△0; met15△0; ura3△0	EUROSCARF (Frankfurt, Germany)	Yeast Extract-Peptone-Dextrose (YPD)
ipt1△	Y04007	BY4741; YMR272c::kanMX4	EUROSCARF (Frankfurt, Germany)	YPD
erg6△	Y00568	BY4741; YML008c::kanMX4	EUROSCARF (Frankfurt, Germany)	YPD
scs7△	Y00858	BY4741; YMR272c::kanMX4	EUROSCARF (Frankfurt, Germany)	YPD
sur2△	Y03656	BY4741; Mat a; his3△1; leu2△0; met15△0; YDR297w::kanMX4	EUROSCARF (Frankfurt, Germany)	YPD

2.3. Equipment and accessories

All the equipment used in this work is listed in Table 2.2. For the preparation of yeast cell cultures an autoclave was used for the sterilization of all reagents and material, and an incubator was employed during the handling/preparation of cell cultures to ensure sterile conditions. For the spectroscopic characterization of the living cells a Fluorolog Model 3.22 Spectrofluorimeter from Horiba Jobin Yvon was used (Figure 2.1).

Table 2.2. List of equipment and accessories used to perform the experiments in this project.

Autoclave 88 from A. J. Costa (Agualva-Cacém, Portugal)
Laboratory Incubator POL-EKO Aparatura from Controltecnica (Madrid, Spain)
Incubator Model BE500 from Memmert
Floor Model Shaking Incubator from Shel Lab (OR, USA)
Digital Centrifuge Model 5415D from Eppendorf (Hamburg, Germany)
pH Meter Model Micro pH 2001 from Crison (Barcelona, Spain)
Thermoblock Dri-Block Model DB-3A from Techne
Spectrophotometer Model V-560 UV/VIS from Jasco (MD, USA)
Genesys Spectrophotometer Model 10S UV-VIS from Thermo Scientific (MA, USA)
Fluorolog Model 3.22 Spectrofluorimeter from Horiba Jobin Yvon (Villeneuve D'ascq, France)
nanoLED N-320 and nanoLED N-370 plus UGI-370 band from Horiba Jobin Yvon (Villeneuve D'ascq, France)
Temperature bath from Witeg (Wertheim am Main, Germany)
Sunrise-RC/ST Evolyzer Plate Reader from LaboControle (Linda-a-Velha, Portugal)
Fluorescence Microscope model BX41 from Olympus (Tokyo, Japan)

Figure 2.1. Fluorolog Model 3.22 Spectrofluorimeter from Horiba Jobin Yvon. This is the equipment used for the fluorescence spectroscopy measurements and the identification of each compartment.

2.4. Cell culture

Growth of yeast strains in solid medium

The cell suspensions of the yeast strains were preserved in a 20% (v/v) glycerol solution at a temperature of -80 °C (storage). A few cells were removed from one of the cell suspensions and inoculated in YPD solid medium in a petri dish. YPD solid medium contains 5 g peptone, 2.5 g yeast extract, 5 g agar and 225 mL Millipore water and 25 mL glucose 20%. This culture was incubated in a standard incubator at 30°C for 3 days, and then stored at a temperature of 4°C. The cultures were renewed, from the previous culture, every 15 days. After three renewals, a new culture was made from the cell suspensions.

Suspended cells subculture and culture preparation

Subcultures were made from the inoculated petri dish, which consists of inoculating the cells of the intended strain in YPD liquid growth medium, after which they were incubated in an orbital shaker at a speed of 160 rpm and a temperature of 30°C overnight. The yeast cells were reinoculated in YPD liquid growth medium (5 g peptone, 2.5 g yeast extract and 225 mL Millipore water and 25 mL glucose 20%). with a certain volume of cells from the subculture in order to obtain an initial optical density (OD) of 0.15 at 600 nm. In the mid-exponential phase, upon reaching an OD_{600} of ~0.6, after a 5-6 h of incubation, the cells were harvested. Absorbance measurements were performed on a Thermo Scientific Genesys 10S UV-Vis spectrophotometer. The cells were harvested from the culture in liquid medium and washed twice with sterile Millipore water and then suspended in buffer (PBS, 1 mM EDTA, pH 7.4). Between each wash the solution was centrifuged for 5 minutes at 5000 g.

In this work it was decided to use OD in the context of assessing cell concentration, however, the term "optical density" is no longer being recommended by IUPAC, with a preference for using the term "absorbance". The reason for this decision was because what is being measured is the turbidity of the suspension, without any light absorption process involved.

2.5. Cell growth curve

The growth of a cell culture can be determined by analysing its growth curve. Once the growth curve has been determined for a specific strain under certain conditions, it is possible to estimate the density at which a culture should be before being transferred to a new medium.

The strain of *sur2*Δ yeast cells were grown overnight in YPD liquid medium and then transferred to a new medium in order to begin with an A_{600} of 0.05. The samples were prepared in 96-well cell culture plate (Figure 2.2), each well with 250 µl of the suspended cell solution. A Tecan Sunrise Basic Microplate Reader was used to measure the cell density of each sample at different time points throughout 36 hours, with an agitation of 5 seconds and a temperature of 30º C.

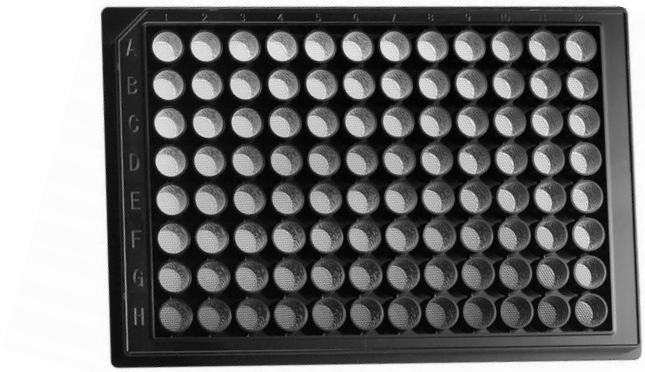

Figure 2.2. Example of a 96-well cell culture plate. These plates are a valuable tool for simultaneously measuring the OD of multiple samples.

The parameters for cell growth include the generation or doubling time (t_g) and the cell growth rate (μ). Considering that the growth of a microbial population is given by:

$$N = N_0 \cdot e^{\mu t} \qquad \text{Equation 2.1}$$

where N corresponds to the number of cells at a specific time t, N_0 to the initial number of cells ($t = 0$), μ to the growth rate, and t to the generation time.

By linearizing Equation 2.1, the growth rate, which represents the change in the number of cells per unit of time, corresponds to the slope of the line. On the other hand, the generation time, which is the time interval required for cells to double, is determined by:

$$t_g = \frac{\ln 2}{\mu} \qquad \text{Equation 2.2}$$

This parameter depends on the composition of the growth medium and environmental conditions.

2.6. Cell Viability

Cell viability refers to the number of live, healthy cells in a sample. Cell viability assays are used to measure the physical and physiological health of cells in response to extracellular stimuli, chemical agents, or therapeutic treatments, or when determining optimal growth conditions in cell culture (Präbst *et al.* 2017).

Trypan blue is a diazo dye (Figure 2.3) that has been widely used to color dead tissues or cells selectively. The mechanism of trypan blue staining is based on it being negatively charged and not interacting with cells unless the membrane is damaged. Therefore, all the cells that exclude the dye are considered viable. By contrast, cells with damaged membranes are stained in a distinctive blue color readily observed under a microscope. Thus, trypan blue dye is described as being a vital stain allowing discrimination between viable cells and cells with damaged membranes that are usually considered to be dead cells (Tran *et al.* 2011).

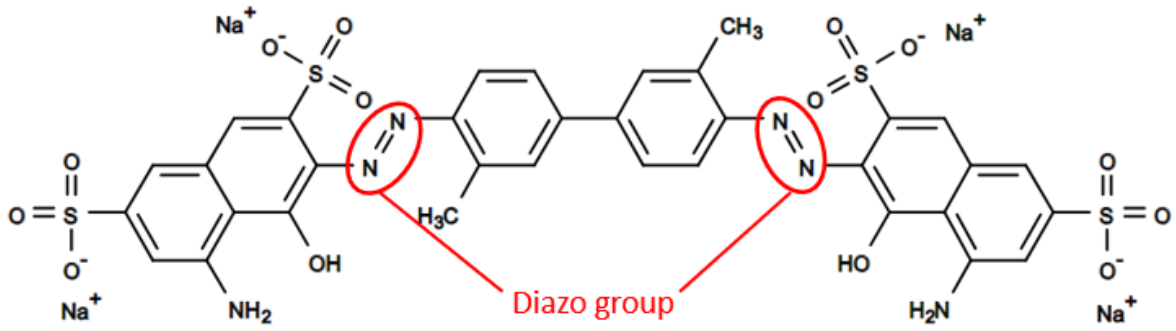

Figure 2.3. Chemical structure of trypan blue.

For this cell viability assay, a protocol was adapted from Gilbert and Friedrich "Cell Viability Assays: Methods and Protocols" (2017). A trypan blue stock solution was prepared by dissolving 4 g of trypan blue in 1000 mL of a sterile 0.9% NaCl solution. The solution was filtered through a 0.2 µm pore size filter to remove undissolved trypan blue crystals. Aliquots of the stock solution were stored frozen at −20 °C. For smaller quantities, 0.4 g of trypan blue was dissolved in 100 mL of 0.9% NaCl solution. For the incubation of the yeast cell suspension with trypan blue, the dye was added from the concentrated stock solution to the cells, to a final concentration of 2 µM. Cells were incubated with trypan blue for 20 minutes at 30 °C in the dark.

An hemocytometer was used to determine cell density and cell viability (Figure 2.4). The device had 2 chambers with grids, each chamber containing 9 large squares, and each large square corner had 16 smaller squares. Before use, the hemocytometer was cleaned with 70% ethanol and dried. The coverslip or cover glass was secured by placing one drop of water on each side of the "mounts." The chambers of the hemocytometer were filled with 10 µl each with the cell suspension stained with trypan blue. The cell count was performed using a wide-field microscope Olympus CK40, with a magnification of 200X. To simplify the process of cell counting, a manual hand counter was utilized.

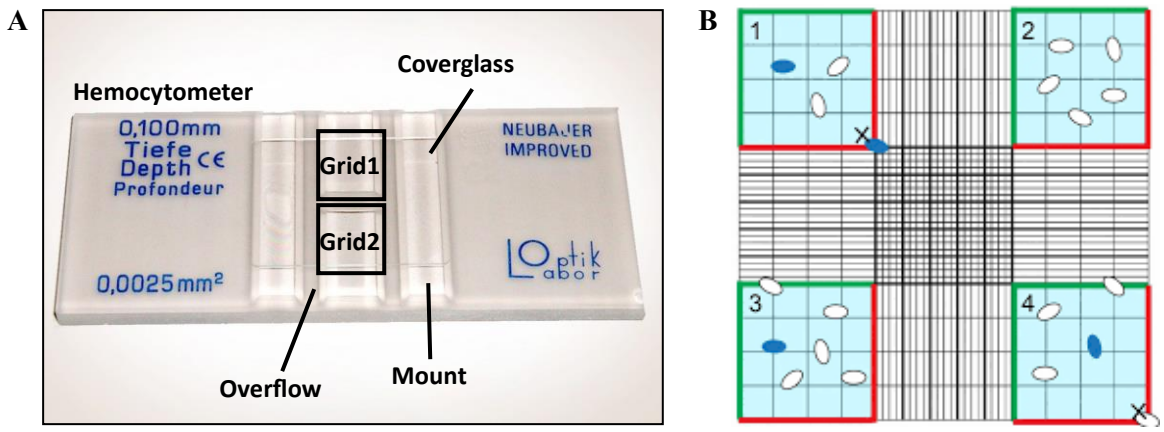

Figure 2.4. Cell counting in a hemocytometer. Hemocytometer assembly (A) and representation of the visuals of one of the grids of the hemocytometer in the fluorescence microscope (B). ○ Not stained/ white cells = living cells; ● Stained/ blue cells = dead cells.

The following equations for the calculation of viable cells and concentration of viable cells were applied:

a) Viable cells:

$$Cell\ viability(\%) = \frac{Total\ number\ of\ cells - number\ of\ stained\ cells}{Total\ number\ of\ cells} \cdot 100 \qquad \text{Equation 2.3}$$

b) Concentration of viable cells/mL:

$$Concentration = cells/square \cdot dilution\ factor \cdot 10^4 \qquad \text{Equation 2.4}$$

, 10^4 being the volume of suspension in mL associated with the hemocytometer characteristics.

2.7. Determination of molar absorption coefficient

The molar absorption coefficient was determined for the membrane fluorescent probes DPH, TMA-DPH and PA-DPH. The Lambert Beer's Law can be applied in order to calculate an unknown concentration of a solution using its absorvance value and the molar absorption coefficient. This law states that molar absorption is constant (and the absorbance is proportional to concentration) for a given substance dissolved in a given solute and measured at a given wavelength (Klostermeier and Rudolph 2017).

$$A_\lambda = \varepsilon\, c\, L = \varepsilon\, c \qquad \text{when L = 1 cm} \qquad \text{Equation 2.5}$$

A: Absorvance λ: Specified wavelength ε: Molar absorption c: Molar concentration L: Light path length in centimeters

The molar absorption coefficients of the fluorescent probes are DPH, $\varepsilon_{ethanol}^{352\ nm}$= 84800 M^{-1} cm^{-1} (Pathak and London 2011), TMA-DPH, $\varepsilon_{methanol}^{354\ nm}$= 53000 M^{-1} cm^{-1} (Cundall *et al.* 1979), however, the coefficient of PA-DPH dissolved in methanol or ethanol cannot be found in the literature. In this project it was determined the molar absorption coefficient of the three DPH probes.

To determine the molar absorption coefficient of the fluorescence probes, a certain amount of powder in an high precision analytical balance with 0.01 mg readability was weighted. The powder was then dissolved in a specific organic solvent (methanol or ethanol analytical grade). Since the powder of DPH and its derivates are difficult to dissolve in methanol or ethanol, the solutions were heated at 30 °C overnight and put in an ultrasound bath for 20 minutes prior to its use. The probe solutions were protected from the sunlight inside ambar colored glass. The absorbance of each probe solution at different concentrations was performed on a Thermo Scientific Genesys 10S UV-Vis spectrophotometer. The molar absorption coefficient was determined by the slope obtained by the graphic representation of the correlation between the probe concentration and the absorvance of the probe's solution.

2.8. Quantification of fluorescent probes

The fluorescent membrane probes DPH, TMA-DPH, PA-DPH and *t*-PnA were quantified before every experiment with the purpose of controlling rigorously its concentration when used to label the cell suspensions. The concentration of each probe was determined from its respective concentrated stock solution (≥ 200 μM), using the following molar absorption coefficients that were determined in this project: DPH, $\varepsilon_{ethanol}^{352\,nm}$= 84102 M^{-1} cm^{-1}, TMA-DPH, $\varepsilon_{ethanol}^{354\,nm}$= 51823 M^{-1} cm^{-1}, PA-DPH, $\varepsilon_{methanol}^{355\,nm}$= 66446 M^{-1} cm^{-1}. For the *t*-PnA probe it was used $\varepsilon_{ethanol}^{300\,nm}$= 89000 M^{-1} cm^{-1} (Bento-Oliveira *et al.* 2020). In order to determine the probes concentration, the Lambert Beer's Law was applied.

2.9. Fluorescence microscopy of labelled yeast cells

Fluorescence microscopy images were taken with an Olympus BX41 fluorescence wide-field microscope, Olympus U-RFL-T burner, Olympus U-CMAD3 ocular. Images were captured using the Software IC Capture 2.4. Yeast cell suspension of each strain was grown overnight and pre-cultures with a OD_{600} = 0.15 were incubated for 5-6 h for a final OD_{600} of 0.6, which indicates that the cells reached their exponential growth phase. The cells were harvested from the culture in liquid medium and washed twice with sterile Millipore water and then suspended in buffer (PBS, 1 mM EDTA, pH 7.4). Between each wash the solution was centrifuged for 3 minutes at 500 G. For the incubation of the fluorescent membrane probe with the yeast cell suspension, the probe was added from a concentrated stock solution to the cells, achieving a final concentration of 2 μM. While the probe was incubating, the fluorescent images were being taken in order to obtain images throughout the incubation time. The images obtained were treated using the software ImageJ 1.54d.

2.10. Fluorescence spectroscopic characterization of cells in suspension labelled with fluorescent probes

Fluorescence spectroscopy measurements were carried out on a Horiba Jobin Yvon FL-1057 Tau 3 spectrofluorometer equipped with double monochromators in both excitation and emission, in a perpendicular angle, and Glan-Thompson polarizers - calcite prisms, providing an high extinction ratio, essential for measuring small changes in anisotropy). Detection was carried out using a photomultiplier tube model TBX. The experiments were performed at 24 °C in a temperature-controlled sample compartment with magnetic stirring to prevent deposition of the cell suspension. The temperature in the cuvette holder was controlled by a water circulation system. The fluorescent probes were added from a concentrated stock solution (≥ 200 μM) to the cell suspensions to a final concentration 2 μM, in quartz cuvettes with dimensions of 0.4 cm × 1 cm (optical path during excitation × optical path during emission) from Hellma.

2.10.1. Optimization of experimental conditions for the use of fluorescent probes in *S. cerevisiae*

2.10.1.1. Steady-state fluorescence anisotropy kinetics measurements for probe incorporation in the plasma membrane of yeast

In order to determine the proper incubation time of each probe, anisotropy kinetics measurements were performed. The incubation of the probe was done directly on a cuvette containing the cell suspension with the purpose of tracking the anisotropy progression over time, to conclude about: i) the suitable incubation time of each probe in subsequent experiments; ii) and the preferential labelling regions on the membrane since, over time, the probes end up being distributed throughout the membrane.

2.10.2. Steady-state fluorescence spectroscopy

For fluorescence measurements in the steady-state, the excitation and emission wavelengths were set to, respectively, 350 and 430 nm for DPH (Bento-Oliveira *et al.* 2020), TMA-DPH and PA-DPH. For *t*-PnA the excitation and emission wavelengths were set to, respectively, 320 and 404 nm (Santos *et al.* 2017). As for incubation times, cells were incubated with DPH and its derivatives for 20 minutes, and they were incubated with *t*-PnA for 5 minutes. The integration time for DPH and its derivatives were 1 s, and for *t*-PnA it was 0.2 s. The steady-state fluorescence spectroscopy measurements were performed both for fluorescent excitation and emission spectra and also steady-state anisotropy. The continuous radiation source used for steady-state fluorescence and calibration of the monochromators was a 450 W Xenon arc lamp, and the reference was a photodiode. A spectrum for the blank was always obtained and subtracted from the spectrum of the respective sample.

2.10.2.1. Fluorescence excitation and emission spectra

Fluorescence excitation and emission spectra were obtained using excitation and emission slits of 3 nm for DPH and *t*-PNA, and slits of 2 nm for TMA-DPH and PA-DPH.

2.10.2.2. Fluorescence anisotropy

The value of steady-state fluorescence anisotropy, $\langle r \rangle$, was determined through Equation 2.6 and Equation 2.7:

$$\langle r \rangle = \frac{I_{VV} - G \times I_{VH}}{I_{VV} + 2G \times I_{VH}} \qquad \text{Equation 2.6}$$

$$G = \frac{I_{HV}}{I_{HH}} \qquad \text{Equation 2.7}$$

, in which I_{VV} and I_{VH} are the fluorescence intensities of the vertically (VV) and horizontally (VH) polarized emission when the sample is excited with vertically polarized light, and G is the ratio of the sensitivity of the system for vertically and horizontally polarized light (Sousa *et al.* 2021)

The total intensity (I_{total}) was calculated through Equation 2.8:

$$I_{TOTAL} = I_{VV} + (2 \cdot G \cdot I_{VH}) \quad \text{Equation 2.8}$$

Anisotropy measurements provide information about the rotational mobility of the probes, which is related to membrane fluidity. Intensity decay measurements provide information about the lifetime of the excited state of the probes, which can be used to infer the dynamics of the membrane. The steady-state anisotropy measurements were obtained using slits of 6 nm for DPH and *t*-PNA, and slits of 4 nm for TMA-DPH and PA-DPH.

2.10.3. Time-resolved fluorescence spectroscopy

For time-resolved measurements, the single photon counting technique is used for the excitation of the fluorescent probes, and the emission wavelength varied according to the light source for lifetime fluorescence used for each probe. A nanoLED N-370 plus UGI-370 band pass filter (Horiba) was used for DPH, TMA-DPH and PA-DPH, and for *t*-PnA the light source utilised was a nanoLED N-320 (Horiba). The light sources were chosen by their proximity with the wavelength of the peak of absorption of the fluorescent probes. The fluorescence intensity decays of the probe were described by the following multiexponential model:

$$I(t) = \sum_{i=1}^{n} \alpha_i \exp\left(-\frac{t}{\tau_i}\right) \quad \text{Equation 2.9}$$

where α_i and τ_i: normalized amplitude and lifetime of component i, respectively. After subtracting the contribution of the cells autofluorescence to the pre-exponential factor in each component *i* with lifetime τ_i, and after the thus obtained pre-exponential factors were normalized to obtain their relative amplitude *i*. Equation 2.10 was used to calculate the intensity weighted fluorescence lifetime, $\langle\tau\rangle$:

$$\langle\tau\rangle = \frac{\sum \alpha_i \tau_i^2}{\sum \alpha_i \tau_i} \quad \text{Equation 2.10}$$

and Equation 2.11 was used to compute the amplitude-weighted mean fluorescence lifetime, $\bar{\tau}$ or τ bar:

$$\bar{\tau} = \sum_{i=1}^{n} \alpha_i \tau_i \quad \text{Equation 2.11}$$

The criteria for good quality of the fitting were the reduced global χ^2 close to 1 and the random distributions of weighted residuals and of residuals autocorrelation (Bento-Oliveira *et al.* 2020). Time-dependent fluorescence intensity and anisotropy measurements of the probe used shown fluorescence decay curves which can best be fit by three exponential functions.

2.11.Statistical Analysis

The results are presented as mean standard deviation (S.D.), unless stated otherwise, and the sample dimension and number of biologically independent replicates are given with the results. The statistical significance was determined using Student's t-test or ANOVA (Analysis of Variance), depending on the number of independent treatments, also known as the samples. Mean values were considered significantly different for *p*-values below or equal to 0.05.

Chapter 3. Results

3.1. *S. cerevisiae sur2*Δ cells growth profile

Analysing the growth curve allows for the evaluation of cell culture development. Once this curve is established for a specific strain under defined conditions, it becomes possible to predict the ideal culture density before transferring it to a new medium. The growth curve of *S. cerevisiae sur2*Δ cells in YPD liquid medium was read in a microplate reader. Figure 3.1 represents the growth curve of the *sur2*Δ cells for 24 hours, in which each dot represents the average absorbance at a certain growth time. The curve showed the usual behaviour comprising a lag phase of ~ 1.40 hours, with similar duration for the 8 replicates tested, followed by an exponential phase of growth.

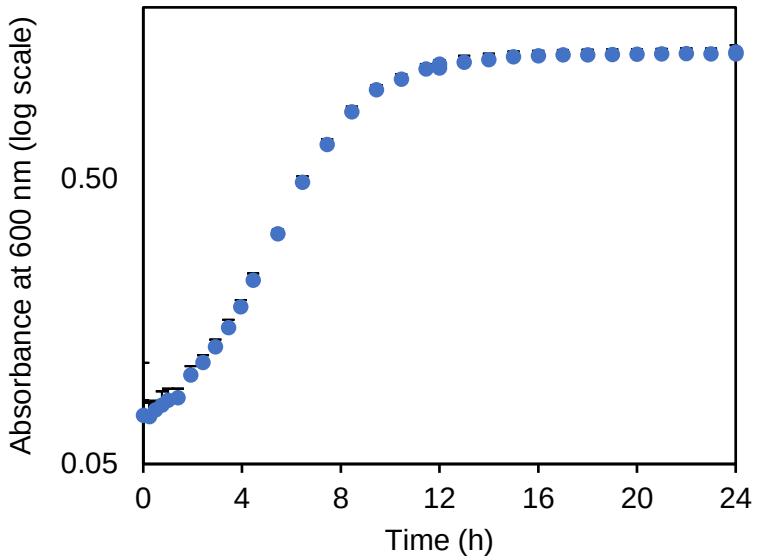

Figure 3.1. *S. cerevisiae sur2*Δ cells growth curve throughout 24 hours, in YPD medium. The cells were inoculated at an initial absorbance of 0.05 at 600 nm A600 (1 $A_{600} \approx 4 \times \mathbf{10^7}$ cells/ mL) and grown at 30° C with an agitation of 160 rpm. Their growth was monitored by measuring its absorbance at 600 nm at short time intervals. The values correspond to the average of 8 biological replicates, standard deviation ± 0.041.

In Table 3.1, the values of growth rate and generation or doubling time for each strain are presented. The growth rate is slower in the *sur2*Δ strains than in the other two strains *wt* and *ipt1*Δ. On the other hand, *sur2*Δ cells present the highest doubling time. The values of the *wt* and *ipt1*Δ strains were used merely for comparison purposes.

Table 3.1. Cell growth parameters obtained from the exponential phase of growth curves for the *wt, ipt1*Δ and *sur2*Δ strains in YPD culture media. The values of *sur2*Δ presented represent the mean ± standard deviation from 8 biological replicates.

	$\boldsymbol{\mu\ (h^{-1})}$	$\boldsymbol{t_g\ (h)}$
***wt* strain in YPD** [(a)]	0.469 ± 0.001	1.478 ± 0.003
***ipt1*Δ strain in YPD** [(a)]	0.446 ± 0.011	1.557 ± 0.040
***sur2*Δ strain in YPD**	0.340 ± 0.007	2.037 ± 0.041

(a) Obtained by (Antunes 2013).

3.2. Cell viability in yeast cells was not affected by DPH and its derivatives

Five *S. cerevisiae* cells strains (*wt*, *ipt1*△, *scs7*△, *sur2*△ and *erg6*△) were incubated with fluorescent probes, namely DPH, TMA-DPH and PA-DPH. These yeast cell strains present single deletion mutations either in the sphingolipid or the sterol biosynthetic pathways. Six samples were prepared to test the cellular viability of each strain, with the following components:

1) Control: the yeast cell suspension;
2) MeOH: the yeast cell suspension and the solvent of the respective probe (in this case, methanol) with the same volume as the probe solution;
3) EtOH: the yeast cell suspension and the solvent of the respective probe (in this case, ethanol) with the same volume as the probe solution;
4) DPH: the yeast cell suspension and 2 μM of DPH solution;
5) TMA-DPH: the yeast cell suspension and 2 μM of TMA-DPH solution;
6) PA-DPH: the yeast cell suspension and 2 μM of PA-DPH solution.

Cellular viability was assessed, using the trypan blue dye to colour dead cells selectively. The cells were incubated with the solvents at 24 ºC for 20 minutes, for a control test. In the presence of organic solvents such as methanol and ethanol, every cell strain tested also has a cell viability above 99.0%, meaning that the solvents in which the probes are dissolved do not compromise the cellular viability.

The cells were then incubated with the fluorescent probes at 24 ºC for 20 minutes. The viability of yeast cells remained consistently above 99.0% across all tested strains, as shown in Figure 3.2. The use of DPH or its derivatives did not impose any notable cytotoxic effects on yeast cells, suggesting their suitability for further experimental investigations without compromising cellular viability. Moreover, the average concentration of viable cells per mL of the 30 samples used in this experiment was $4.0 \times 10^7 \pm 0.4 \times 10^7$.

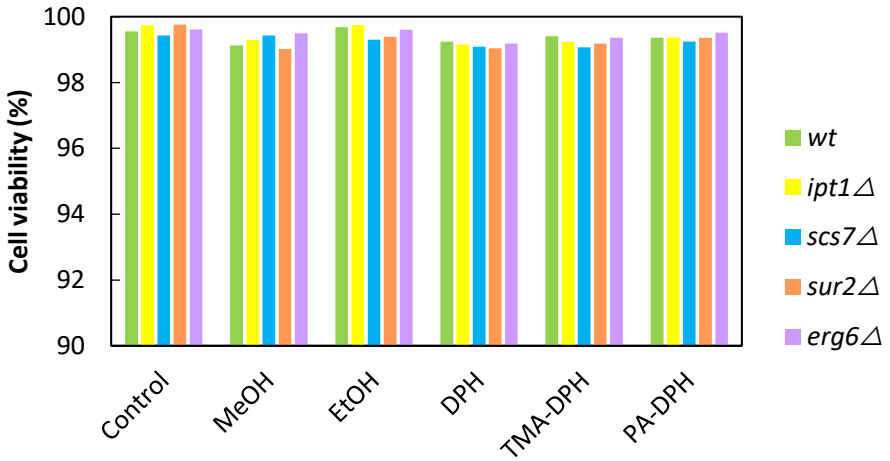

Figure 3.2. The presence of DPH and its derivatives did not show any adverse effects on cell viability in *wt* strains and mutated *S. cerevisiae* cells strains, in YPD medium at 24 ºC. The cell viability was assessed using the trypan blue cell viability method.

3.3. Intracellular location of the probes in *wt S. cerevisiae* cells

The probes distribution in *wt* cells yeast cells was assessed qualitatively, by widefield florescence microscopy after 20 min of incubation. Figures 3.3 shows that the DPH fluorescence signal is emitted from both the plasma membrane and from the inner membranes of the cell. Also, the neck of the budding yeast appears to emit more signal, probably because the plasma membranes of both cells are overlapped. On the other hand, TMA-DPH and PA-DPH seem to emit signal mainly from the plasma membrane of the cells. The fluorescent microscope images have to be interpreted taking in account that *S. cerevisiae* yeast cells have autofluorescence, which primarily correlates with the presence of tryptophan, pyridoxine, flavins, and NAD(P)H (Maslanka *et al.* 2018).

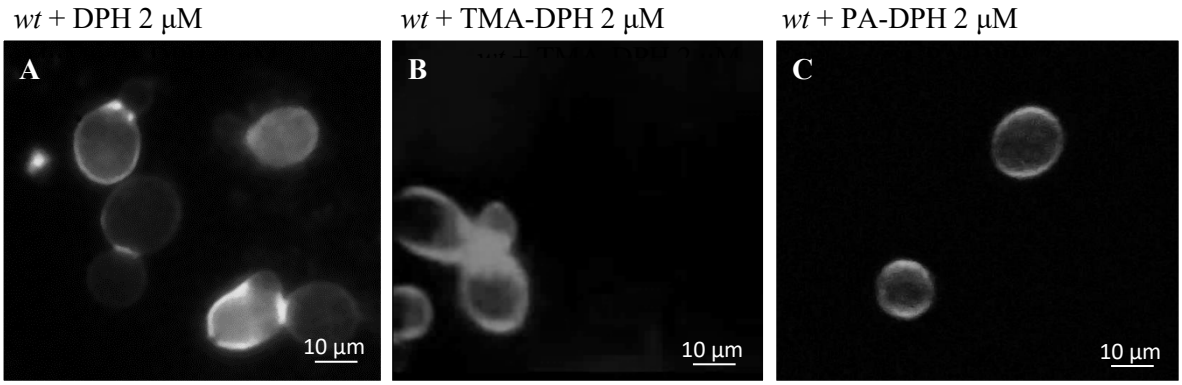

Figure 3.3. Fluorescence imaging of *wt* cells labelled with the probes DPH (A), TMA-DPH (B) and PA-DPH (C) after 20 minutes of incubation time, using a wide-field fluorescence microscope. Magnification 1000X. The images were obtained with IC Capture 2.4 software and analysed in ImageJ software.

3.4. Determination of the molar absorption coefficient of fluorescent probes

The molar absorption coefficients of the fluorescent probes DPH and TMA-DPH had been previously determined, being $\varepsilon^{350\,nm}_{methanol}$= 88000 M^{-1} cm^{-1} for DPH (Bento-Oliveira *et al.* 2020), DPH, $\varepsilon^{352\,nm}_{ethanol}$= 84800 M^{-1} cm^{-1} (Pathak and London 2011), TMA-DPH, $\varepsilon^{354\,nm}_{methanol}$= 53000 M^{-1} cm^{-1} (Cundall *et al.* 1979). However, the value for TMA-DPH dissolved in ethanol and PA-DPH dissolved in either methanol or ethanol is absent in the literature. For this reason, the molar absorption coefficient of these fluorescent probes was determined. The coefficient was also determined for the DPH to ensure that the protocol followed was adequate and optimized with a sample with a known molar absorption coefficient value.

Throughout this experiment, there was a difficulty in dissolving the crystals of DPH and its derivatives in methanol or ethanol. This might happen because the stock concentrations at ≥ 200 µM may surpass its solubility limit. It was observed that the crystals with be more dissolved (not totally), if it was employed an ultrasonic bath to treat the samples at a temperature of 24 ºC for 15 minutes. Regarding DPH and TMA-DPH, it was found that their solubility was higher in ethanol than in methanol. The PA-DPH probe presents very limited solubility in ethanol or in methanol.

First, the molar absorption coefficient of DPH was determined, in order to check if the literature values could be reproduced (Figure 3.4 and Table 3.2). The value determined for DPH was indeed similar to the value found in the literature, in the same solvent – ethanol – at the same wavelength of 354 nm. The molar absorption coefficients were calculated by the Lambert-Beer Law (Figure 3.4).

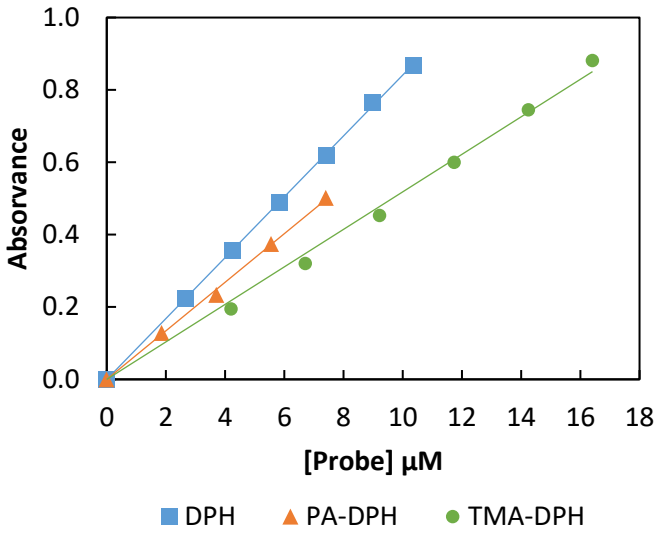

Figure 3.4. Determination of the molar absorption coefficients (ε) of DPH. TMA-DPH and PA-DPH in different solvents. The absorbance of the fluorescence probes solutions at different concentrations were measured and ε values were determined through the Beer-Lambert law.

Table 3.2. Molar absorption values of DPH and its derivatives dissolved in different solvents.

Probe	ε literature (M^{-1} cm^{-1})	ε exp (M^{-1} cm^{-1})	R^2
DPH (in methanol)	88000 at 350 nm [b]	-	-
DPH (in ethanol)	84800 at 352 nm [c]	84102 (ethanol at 352 nm)	0.9999
TMA-DPH (in metanol)	53000 at 355 nm [d]	-	-
TMA-DPH (in etanol)	-	51823 (ethanol at 354 nm)	0.9975
PA-DPH (in metanol)	-	66446 (methanol at 355 nm)	0.9994

(b) Obtained by (Bento-Oliveira *et al.* 2020)
(c) Obtained by (Pathak and London 2011)
(d) Obtained by (Cundall *et al.* 1979).

3.5. Characterization of the plasma membrane of *wt* and *sur2*Δ *S. cerevisiae* cells using DPH, TMA-DPH and PA-DPH

The research presented in this topic delves into the insights that three distinct fluorescent probes, DPH, TMA-DPH, and PA-DPH bring on the biophysical properties of the plasma membrane of two *S. cerevisiae* strains: *wt* and the *sur2*Δ. By exploring the fluorescence properties of these probes, the complex behaviour of yeast plasma membranes can, in principle, be unravelled, since it is expected that different regions of the plasma membrane are differentially labelled by each probe, as a consequence of their characteristics. This section of the results will be focused on the comparison of the behaviour of the different probes, regardless of the yeast cell strain. A comparison of the biophysical properties of *wt* versus *sur2*Δ will be carried out in section 3.6.

3.5.1. Excitation and emission spectras of DPH and its derivatives

The fluorescence excitation spectra of DPH and its derivatives have a very intense band where three vibronic transitions at 345, 360 (absolute maximum) and 380 nm can be distinguished. On the other hand, the fluorescence emission band of DPH and its derivatives has also a clear vibronic progression with peaks at 408, 430 (absolute maximum) and 454 nm; however, the emission spectrum of TMA-DPH presents a different behaviour from the other spectra presented in Figure 3.5, especially in *sur2*Δ cells where its maximum is red-shifted to 460 nm.

There is a study in which the authors determined the excitation and emission spectra for a DPH/ ethanol solution dissolved in dimethyl sulfoxide (DMSO). The excitation and emission spectra showed an intense band with three vibronic transitions at approximately ~340, 351 and 375 nm, and ~402, 425 and 450 nm, respectively (Gracetto *et al.* 2010). For both spectras, the wavelengths of the three vibronic transitions are very similar comparing the results of the experiment in this project with the results in the literature, despite the probe being dissolved in DMSO and not in a yeast solution.

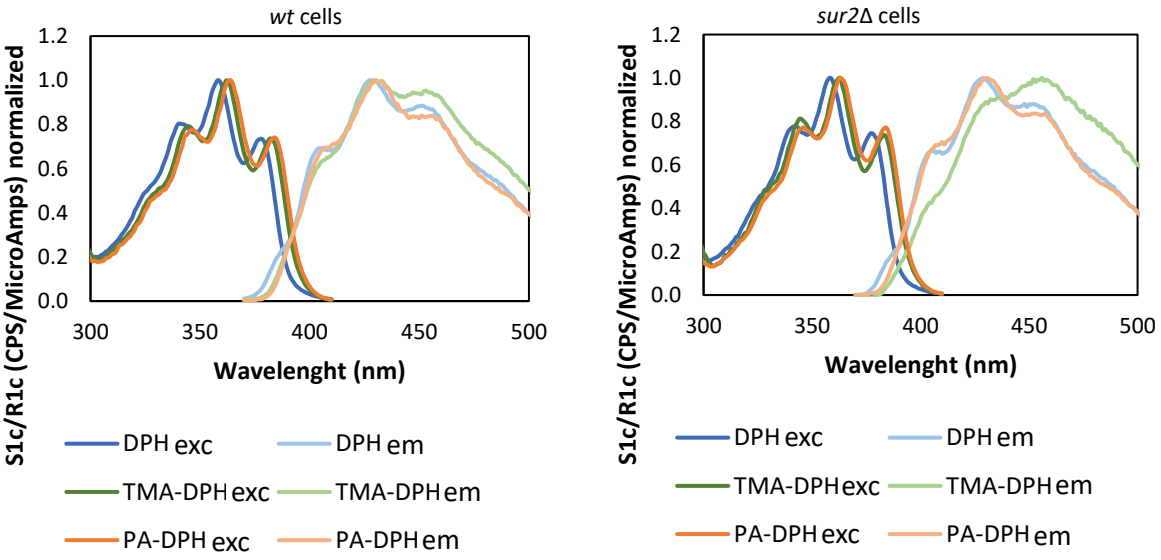

Figure 3.5. Representation of normalized excitation (exc) (λexc = 350 nm) and emission (em) (λem = 430 nm) spectra of DPH and its derivatives in *wt* (left) and *sur2*Δ (right) *S. cerevisiae* cell suspensions at 24 ºC. The represented spectra are the mean of at least three independent experiments. S1c, corrected signal. R1c, corrected noise. CPS, counts per second.

3.5.2. Steady-state fluorescence anisotropy

Fluorescence anisotropy provides information on the molecular rotation, size, shape, and flexibility of a fluorescent probe. The anisotropy values can translate the fluidity or rigidity of the plasma membrane of the yeast cells. Comparing the anisotropy associated with the fluorescent probes DPH, TMA-DPH and PA-DPH can highlight the differential labelling of the fungal membranes, since each probe presents different charge.

The DPH probe presents significantly lower values of anisotropy compared to TMA-DPH and PA-DPH (Figure 3.6), which can be explained by DPH being located deep in the membrane and there may be a gradual increase in the disorder of the chains from the interfacial region (where the charged DPHs fluorophore will be located) until membrane/water to the center of the bilayer (where the DPH fluorophore will be). The probes show this behaviour both in *wt* and *sur2*Δ *S. cerevisiae* cells.

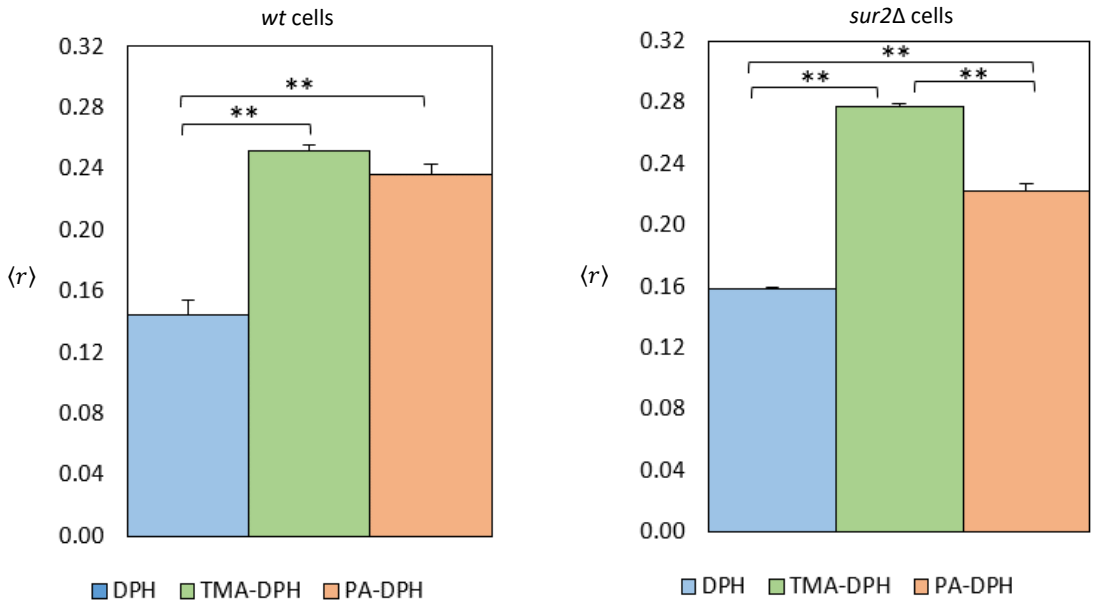

Figure 3.6. Steady-state anisotropy ($\langle r \rangle$) measurements of DPH and its derivatives in *wt* (left) and *sur2*Δ (right) yeast cells, after 20 minutes of incubation. The values are the mean ± S.D. of three biological replicates. **, $p < 0.01$.

Table 3.3 comprises the steady-state anisotropy values of DPH and its derivatives labelling *wt* and *sur2*Δ *S. cerevisiae* cells in mid exponential phase. It is important to highlight that the values presented in this table were obtained both in this work, which are the ones for cells grown in YPD liquid medium; or literature values for cells grown either in Synthetic Complete (SC) medium containing 6.8% (w/v) yeast nitrogen base, 2% (w/v) glucose, and the aminoacids as indicated in (Branco *et al.* 2004) or in Rich Medium (1% yeast extract, 2% peptone, 2% glucose, and 40 mg/l uracil and adenine). Despise the different culture media, the average steady-state anisotropy of DPH in *wt* cells is similar to the reference value (~ 0.15). In Rich Medium the values present some differences compared with the YPD medium values. The average anisotropy values of TMA-DPH in *wt* and *sur2* mutated cells are 0.25 and 0.28, respectively, in YPD medium. However, in Rich Medium the average anisotropy values of TMA-DPH in *wt* and *sur2* mutated cells are 0.28 and 0.27, respectively.

Table 3.3. Steady-state anisotropy (mean +/- standard deviation) and *p*-values of the probes in *wt* and *sur2*Δ yeast cells after 20 minutes of incubation time.

Cell strain and its culture medium	Fluorescent probe	⟨r⟩	*p*-value
***wt* (in YPD)**	DPH	0.145 ± 0.009	1.40×10^{-5}
	TMA-DPH	0.252 ± 0.004	
	PA-DPH	0.236 ± 0.006	
***wt* (in SC)**	DPH	~ 0.145[(e)]	-
***wt* (in Rich Medium)**	TMA-DPH	0.283 ± 0.004[(f)]	-
***sur2*Δ (in YPD)**	DPH	0.159 ± 0.001	1.46×10^{-7}
	TMA-DPH	0.277 ± 0.002	
	PA-DPH	0.222 ± 0.005	
***sur2*Δ (in Rich Medium)**	TMA-DPH	0.270 ± 0.015[(f)]	-

(e) The reference anisotropy values were obtained by (Aresta-Branco *et al.* 2011).
(f) The reference anisotropy values were obtained by (Heese-Peck *et al.* 2002).

3.5.3. Steady-state fluorescence anisotropy kinetics

In order to evaluate how the fluorescent probes spread through the membranes over a period of incubation time, anisotropy measurements over incubation time were performed with two *S. cerevisiae* strains: *wt* and *sur2*Δ. The fluorescence intensity was also tracked over time, to monitor the probe incorporation in the cells. This method also elucidates on the proper incubation time for each probe.

In *wt* cells, the value of the DPH anisotropy increases from 0.11 to 0.13 in the first 2 minutes of incubation time and remains significantly stable throughout 40 minutes. This behaviour corroborates that for DPH a fast distribution among the plasma membrane and inner membranes occurs. In fact, the value of DPH anisotropy is 0.145 in intact cells and 0.22 in isolated plasma membrane in SC medium (Bento-Oliveira *et al.* 2020), which indicates that the more disordered inner membranes contribute to the lower values observed in intact cells. However, the DPH derivatives started at very different anisotropy values, and after ≈ 25 minutes the anisotropy values become very similar, around 0.25 (Figure 3.7). DPH derivatives seem to concentrate at the plasma membrane due to their charge that anchors the probe at the membrane/water interfacial region. Also, the derivatives label different membrane domains at short times.

On the other hand, in *sur2*Δ cells, DPH anisotropy remains fairly constant throughout the 20 minutes of measurement, which is similar to the behaviour in *wt* cells. In *sur2* mutated cells, the PA-DPH probe has an initial anisotropy value of 0.22, at 20 minutes of incubation time the anisotropy has increased to 0.24 and remains around this value until a 40 minutes incubation time is reached. For TMA-DPH, the initial fluorescence anisotropy value is 0.28, decreases to 0.26 at 20 minutes of incubation and by the end of the experiment, at 40 minutes of incubation, the anisotropy returns to a value of ~0.28. This was observed in 2 individual replicates. The behaviour of the probes is different between the two strain of *S. cerevisiae* cells, since the anisotropy of the DPH derivatives do not have a tendency to reach the same values after a certain amount of time in *sur2*Δ cells as it happens in *wt* cells.

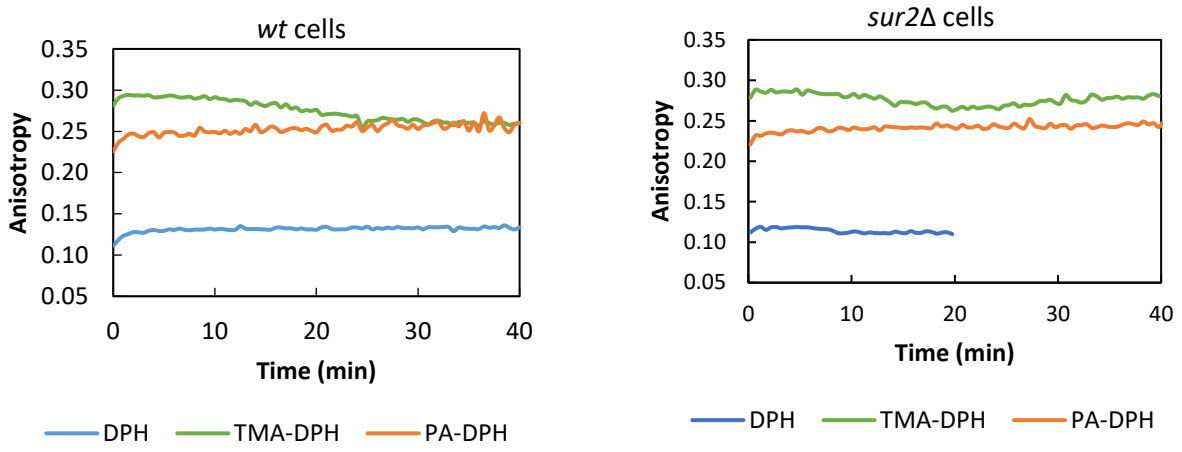

Figure 3.7. Anisotropy kinetics curves throughout the incorporation of the probes in the *wt* (left) and *sur2*Δ (right) *S. cerevisiae* cells, for 40 minutes. The values are the mean ± S.D. of three and two biological replicates for *wt* and *sur2*Δ cells, respectively. **, $p < 0.01$.

Table 3.4 condenses and highlights the kinetic anisotropy values - from Figure 3.7 - of the fluorescent probes at specific incubation times: 2, 5, 10, 20, 30 and minutes, in both *S. cerevisiae* strains. It also contains the average anisotropy values and their respective standard deviation. The Tukey HSD test was applied to the data in Table 2 for multiple comparison tests to identify which of the pairs of treatments are significantly different from each other. The pairs of treatment chosen for each cell strain were: i) DPH against TMA-DPH; ii) TMA-DPH against PA-DPH; iii) and DPH against PA-DPH. The *p*-value corresponding to the F-statistics of one-way ANOVA is lower than 0.01 in every pair, which strongly suggests that one or more pairs of treatments are significantly different.

Table 3.4. Statistical analysis of the anisotropy values of the fluorescent probes incorporated in the *S. cerevisiae* cells at certain time points. The values are the mean ± S.D. of three and two biological replicates for *wt* and *sur2*Δ cells, respectively. **, $p < 0.01$.

Time(min)	*wt* cells				*sur2*Δ cells			
	DPH	TMA-DPH	PA-DPH	Total	DPH	TMA-DPH	PA-DPH	Total
2	0.128	0.293	0.247		0.118	0.288	0.235	
5	0.129	0.292	0.248		0.118	0.282	0.237	
10	0.131	0.291	0.249		0.113	0.283	0.242	
20	0.131	0.276	0.249		0.111	0.273	0.241	
30	0.133	0.264	0.252		0.110	0.262	0.242	
40	0.134	0.260	0.260		-	-	-	
Mean	0.131	0.280	0.251	0.221	0.114	0.278	0.240	0.211
Standard deviation of the mean	0.001	0.006	0.002	0.016	0.002	0.005	0.001	0.019
p-value	4.67×10^{-14}				1.17×10^{-13}			

3.5.4. Steady-state fluorescence intensity kinetics

The fluorescence intensity associated with the previous kinetic anisotropy measurements in section 3.5.3. was calculated and it is shown in Figure 3.8. The incorporation of DPH in *S. cerevisiae* membranes stabilizes after 5 minutes in *wt* cells and 15 minutes in *sur2* mutated cells, which is shown in the graphic where the total intensity increases drastically in the beginning of the incubation time and stabilizes after that period of time.

The behaviour of TMA-DPH is different from DPH because the total intensity values remain constant throughout the 20 minutes of incubation, for both yeast cell strains. This observation could mean that the probe incorporates in the cell membranes rapidly, first in the gel-like domains due to its positive charge and then in more disordered domains. The effect on the fluorescence intensity of probe incorporation in less rigid domains would be compensated with a more extensive global membrane incorporation. Notably, this interpretation is consistent with the fluorescence anisotropy trend over time.

The probe PA-DPH total intensity decreases significantly from the starting point until the 20 minutes of incubation. This negative charged probe requires further studies and more complementary experiments in order to understand its behaviour in the *S. cerevisiae* cell membranes. We will explore two non-mutually exclusive hypotheses, a self-quenching mechanism and no alteration of the probe ionization state upon membrane incorporation leading to a probe redistribution.

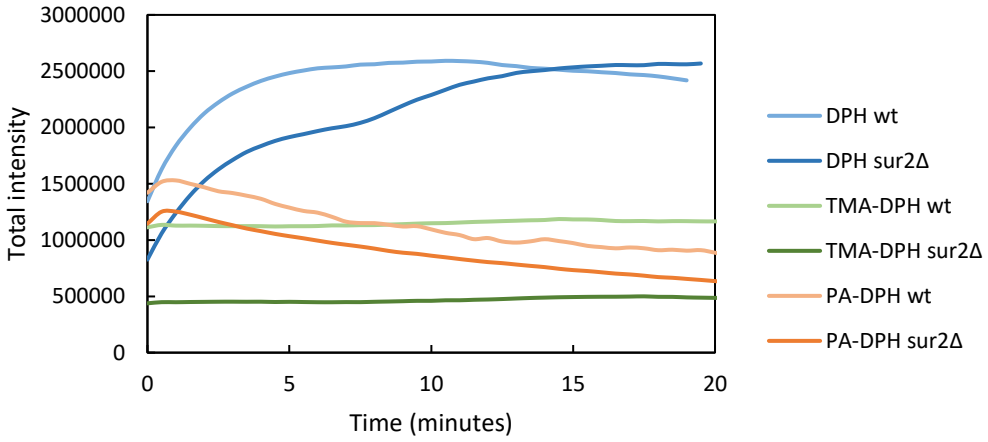

Figure 3.8. Total intensity kinetics curves throughout the incorporation of the probes in the *wt* and *sur2*Δ *S. cerevisiae* cells, for 20 minutes. The values are the mean ± S.D. of three and two biological replicates for *wt* and *sur2*Δ cells, respectively.

3.5.5. Fluorescence intensity decays

The fluorescence intensity decays were measured in *wt S. cerevisiae* living cells suspensions labelled with DPH, TMA-DPH and PA-DPH probes at a temperature of 24 °C. In Figure 3.9, a fluorescence intensity decay of DPH is represented. These decays did not require global analysis since the excitation was performed at 370 nm, significantly distant from the excitation wavelength of proteins and sterols. The decay of the three probes are described by three exponentials. DPH exhibits a shorter lifetime of approximately 1.5 ± 0.3 ns and a longer lifetime of around 9.2 ± 0.2 ns. The fluorescence intensity decays of DPH in cell membranes are described by a lifetime of ~8-12 ns, where the upper limit of this range will be associated with a gel phase. The TMA-DPH decay reveals a shorter lifetime of approximately 1.7 ± 0.1 ns, while the other component exhibits a longer lifetime of around 16.5 ± 0.7 ns. The probe PA-DPH decay exhibits a shorter lifetime of approximately 1.3 ± 0.1 ns, alongside another

component demonstrating a longer lifetime of around 6.5 ± 0.2 ns. The short component is similar for the three probes, however, the long component is clearly distinct in all three. Each fluorescent probe presents a characteristic lifetime, however, PA-DPH shows lower values of count number after 26 ns than the other probes (Figure 3.9A).

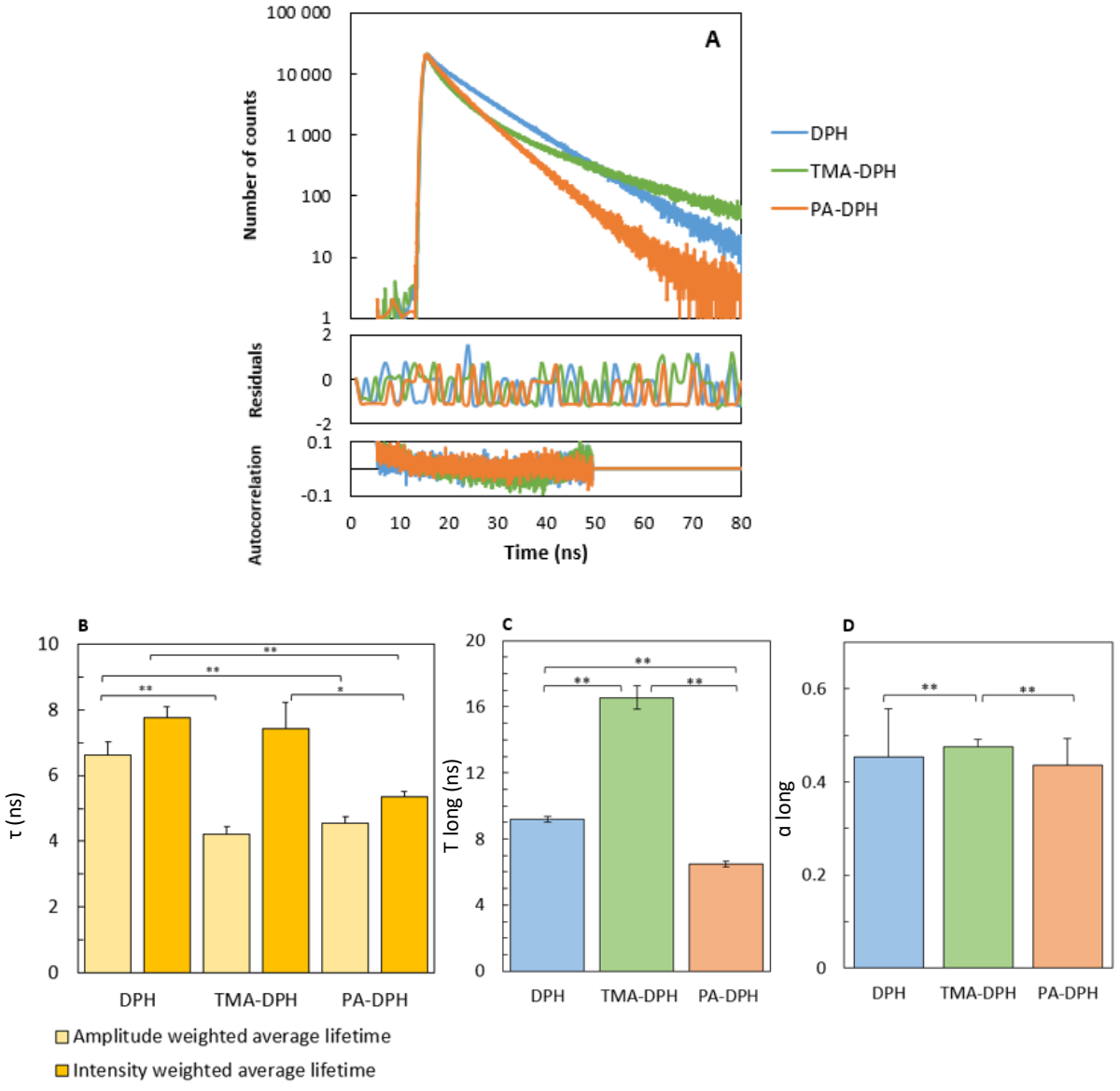

Figure 3.9. Fluorescence lifetime components obtained from *wt S. cerevisiae* living cells labelled with DPH, TMA-DPH and PA-DPH probes, incubated for 20 minutes. Decay of DPH fluorescence intensity, residuals of the fit and the autocorrelation of the residuals are also shown (A), amplitude and intensity weighted average lifetime (B), lifetime of the long component (C), amplitude of the long component (D). The fit of the decay of fluorescence intensity was carried out with a 3 exponential function for the DPH probe and its derivatives. The values are the mean ± S.D. of three biological replicates. *, $p<0.05$ **, $p < 0.01$.

3.5.6. Fluorescence lifetimes associated with each probe did not vary with incubation time

Time-resolved fluorescence spectroscopy was used to measure the lifetimes of the fluorescent probes DPH, TMA-DPH and PA-DPH labelling *wt* yeast cells. Measurements were taken at different incubation times: 5, 15 and 30 minutes. The fluorescence lifetime values remain unchanged throughout the incubation times of the probes, which suggest that the probe itself primarily defines the observed lifetime values, rather than the incubation time (as represented in Figure 3.10).

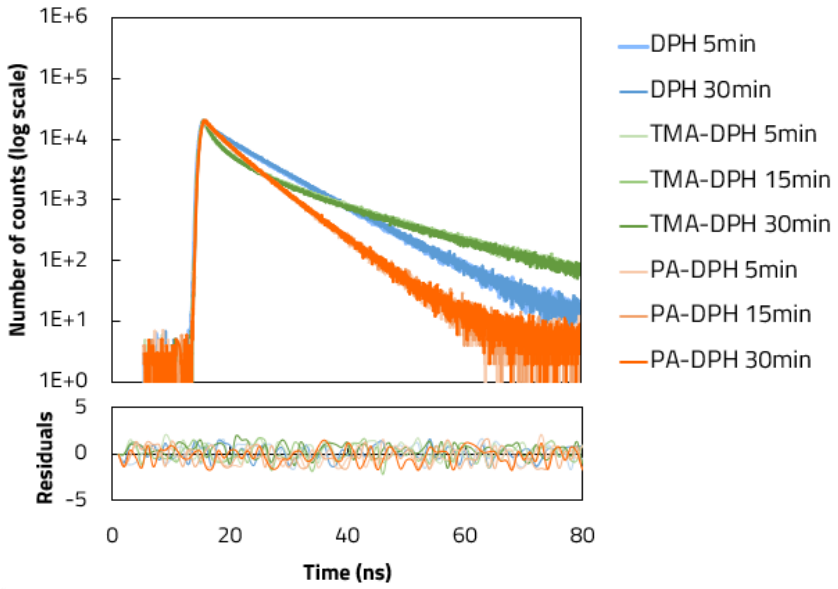

Figure 3.10. Fluorescence intensity decay curve of the fluorescent probes labelling *wt S. cerevisiae* cells at different incubation times. The decay curves shown were fitted to three exponentials decay.

3.6. Biophysical impact of sphingolipid and ergosterol profile in *S. cerevisiae* cells

The biophysical properties of cellular membranes play a pivotal role in various physiological processes, as detailed in Chapter 1, and their integrity is contingent upon the intertwined sphingolipid and ergosterol synthesis. The focus of this topic is the biophysical impact of mutations affecting these critical pathways in *S. cerevisiae* cells. Specifically, the consequences of mutations affecting sphingolipid and ergosterol synthesis, with particular attention on three key mutations: *sur2*Δ, *scs7*Δ and *erg6*Δ, were investigated. The fluorescent probes used were, again, DPH, TMA-DPH, PA-DPH and, additionally, *t*-PNA.

3.6.1. Global order of cell membranes and SLEDs characterization in *S. cerevisiae*

Considering that a substantial portion of the plasma membrane surface contains proteins proposed to be localized in rafts, we opted to evaluate the plasma membrane fluorescence anisotropy using DPH and its derivatives, and *t*-PNA as our chosen fluorescent probes. Initially, *t*-PnA was only chosen for fluorescence intensity decay measurements (see section 3.5.2) since it is as a distinctive marker for gel domains, however, it would also be interesting to evaluate the anisotropy values on *S. cerevisiae cells* and what information it gives for the global order of the plasma membrane. As explained previously, these fluorescent probes can be inserted into the yeast plasma membrane, and their steady-state fluorescence anisotropy values serve as indicators of membrane rigidity and lipid order. The mutant *sur2*Δ cells were examined to assess the impact that the C4 hydroxylation at the sphingoid base might have in the plasma membrane biophysical properties.

The anisotropy of DPH, TMA-DPH and *t*-PnA is similar for both *wt* and *sur2*Δ cells (as depicted in Figure 3.11), which suggests that the hidroxilation in C4 of the sphingoid base catalysed by the *SUR2* gene product does not change significantly the global order of the plasma membrane of *S. cerevisiae* cells. However, with the exception of PA-DPH, in *sur2*Δ there is a slight increase in anisotropy compared to *wt* cells, which corresponds to a lower membrane fluidity.

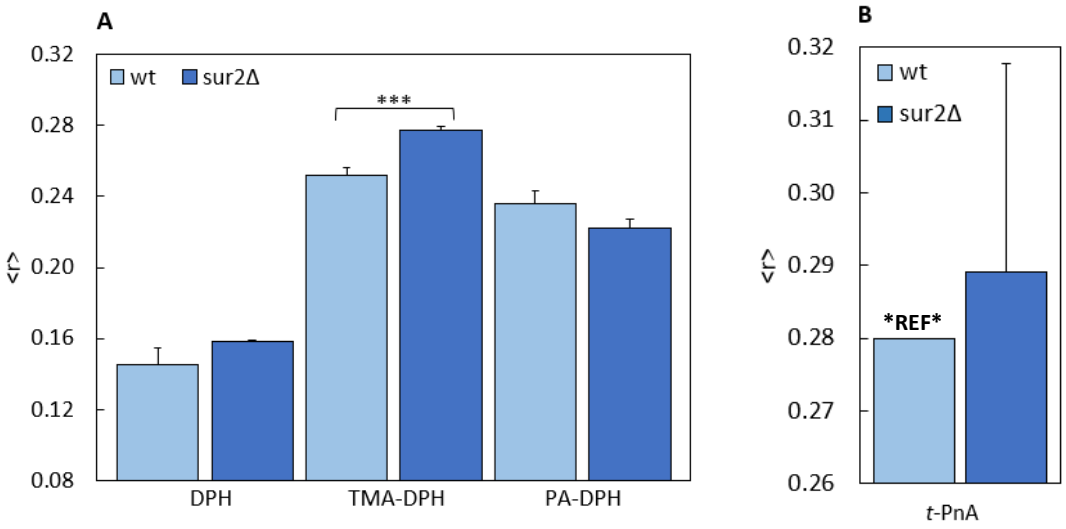

Figure 3.11. Order of the membranes of *S. cerevisiae* in *wt* (light blue) and in *sur2*Δ (blue) whole cells. The steady-state anisotropy values were obtained for DPH, TMA-DPH, PA-DPH (A) and for t-PnA (B), at 24 ºC in mid-exponential phase. The reference (REF) anisotropy value of t-PnA in *wt* cells was obtained by (Aresta-Branco *et al.* 2011). The values are the mean ± S.D. of three biological replicates. ***, $p<0.005$.

Table 3.5 comprises the steady-state anisotropy values of the DPH probe and its derivatives incubated in *wt*, *sur2*Δ, *scs7*Δ and *erg6*Δ *S. cerevisiae* cells, in mid exponential phase of the cells. It is important to highlight that this table presents both values reproduced in this project, which are yeast cells that were grown in YPD liquid medium; and also reference anisotropy values from cells that were grown in SC medium. For more information about the SC medium or the experimental procedure of that experiment, it is highly suggest to read the article from Aresta-Branco *et al.* 2011. The reference values were chosen to compare the steady-state anisotropy differences between the different mutations both in sphingolipid and ergosterol pathways.

Table 3.5. Steady-state anisotropy of the fluorescent probes in *wt*, *sur2*Δ, *scs7*Δ and *erg6*Δ yeast cells. The values are the mean ± S.D. of three biological replicates.

Fluorescent probe	Culture media	*wt*	*sur2*Δ	*erg6*Δ	*scs7*Δ
DPH	YPD	0.145 ± 0.009	0.159 ± 0.001	-	-
	SC	~ 0.145 (e)	-	~ 0.155 (e)	~ 0.165 (e)
TMA-DPH	YPD	0.252 ± 0.004	0.277 ± 0.002	-	-
	SC	0.283 ± 0.004 (g)	-	0.272 ± 0.007 (g)	-
	Rich Medium	~0.283 (f)	~0.270 (f)	-	-
PA-DPH	YPD	0.236 ± 0.006	0.222 ± 0.005	-	-
t-PnA	YPD	-	0.289 ± 0.029	-	-
	SC	~ 0.280 (e)	-	-	-

(e) Values obtained by (Aresta-Branco *et al.* 2011).
(f) Values obtained by (Heese-Peck *et al.* 2002).
(g) Values by (Abe and Hiraki 2009).

3.6.2. Characterization of gel and fluid domains

To discern the nature of gel and fluid domains within the membrane, it was measured time-resolved lifetime decay with the goal to unveil the presence or absence of gel domains based on a crucial parameter: long lifetime decay. When this component exceeds the 30 nanosecond threshold in *t*-PnA, it signals the existence of gel domains within the membrane (Aresta-Branco *et al.* 2011). Thus, this investigation centers on different fluorescence lifetime measurements, offering insights into the membrane structural intricacies and unraveling the interplay between gel and fluid domains within the plasma membranes of *wt* and *sur2*Δ *S. cerevisiae* cells.

Figure 3.12D depicts the fluorescence intensity decay of *t*-PnA in *sur2*Δ *S. cerevisiae* cells, along with the resulting curve from a global analysis involving the linkage of the lifetime of all components except the longest one. The fluorescence intensity decays obtained in the presence of *t*-PnA are described by the sum of five exponentials, while the decays in the sample without probe, here treated not as a background, but as cell auto-fluorescence are described by four exponentials. Therefore, the application of global analysis was necessary to eliminate the contribution of fluorescent proteins and sterols emissions in the different components of the *t*-PnA fluorescence decay (Mukhopadhyay *et al.* 2002). In the case of *sur2*Δ cells labelled with *t*-PnA probe, the long lifetime component measured was 44.3 ± 0.6 ns (Figure 3.12F). Thus, the long lifetime component in *sur2*Δ labelled with *t*-PnA clearly surpasses the 30 nanoseconds, demonstrating the presence of gel domains within the membrane. Thus the hydroxylation at the C-4 of the sphingoid base is not required for the formation of SLEDs. In fact, the long component lifetime in *sur2*Δ cells is significantly longer than in *wt* cells that measures 40.9 ± 0.4 ns in YPD as reported in a previous work (Bento-Oliveira *et al.* 2020) and it is also longer than in other mutant cells represented in Table 3.6, such as *ipt1*Δ and *erg6*Δ *S. cerevisiae* cells. The absence of the C4-OH in the sphingoid base thus leads to the formation of more rigid gel domains, as was previously

observed for cells lacking the C2-OH in the acyl chain of sphingolipids, and its impact is more noticeable than the absence of $M(IP)_2C$/accumulation of MIPC instead (*ipt1*Δ cells).

The lifetime components of *S. cerevisiae* cells labelled with DPH and PA-DPH, represented in Figure 3.12E, show values in *sur2*Δ cells that are either not significantly different or shorter than in *wt* cells. On the other hand, TMA-DPH presents a longer intensity weighted average lifetime in *sur2*Δ cells of 10.1 ± 0.5 ns than in *wt* cells is (7.4 ± 0.8 ns). This result suggests a preferential labelling of SLEDs by TMA-DPH, as a similar trend was observed in the fluorescence lifetime of *t*-PnA,

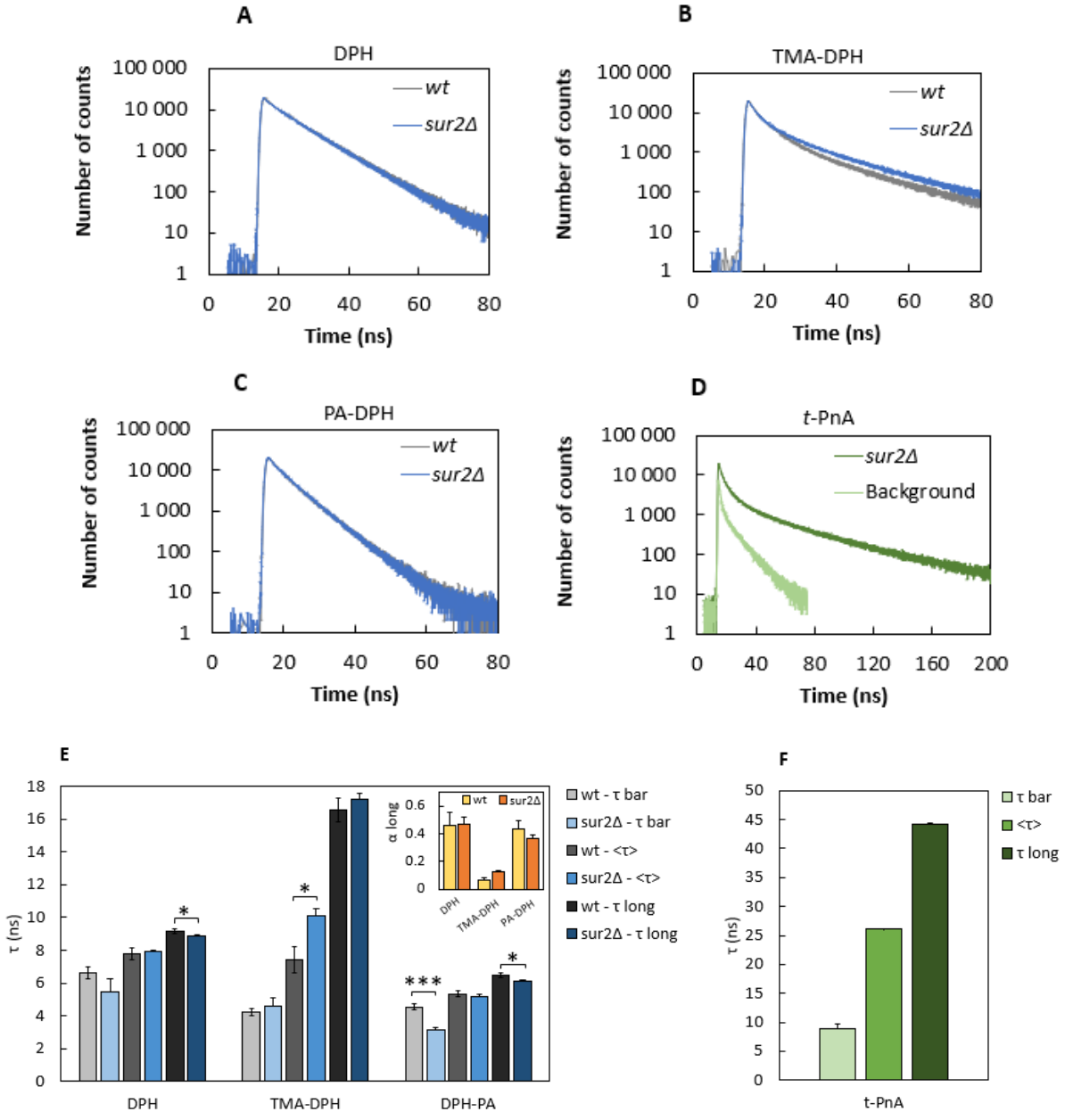

Figure 3.12. Time-resolved fluorescence lifetime decay measurements in *S. cerevisiae* cells labelled with fluorescent probes. Analysis of the fluorescence intensity decay of DPH, TMA-DPH and PA-DPH in *wt* and *sur2*Δ yeast cells, 20 minutes of incubation (A, B, C). Global analysis of the fluorescence intensity decay of *t*-PnA in the plasma membrane of *sur2*Δ cells, 5 minutes of incubation (D). Amplitude ($\bar{\tau}$) and intensity weighted average lifetime ($\langle\tau\rangle$), lifetime of the long component (τ_{long}) and amplitude of the long component (α long) (E, F). The graphics A, B, C and E represent both *wt* and *sur2*Δ cells; the graphics D and F represent just *sur2*Δ cells. The fit of the decay of fluorescence intensity was applied 3 exponentials for the DPH probe and its derivatives and 5 exponentials for the *t*-PnA probe. The values are the mean ± S.D. of three biological replicates. *, $p<0.05$ ***, $p < 0.001$.

Table 3.6. Fluorescence lifetime decay measurements of *t*-PnA in *S. cerevisiae* cells for the characterization of gel domains in *wt S. cerevisiae* cells and its deletion mutants *sur2*Δ, *scs7*Δ, *erg6*Δ and *ipt1*Δ. For the analysis, the decay measurements were fitted to five exponentials decay, except the auto-fluorescence decays which were fitted to four exponentials. The values are the mean ± S.D. of three biological replicates.

Cell strain	$\bar{\tau}$ (ns)	$\langle\tau\rangle$ *(ns)*	τ_{long} (ns)	α_{long}
wt (in YPD)	-	-	40.9 ± 0.4 [(b)]	-
wt (in SC)	-	~26 [*(e)*]	~41 [*(e)*]	~0.13 [*(e)*]
***sur2*Δ (in YPD)**	9.0 ± 0.8	26.0 ± 1.9	44.3 ± 0.6	0.10 ± 0.01
***scs7*Δ (in SC)**	-	~25 [*(e)*]	~46 [*(e)*]	~0.08 [*(e)*]
***erg6*Δ (in SC)**	-	~21 [*(e)*]	~41 [*(e)*]	~0.08 [*(e)*]
ipt1*Δ *(in YPD)	-	-	~43 [(b)]	-

(b) The reference anisotropy values were obtained by (Bento-Oliveira *et al.* 2020).
(e) The reference anisotropy values were obtained by (Aresta-Branco *et al.* 2011).

Chapter 4. Discussion

The cell membrane of fungi is a lipid bilayer enriched with several lipids, including sphingolipids that constitute around 30% of the phospholipids in the plasma membrane of the fungus *S. cerevisiae* (Patton and Lester 1991). This class of lipids is the object of interest in this project, given that sphingolipids can present different hydroxylations, either in the sphingoid group or in the acyl chain, which can influence certain biophysical properties and the organization of the plasma membrane (Marquês *et al.* 2018). It is hypothesized that the degree of hydroxylation has a major impact, namely on the stabilization of gel domains (SLEDs) that are present in the plasma membrane of fungi under physiological conditions, but not in mammals. Recent studies show that the highly rigid SLEDs found at the plasma membrane of fungi, such as *S. cerevisiae*, appear to be absent in mammalian cells, which qualifies as potential targets for antifungal drug therapies (Santos *et al.* 2020).

One of the goals of this dissertation was to study the influence of the charge of fluorescent membrane probes in the labelling of lipid domains of the *S. cerevisiae* plasma membrane. The plasma membrane was labelled with DPH and two DPH derivatives, namely the cationic TMA-DPH and the anionic PA-DPH, which have the potential to label different regions of the yeast plasma membrane as a consequence of their charge. It is reported that TMA-DPH is retained in the outer leaflet of the plasma membrane due to its positive charge (Chazotte 2011). On another hand, anionic PA-DPH is being used for the biophysical characterization of yeast plasma membrane for the first time and should behave distinctly from TMA-DPH, though it is expected to be also retained in the outer leaflet of the plasma membrane due to its charge.

The second goal was to identify the impact on the biophysical properties of the yeast plasma membrane of the sphingolipid hydroxylation pattern. The deletion of the genes *SUR2* and *SCS7* prevents the hydroxylation of the sphingolipid sphingoid base and acyl chain, respectively, *IPT1* gene deletion leads to the accumulation of the complex sphingolipid MIPC but averts the formation of $M(IP)_2Cs$ (Marquês *et al.* 2018), and lastly the gene deletion of *ERG6* prevents the formation of ergosterol since it accumulates zymosterol and colesta-5,7,24-trienol (Jordá and Puig 2020). The latter mutant strain has a different sterol profile but similar sphingolipid profile, when compared to the *wt*, and allows testing whether the biophysical changes observed in the other mutant are specifically due to alterations in sphingolipids or can be perceived just as a consequence of general changes in the plasma membrane lipid composition. Moreover, the long lifetime component of *t*-PnA fluorescence intensity decay was also determined in the previous yeast mutants, since this probe can serve as a fingerprint for gel domains, especially when it exceeds 30 nanoseconds (Bento-Oliveira *et al.* 2020). In this thesis, the parameters of *wt* and *sur2*Δ were evaluated, although they will later be compared with other mutant strains. The *sur2*Δ mutant strain can serve as a valuable tool for identifying genetically related genes encoding proteins whose functional properties are influenced by C4 hydroxylation at the sphingoid base (Haak *et al.* 1997). Additionally, the deletion of *SUR2* significantly enhances cells' resistance to the morpholine fungicide fenpropimorph, an inhibitor of several enzymes in the ergosterol synthesis pathway.

Before starting any of the experiments previously mentioned, the cell viability was assessed in *wt*, *sur2*Δ, *scs7*Δ, *ipt1*Δ and *erg6*Δ *S. cerevisiae* cells, and it was not affected by any of the fluorescent probes (> 99.0 %) (Figure 3.2). The use of DPH and its derivatives do not impose any notable cytotoxic effects both on healthy and mutant *S. cerevisiae* cells, suggesting that neither the probes or the mutations regarding the sphingolipid and ergosterol pathways compromise cellular viability. The solvents in which the fluorescent membrane probes were dissolved - methanol and ethanol – do not seem to destabilize the normal function of the cell and its environment, at the low concentrations employed. However, the

probes showed different solubility; DPH and TMA-DPH presented higher solubility in ethanol, whereas PA-DPH showed higher solubility in methanol.

Characterization of the plasma membrane of *wt* and *sur2*Δ *S. cerevisiae* cells using DPH, TMA-DPH and PA-DPH

To gain deeper insights into how changes in the sphingolipid composition affect the plasma membrane, the membranes of *S. cerevisiae* were labelled with membrane fluorescent probes. The two lipophilic molecules DPH and TMA-DPH are commonly employed in experiments of this nature. (Kinosita *et al.* 1977; Prendergast *et al.* 1981; Lentz 1993). DPH, due to its even distribution across various lipid phases, is particularly sensitive to the overall membrane properties rather than being specific to any particular domain, except for ceramide-rich phases with low hydration (Florine-Casteel and Feigenson 1988; Davenport 1997; Marquês *et al.* 2015), from which is mostly excluded. The steady-state fluorescence anisotropy, $\langle r \rangle$, of DPH serves as a well-established parameter for assessing alterations in the overall fluidity of the plasma membrane (Aresta-Branco *et al.* 2011; Santos *et al.* 2017; Bento-Oliveira *et al.* 2020). The fluorescence anisotropy of DPH exhibits a linear response to changes in composition (and temperature) within the gel/Ld and Ld/Lo phase coexistence region (De Almeida *et al.* 2009). The measurement of DPH steady-state anisotropy considers both the fluid and less fluid regions within the membrane (Lentz *et al.* 1976). These collective findings support the use of DPH anisotropy as a reliable indicator of global membrane fluidity in yeast membranes. TMA-DPH, as a derivative of DPH, offers a unique advantage. Owing to its cationic moiety, it is anchored at the lipid–water interface, providing insights into in the interfacial region of the membrane. Moreover, in mammalian cells, TMA-DPH tends also to distribute randomly in the plasma membrane (Prendergast *et al.* 1981; Kuhry *et al.* 1983). Nevertheless, it is essential to recognize that steady-state anisotropy alone may not precisely describe the dynamic properties of the membrane because not only probe motion but also fluorescence lifetime can influence fluorescence anisotropy, and in complex systems, the value measured depends on the relative fluorescence quantum yield and partition among different cellular membranes and membrane domains (Abe and Hiraki 2009).

In 2009 it was published an article that presented fluorescence microscopy imaging of *S. cerevisiae* cells labelled with DPH and TMA-DPH. This study revealed that yeast cells labelled with DPH molecules, emitted fluorescence signal mainly within the cytoplasm, rather than adhering to the plasma membrane in both *wt* and *erg2*Δ cells. Conversely, in TMA-DPH distinctly adhered to the plasma membrane in the cell, with a distribution that seemed nearly consistent across the entire plasma membrane (Abe and Hiraki 2009). In this thesis, the fluorescence microscopy imaging analysis corroborated the initial hypothesis, since it suggests that DPH distributes evenly among the plasma membrane and inner membranes, whereas TMA-DPH and PA-DPH exhibited a clear localization on the plasma membrane, with a nearly uniform distribution throughout on the length scale of the resolution of epifluorescence microscopy (Figure 3.3). Importantly, it seemed unlikely that TMA-DPH or PA-DPH were internalized via endocytosis, as they remained confined to the plasma membrane even when labeled for an extended period of almost 1 hour in the growth medium, while DPH was-observed to accumulate in the inner membranes of the cell within the first 20 minutes of labeling.

To assess the parameters that characterize the fluidity of the plasma membrane labelled with the probes, both steady-state and time-resolved fluorescence spectroscopy were conducted. Both in *wt* and *sur2*Δ cells, it is suggested that DPH tends to label regions that are more fluid, incorporating first in the plasma membrane and then spreading to inner membranes due to its apolar nature (Figure 3.7). After

the first moments of incubation with DPH, the anisotropy values were constant throughout time, which can indicate that it spreads rapidly throughout the intracellular membranes. It was observed that the DPH derivatives tend to spread to the same membrane domains after ~24 minutes of incubation time. On the other hand, TMA-DPH and PA-DPH seem to incorporate in membrane domains with different characteristics in the initial moments of incubation. It is expected that the anisotropy value of these two probes should be similar in domains with identical properties, as both have a more superficial location. There were parallel studies taking place during the making of this thesis, to confirm this hypothesis in model systems (unpublished data). At short incubation times, the anisotropy values of TMA-DPH are higher than those of PA-DPH. These results suggest that the cationic TMA-DPH may interact preferentially with SLEDs due to the negative charge of complex sphingolipids (inositolphosphorylceramide based) in yeast, and there is the possible saturation of those domain with the probe that then starts to incorporate in remaining regions of the plasma membrane and therefore tends towards a similar anisotropy value to the probe PA-DPH. DPH has slightly lower anisotropy than its derivatives, even if it is inserted into a bilayer with identical properties, because DPH is located deeper in the bilayer, it is not anchored and also it has more "freedom" to spread across the membranes.

Until now, the only tool to detect and characterize SLEDs was *t*-PnA, with the disadvantage of being a probe whose absorption spectrum strongly overlaps with the ones of yeast proteins and sterols and is very susceptible to photobleaching, unlike DPH. Therefore, it being of enormous importance to develop alternative or complementary tools to study this type of characteristic domains of the fungal plasma membrane, hence the use of less studied probes such as DPH and its derivatives.

To sum up, the main findings were: (i) DPH labels both the plasma membrane and inner membranes, however, DPH derivatives seem to concentrate at the plasma membrane. (ii) TMA-DPH and PA-DPH present different anisotropy values in short incubation times, suggesting that the derivatives label different membrane domains. (iii) PA-DPH presents a lower anisotropy than TMA-DPH, which suggests that TMA-DPH rapidly incorporates in more gel-like regions of the plasma membrane, such as SLEDs.

Biophysical impact of sphingolipid and ergosterol profile in *S. cerevisiae* cells

The role of sphingolipid hydroxylation pattern in the organization of cell membranes, the formation of complex sphingolipids and the absence of ergosterol in the yeast plasma membrane was also studied. To this end, the parameters characterizing membrane properties were compared in *wt* strain, and *sur2*Δ, scs7Δ, *ipt1*Δ and *erg6*Δ mutants in *S. cerevisiae* cells.

As stated previously in Chapter 1, Sur2p, an enzyme known as sphinganine C4-hydroxylase, plays a pivotal role in modulating the levels of sphingolipids derived from phytosphingosines by catalyzing the C4 hydroxylation of DHS and dihydroceramides (Marquês *et al.* 2018). In yeast, the enzymatic conversion of DHS at the C4 position of the LCB leads to the formation of a trihydroxylated long-chain base known as phytosphingosine (PHS, 4-hydroxysphinganine). This conversion is facilitated by sphinganine C4-hydroxylase, which is encoded by the *SUR2* gene (Haak *et al.* 1997; Grilley *et al.* 1998). Consequently, the sphingolipid biosynthesis pathway in yeast, under the influence of Sur2p, diverges into two distinct branches, one centered on DHS and the other on PHS, with PHS being the predominant long-chain base, constituting over 90% of yeast sphingolipids (Megyeri *et al.* 2016).

In this thesis, the results obtained with *sur2*Δ cells suggest that the hydroxylation of C4 in the LCB of ceramides and sphingolipids influences the steady-state anisotropy values of the fluorescence membrane probes DPH, TMA-DPH and *t*-PnA, which can have an impact on both global membrane order and order of specific domains, namely SLEDs. The fluorescence anisotropy values are higher in *sur2*Δ cells than in *wt* cells labelled with DPH and TMA-DPH. In contrast, the anionic PA-DPH probe showed anisotropy values lower in the yeast plasma membrane of *sur2*Δ cells than in *wt* cells (Figure 3.6). This behavior suggests that PA-DPH may mark less SLEDs in *sur2*Δ because electrostatic repulsion may be felt more because the SLEDs are more rigid and compact in this strain and could, for example, actually be labelling other domains. Considering that the probe distribution is similar in *wt* and *sur2*Δ cells, then the results suggest that the non-SLED regions of the plasma membrane will be more fluid in the *sur2*Δ. However, there is not sufficient data to prove this hypothesis.

Unlike the probes DPH and its derivatives, the probe *t*-PnA has previously been employed for identifying ordered domains in mammalian cells. In those cases, the long lifetime decay component observed had values lower than 21 ns, aligning with cholesterol-enriched liquid ordered domains (Bastos *et al.* 2012). It was the inaugural discovery of a long lifetime component, characteristic of the gel phase (clearly above 30 ns), within living cells (Aresta-Branco *et al.* 2011).The presence of gel phase was confirmed in the present study in *wt* strains (τ_{long}= 40.9 ± 0.4 ns) and identified for the first time in *sur2*Δ (τ_{long} = 44.3 ± 0.6 ns). The intensity-weighted lifetime component in *sur2*Δ was very similar to *wt* cells (data from (Aresta-Branco *et al.* 2011), both being approximately around 26 ns. Conversely, the long amplitude component in *sur2*Δ (α_{long} = 0.10 ± 0.01) was lower than in *wt* cells ($\alpha_{long} \approx 0.13$) (data from(Aresta-Branco *et al.* 2011) (See results in Table 3.6). The fluorescent lifetime components obtained suggest that the plasma membrane of *sur2*Δ cells present an higher rigidity profile, which seem to correlate with the presence and higher abundance of SLEDs in *sur2*Δ versus *wt* cells. Previous studies' findings strongly suggest that the biophysical data presented in this study indicate a close association between the sphingolipid-enriched domains identified by *t*-PnA and the plasma membrane domain referred to as MCP. More rigid SLEDs could make it difficult for an antifungal compound to enter the cell, however, recent studies support the hypothesis that SLEDs are a target for azole antifungal drugs in the plasma membrane of fungi since it has the ability of nystatin to form active pores as long as gel phase is present. Therefore, it is important to direct future work to study the heterogeneity and molecular environment of MCPs and MCCs by confocal microscopy and FLIM (Fluorescence Lifetime Imaging Microscopy).

Similarly, to *sur2*Δ mutant yeast cells, *scs7*Δ cells also have an altered sphingolipid biosynthesis pathway and thus a sphingolipid profile distinct from the *wt* cells (as mentioned in Chapter 1). Scs7p is a sphingolipid fatty acyl 2-hydroxylase, and it plays a role in catalyzing the hydroxylation at the C2 position of very long-chain fatty acids (VLCFA) found in dihydroceramides and phytoceramides (Marquês *et al.* 2018). Therefore, ceramides from *wt* cells are hydroxylated at both the sphingoid base and acyl chain, while those from *scs7*Δ mutant cells lack the 2-OH in the acyl chain. *Scs7*Δ mutant cells grown in SC medium labelled with DPH showed higher anisotropy values than *wt* strains in YPD, *sur2*Δ in YPD and even *erg6*Δ in SC cells (Table 3.5). It seems that the absence of C2-OH and C4-OH allows for greater packaging of sphingolipids. An article published in 2018, evaluated the melting temperatures of model systems, specifically mixtures of sphingomyelin and phytosphingomyelin: the average melting temperature of these mixtures is lower than the average of the individual melting temperatures of the two lipids. This indicates that there is incomplete mixing of the two components in the gel phase, highlighting inadequate packing between these two species within that phase. The authors suggest that the molecular interactions involving sphingolipids containing extra hydroxyl groups in their structures could significantly differ from those without hydroxyl groups. The presence of an -OH increases the

rigidity and/or stability of the gel domains, but in the presence of two -OHs, as happens in *wt S. cerevisiae cells,* it once again leads to smaller packaging or stability(Marquês *et al.* 2018). In addition, the previous article states that sphingolipid-sterol interactions are compromised by the competing influence of sphingolipid hydroxyl groups. E.g. the mechanism by which polyene drugs operate heavily relies on membrane sterols, since there is a decreased susceptibility of fungi to polyenes when cells undergo depolarization can reduce the availability of sterols. This reduction might occur because of a decline in the concentration of sterols in depolarized plasma membranes, leading to diminished accessibility (Marquês *et al.* 2018). In contrast to *scs7*Δ and *sur2*Δ cells, *wt* cells have two additional hydroxylations, which may explain why the sterols may be less accessible and affect the effectiveness of polyene treatments. This could be a significant factor contributing to the existence of sphingolipid-rich regions depleted of ergosterol, such as SLEDs, in the plasma membrane of live yeast cells.

The removal of the *IPT1* gene, leading to the absence of $M(IP)_2C$ replaced by MIPC (Leber *et al.* 1997; Dickson *et al.* 1997), enables us to explore the impact of altering the polar headgroup of complex sphingolipids on various plasma membrane lipid domains (Bento-Oliveira *et al.* 2020). Specifically, we are interested in sphingolipid-enriched gel domains and how this change affects protein distribution and the microenvironment. A study published in 2020 (Bento-Oliveira *et al.* 2020) indicates that the absence of $M(IP)_2C$ does not impede the formation of gel domains. The relative abundance of these domains in the plasma membrane remains similar for both *S. cerevisiae wt* cells and *ipt1*Δ cells. Surprisingly, in *ipt1*Δ cells, the plasma membrane gel domains exhibit even greater rigidity (τ long = ~43 ns) than those found in *wt* cells (τ long = 40.9 ± 0.4 ns), as indicated by *t*-PnA time-resolved fluorescence. This phenomenon can be explained by the fact that $M(IP)_2C$, a component of gel domains, is replaced by MIPC in *ipt1*Δ cells. The polar head of MIPC is smaller and less charged than that of $M(IP)_2C$. This difference may facilitate a tighter packing of these complex sphingolipids due to reduced electrostatic repulsion and/or steric hindrance at the headgroup level, resulting in a denser and more rigid environment within the hydrophobic membrane core (Bento-Oliveira *et al.* 2020). A similar explanation has been proposed to account for the increased packing density of gel domains in the plasma membrane of *scs7*Δ cells, which lack the 2-OH group in the fatty acyl chain of all sphingolipids, in comparison to *wt* cells (Aresta-Branco *et al.* 2011). The deletion of the *IPT1* gene leads to increased calcium tolerance (Dickson *et al.* 1997; Dickson 2008) and different drug resistance/sensitivity profiles (Hallstrom *et al.* 2001), along with impaired miconazole uptake (Morimoto and Tani 2014). These outcomes suggest that $M(IP)_2C$ affects membrane permeability or the function of membrane proteins differentially. This implies that a variety of direct and indirect mechanisms may be at play (Bento-Oliveira *et al.* 2020).

Recent investigations in both yeast and mammalian cells have posed a challenge to the notion that sterols serve exclusively to create lateral membrane heterogeneity between Lo and Ld phases (Ferraz-De-Souza *et al.* 2011; Khmelinskaia *et al.* 2020)). Findings from FLIM studies, along with the high sterol content observed in eukaryotic plasma membranes, suggest that an Lo-like phase might actually constitute a substantial portion of the cell membrane (Owen et al., 2006; De Almeida and Joly, 2014; Kilin et al., 2015). While in mammalian cells, sphingolipids and cholesterol coexist in the same plasma membrane leaflet, there is evidence that in yeast ergosterol predominantly occupies the inner leaflet, while sphingolipids accumulate in the outer leaflet (Solanko *et al.* 2018). The deletion of the *ERG6* gene in yeast has significant biophysical implications for the plasma membrane due to the accumulation of zymosterol and colesta-5,7,24-trienol. The accumulation of zymosterol in the plasma membrane can have several biophysical implications in the membrane fluidity, since ergosterol is known to modulate membrane fluidity. Its absence and the accumulation of zymosterol can lead to changes in the membrane physical properties (Jordá and Puig 2020). Zymosterol may not provide the same level of

regulation of membrane fluidity as ergosterol, which could affect the overall membrane structure and properties (Khmelinskaia *et al.* 2020). The yeast plasma membrane of *erg6*Δ cells labelled with DPH or TMA-DPH present higher steady-state anisotropy values than in *wt* cells, which suggests that in the presence of zymosterol and in the absence of ergosterol, these probes spread to more rigid domains in *erg6*Δ cells than in *wt* cells (Abe and Hiraki 2009; Aresta-Branco *et al.* 2011).

To sum up, the absence of the enzymes Sur2p, Scs7p, Ipt1p and Erg6p impact the global order of the plasma membrane in *S. cerevisiae*, leading to increased anisotropy values for membrane probes comparing to the *wt* cell. The presence of gel phase was identified in all *wt* strains, and *sur2*Δ, *scs7*Δ, *ipt1*Δ and *erg6*Δ mutated cells. This comparison study showed that the biophysical properties and the global order of the plasma membrane of *S. cerevisiae* cells are highly affected by the hydroxylation pattern of the sphingolipids in C4 of the sphingoid chain and C2 of the acyl chain; moreover, it is influenced by the replacement of $M(IP)_2C$ by MIPC in *ipt1*Δ cells; and finally, by the absence of ergosterol in the plasma membrane. All these factors can result in a denser and more rigid environment within the hydrophobic membrane core. The highly rigid SLEDs that are present in fungi like *S. cerevisiae* but absent in mammalian cells makes sphingolipid domains on the plasma membrane potential candidates for antifungal drug treatments. Exploring these distinct biophysical characteristics could offer a means to mitigate drug side effects and toxicity, ultimately aiding in the creation of more efficient therapies while reducing the likelihood of resistance development.

Chapter 5. Conclusions and future remarks

In this thesis plasma membrane biophysical properties of *S. cerevisiae* cells were characterized by taking advantage of fluorescence membrane probes bearing the same fluorophore, but having different net charge, namely DPH, TMA-DPH and PA-DPH probes, in *wt* strain and *sur2*Δ mutants. The main findings were: (i) DPH distributes evenly among the plasma membrane and inner membranes, however, DPH derivatives seem to concentrate at the plasma membrane a conclusion that is corroborated not only by fluorescence microscopy imaging, but also the much higher fluorescence anisotropy values of the charged probes as compared to those of DPH. (ii) The derivatives label different membrane domains at short incubation times. (iii) PA-DPH presents a lower anisotropy than TMA-DPH, which suggests that TMA-DPH rapidly incorporates in more rigid/ ordered regions of the plasma membrane, such as SLEDs. SLEDs have distinct characteristics that are vital beyond just influencing probe interactions. While TMA-DPH tends to bind preferentially to these domains due to the negative charge of specific sphingolipids in yeast, once saturated, it spreads across the membrane, corresponding to the same anisotropy as PA-DPH. The traditional tool for studying SLEDs, *t*-PnA, has significant drawbacks, such as overlapping absorption with yeast components and high photobleaching susceptibility. This underscores the need for alternative research methods, highlighting the promise of probes like DPH.

Since the steady-state values of the DPH derivatives varied throughout the incubation time, it was tested if the fluorescence lifetime components would also be affected by the incubation time of the probes. The stability of the fluorescence lifetime values throughout the incubation times of the probes suggest that the probe itself primarily defines the observed lifetime values, rather than the incubation time. The lifetimes of the DPH family probes are not as sensitive to lipid phases, as for example in *t*-PnA (Santos *et al.* 2018), and this confirms that the fluorescence anisotropy for these probes a crucial parameter to be explore to achieve a better characterization of SLEDs.

The role of sphingoid base hydroxylation in the yeast plasma membrane was also studied. Considering previous studies performed in the laboratory, the parameters characterizing membrane properties in *wt* strain, and *sur2*Δ, *scs7*Δ and *erg6*Δ mutants of *S. cerevisiae* cells were compared. It is important to highlight that this master thesis dissertation is part of a broader project in which other strains are or have been characterized and the results must be considered together to make the most of them, justifying including these results here and making such a detailed discussion of them. Comparing not only the results obtained with *wt* and *sur2*Δ obtained in this work, but also with previous results with those strains, allows to draw conclusions about the role of sphingolipid hydroxylation pattern and headgroup structure in a more general fashion, and also compare the impact on global order and SLEDs rigidity of sphingolipid profile versus sterol profile alterations. The global fluidity of the membrane seems to be lower in mutant yeast cells that accumulate dihydroceramide-based complex sphingolipids, lacking the hydroxylation in C4 of the sphingosine chain, comparing with the *wt* cells.

The gel domains of the plasma membrane were studied with *t*-PnA probe. The fluorescence lifetime of the DPH probes is not as sensitive to the gel phase. Despite tending to present a higher long lifetime component in the gel, it is not as evident and characteristic as in the *t*- PnA. Furthermore, *t*-PnA has a preferential partition to the gel phase, even in very rigid phases containing ceramides, making it even more sensitive to detect and characterize this type of domains. Conversely, the DPH probes do not incorporate preferably the gel, which can be excluded from it when it is very rigid and poorly hydrated. The *t*-PnA probe was used to compare the long lifetime component in several mutant strains, such as *sur2*Δ, *scs7*Δ, *ipt1*Δ and *erg6*Δ. The absence of hydroxylation either in C4 of the sphingosine chain or in C2 of the acyl chain in the yeast plasma membrane presents a great impact in the long lifetime

component value, compared to the *wt* strain and even the ergosterol-absent yeast cells. Overall, these results corroborate our hypothesis that sphingolipid backbone hydroxylation is of crucial importance for a proper rigidity of the SLEDs and the competition with hydroxyl groups and sterols influence the overall membrane biophysical properties (Marquês et al. 2018).

This study represents a significant methodological advancement as it hints at the development of a new method to study SLEDs. Furthermore, it provides valuable insights into the characteristics of SLEDs, specifically the hydroxylation of their structure, and its role in the organization and properties of the yeast plasma membrane. The findings from these advancements could potentially apply to other fungi. These studies may help to better understand the role of SLEDSs in antifungal resistance or mode of action. Polyene antifungals, such as nystatin, do not need sterols to form pores in the membrane in model systems. For this compound, changes in the rigidity and abundance of SLEDs have a direct implication in anti-fungal activity (Dos Santos *et al.* 2017). This might be explained by the additional two hydroxylations that *wt* cells have, in contrast to *sur2*Δ and *scs7*Δ yeast cells, which reduce the accessibility of the sterols, potentially impacting the efficacy of polyene treatments.

In future studies, it is important to monitor the steady-state fluorescence anisotropy kinetics of the fluorescent probes DPH, TMA-DPH and PA-DPH in other yeast strains, with altered sphingolipid and sterol profiles, since the anisotropy results confirm that, at short incubation times, these probes are a promising strategy to further reveal membrane heterogeneity in the yeast plasma membrane and, perhaps, the plasma membrane of other organisms. As a future study, it should be also explored other membrane probes such as ANEPPS (Aminonaphthylethenylpyridinium potential sensitive) in *sur2*Δ and the double mutant *scs7*Δ:*sur2*Δ. As for membrane compartments, MCC and MCP could be studied in *sur2*Δ cells by FLIM. Also, since it is not possible to directly compare fluorescence anisotropy or lifetime component values between *S. cerevisiae* cultured in different media, strains previously studied in SC medium, should be characterized in YPD, namely *scs7*Δ and *erg6*Δ. Moreover, all the tests in this thesis were performed using only *S. cerevisiae* whole cells, and they should be replicated using the same probes to label isolated plasma membrane of *S. cerevisiae* cells instead of whole cells, as a complementary study.

References

Abe F, Hiraki T (2009). Mechanistic role of ergosterol in membrane rigidity and cycloheximide resistance in Saccharomyces cerevisiae. *Biochimica et Biophysica Acta* **1788**, 743–752. doi:10.1016/J.BBAMEM.2008.12.002

Ahmad S, Asadzadeh M (2023). Strategies to Prevent Transmission of Candida auris in Healthcare Settings. *Current Fungal Infection Reports* **17**, 36–48. doi:10.1007/s12281-023-00451-7

Ahmed SN, Brown DA, London E (1997). On the Origin of Sphingolipid/Cholesterol-Rich Detergent-Insoluble Cell Membranes: Physiological Concentrations of Cholesterol and Sphingolipid Induce Formation of a Detergent-Insoluble, Liquid-Ordered Lipid Phase in Model Membranes. *Biochemistry* **36**, 10944–10953. doi:10.1021/BI971167G

Alberts B, Johnson A, Lewis J, Raff M, Roberts K, Walter P (2008). 'Molecular Biology of the Cell' 5th ed. (Garland Science) doi:10.1093/aob/mcg023

De Almeida RFM, Loura LMS (2004). 'Tópicos de Biofísica de Membranas' 1st ed. (Lidel)

De Almeida RFM, Loura LMS, Prieto M (2009). Membrane lipid domains and rafts: current applications of fluorescence lifetime spectroscopy and imaging. *Chemistry and Physics of Lipids* **157**, 61–77. doi:10.1016/J.CHEMPHYSLIP.2008.07.011

Antunes C (2013). Papel dos esfingolípidos complexos na organização da membrana plasmática da levedura Saccharomyces cerevisiae. Universidade de Lisboa. Available at: http://hdl.handle.net/10451/10349

Aresta-Branco F, Cordeiro AM, Marinho HS, Cyrne L, Antunes F, De Almeida RFM (2011). Gel Domains in the Plasma Membrane of Saccharomyces cerevisiae: Highly-ordered, ergosterol-free, sphingolipid-enriched lipid rafts. *Journal of Biological Chemistry* **286**, 5043–5054. doi:10.1074/JBC.M110.154435

Arora A, Raghuraman H, Chattopadhyay A (2004). Influence of cholesterol and ergosterol on membrane dynamics: a fluorescence approach. *Biochemical and biophysical research communications* **318**, 920–926. doi:10.1016/J.BBRC.2004.04.118

Bae JH, Sohn JH, Park CS, Rhee JS, Choi ES (2004). Cloning and functional characterization of the SUR2/SYR2 gene encoding sphinganine hydroxylase in Pichia ciferrii. *Yeast* **21**, 437–443. doi:10.1002/YEA.1082

Bastos AEP, Scolari S, Stöckl M, De Almeida RFM (2012). Applications of Fluorescence Lifetime Spectroscopy and Imaging to Lipid Domains In Vivo. *Methods in Enzymology* **504**, 57–81. doi:10.1016/B978-0-12-391857-4.00003-3

Bento-Oliveira A, Santos FC, Marquês JT, Paulo PMR, Korte T, Herrmann A, Marinho HS, De Almeida RFM (2020). Yeast Sphingolipid-Enriched Domains and Membrane Compartments in the Absence of Mannosyldiinositolphosphorylceramide. *Biomolecules* **10**, 1–24. doi:10.3390/BIOM10060871

Branco MR, Marinho HS, Cyrne L, Antunes F (2004). Decrease of H2O2 plasma membrane permeability during adaptation to H2O2 in Saccharomyces cerevisiae. *The Journal of biological chemistry* **279**, 6501–6506. doi:10.1074/JBC.M311818200

Brown GD, Denning DW, Gow NAR, Levitz SM, Netea MG, White TC (2012). Hidden killers: Human fungal infections. *Science Translational Medicine* **4**. doi:10.1126/SCITRANSLMED.3004404

Carquin M, D'auria L, Pollet H, Bongarzone ER, Tyteca D (2016). Recent progress on lipid lateral heterogeneity in plasma membranes: from rafts to submicrometric domains HHS. *Progress in lipid*

research **62**, 1–24. doi:10.1016/j.plipres.2015.12.004

Castelli MV, Butassi E, Monteiro MC, Svetaz LA, Vicente F, Zacchino SA (2014). Novel antifungal agents: A patent review (2011-present). *Expert Opinion on Therapeutic Patents* **24**, 323–338. doi:10.1517/13543776.2014.876993

Chazotte B (2011). Labeling the Plasma Membrane with TMA-DPH. *Cold Spring Harbor Protocols* **2011**, pdb.prot5622. doi:10.1101/PDB.PROT5622

Cowen LE, Sanglard D, Howard SJ, Rogers PD, Perlin DS (2015). Mechanisms of Antifungal Drug Resistance. *Cold Spring Harbor Perspectives in Medicine* **5**. doi:10.1101/CSHPERSPECT.A019752

Cundall RB, Johnson I, Jones MW, Thomas EW, Munro IH (1979). Photophysical properties of DPH derivatives. *Chemical Physics Letters* **64**, 39–42. doi:10.1016/0009-2614(79)87270-X

Davenport L (1997). Fluorescence probes for studying membrane heterogeneity. *Methods in enzymology* **278**, 487–512. doi:10.1016/S0076-6879(97)78026-1

Denning DW, Pleuvry A, Cole DC (2011). Global burden of chronic pulmonary aspergillosis as a sequel to pulmonary tuberculosis. *Bulletin of the World Health Organization* **89**, 864–872. doi:10.2471/BLT.11.089441

Dickson RC (2010). Roles for Sphingolipids in Saccharomyces cerevisiae. *Advances in Experimental Medicine and Biology* **688**, 217–231. doi:10.1007/978-1-4419-6741-1_15

Dickson RC (2008). Thematic Review Series: Sphingolipids. New insights into sphingolipid metabolism and function in budding yeast *. *Journal of Lipid Research* **49**, 909–921. doi:10.1194/JLR.R800003-JLR200

Dickson RC, Lester RL (1999). Yeast sphingolipids. *Biochimica et Biophysica Acta* **1426**, 347–357. doi:10.1016/S0304-4165(98)00135-4

Dickson RC, Nagiec EE, Wells GB, Nagiec MM, Lester RL (1997). Synthesis of mannose-(inositol-P)2-ceramide, the major sphingolipid in Saccharomyces cerevisiae, requires the IPT1 (YDR072c) gene. *The Journal of biological chemistry* **272**, 29620–29625. doi:10.1074/JBC.272.47.29620

Dufourc EJ (2008). Sterols and membrane dynamics. *Journal of Chemical Biology* **1**, 63–77. doi:10.1007/s12154-008-0010-6

Eeman M, Magali D (2010). From biological membranes to biomimetic model membranes. *Biotechnology, Agronomy, Society and Environment* **14**, 719–736.

Feldmann H (2012). 'Yeast Molecular Cell Biology' 2nd ed. (Wiley-Blackwell) doi:10.1002/9783527659180

Ferraz-De-Souza B, Hudson-Davies RE, Lin L, Parnaik R, Hubank M, Dattani MT, Achermann JC (2011). Sterol O-acyltransferase 1 (SOAT1, ACAT) is a novel target of steroidogenic factor-1 (SF-1, NR5A1, Ad4BP) in the human adrenal. *The Journal of clinical endocrinology and metabolism* **96**. doi:10.1210/JC.2010-2021

Florine-Casteel K, Feigenson GW (1988). On the use of partition coefficients to characterize the distribution of fluorescent membrane probes between coexisting gel and fluid lipid phases: an analysis of the partition behavior of 1,6-diphenyl-1,3,5-hexatriene. *Biochimica et Biophysica Acta (BBA) - Biomembranes* **941**, 102–106. doi:10.1016/0005-2736(88)90218-0

Frackowiak D (1988). The Jablonski diagram. *Journal of Photochemistry and Photobiology* **2**, 399. doi:10.1016/1011-1344(88)85060-7

Giaever G, Nislow C (2014). The Yeast Deletion Collection: A Decade of Functional Genomics. *Genetics* **197**, 451–65. doi:10.1534/genetics.114.161620

Gilbert DF, Friedrich O (2017). Cell Viability Assays: Methods and Protocols. *Methods in Molecular Biology* **1601.** doi: 10.1007/978-1-4939-6960-9

Goffeau A, Barrell G, Bussey H, Davis RW, Dujon B, Feldmann H, Galibert F, Hoheisel JD, Jacq C, Johnston M, Louis EJ, Mewes HW, Murakami Y, Philippsen P, Tettelin H, Oliver SG (1996). Life with 6000 Genes. *Science* **274**, 546, 563–7. doi:10.1126/SCIENCE.274.5287.546

Gorter E, Grendel F (1925). On Bimolecular Layers of Lipoids on the Chromocytes of the Blood. *The Journal of Experimental Medicine* **41**, 439. doi:10.1084/JEM.41.4.439

Gracetto AC, Batistela VR, Caetano W, De Oliveira HPM, Santos WG, Cavalheiro CCS, Hioka N (2010). Unusual 1,6-diphenyl-1,3,5-hexatriene (DPH) spectrophotometric behavior in water/ethanol and water/DMSO mixtures. *Journal of the Brazilian Chemical Society* **21**, 1497–1502. doi:10.1590/S0103-50532010000800013

Grilley MM, Stock SD, Dickson RC, Lester RL, Takemoto JY (1998). Syringomycin action gene SYR2 is essential for sphingolipid 4-hydroxylation in Saccharomyces cerevisiae. *The Journal of biological chemistry* **273**, 11062–11068. doi:10.1074/JBC.273.18.11062

Haak D, Gable K, Beeler T, Dunn T (1997). Hydroxylation of Saccharomyces cerevisiae ceramides requires Sur2p and Scs7p. *The Journal of biological chemistry* **272**, 29704–29710. doi:10.1074/JBC.272.47.29704

Hallstrom TC, Lambert L, Schorling S, Balzi E, Goffeau A, Moye-Rowley WS (2001). Coordinate Control of Sphingolipid Biosynthesis and Multidrug Resistance in Saccharomyces cerevisiae. *Journal of Biological Chemistry* **276**, 23674–23680. doi:10.1074/jbc.M101568200

Hama H, Young DA, Radding JA, Ma D, Tang J, Stock SD, Takemoto JY (2000). Requirement of sphingolipid alpha-hydroxylation for fungicidal action of syringomycin E. *FEBS letters* **478**, 26–28. doi:10.1016/S0014-5793(00)01821-4

Heese-Peck A, Pichler H, Zanolari B, Watanabe R, Daum G, Riezman H (2002). Multiple functions of sterols in yeast endocytosis. *Molecular Biology of the Cell* **13**, 2664–2680. doi:10.1091/mbc.E02-04-0186

Hishikawa D, Hashidate T, Shimizu T, Shindou H (2014). Diversity and function of membrane glycerophospholipids generated by the remodeling pathway in mammalian cells. *Journal of Lipid Research* **55**, 799–807. doi:10.1194/JLR.R046094

Huang Z, Haugland RP (1991). Partition coefficients of fluorescent probes with phospholipid membranes. *Biochemical and biophysical research communications* **181**, 166–171. doi:10.1016/S0006-291X(05)81396-8

Ipsen JH, Karlström G, Mourtisen OG, Wennerström H, Zuckermann MJ (1987). Phase equilibria in the phosphatidylcholine-cholesterol system. *Biochimica et Biophysica Acta (BBA) - Biomembranes* **905**, 162–172. doi:10.1016/0005-2736(87)90020-4

Jabłoństski A (1933). Efficiency of Anti-Stokes Fluorescence in Dyes. *Nature* **131**, 839–840. doi:10.1038/131839b0

Jordá T, Puig S (2020). Regulation of Ergosterol Biosynthesis in Saccharomyces cerevisiae. *Genes* **11**, 1–18. doi:10.3390/GENES11070795

Kane PM (2016). Proton Transport and pH Control in Fungi. *Advances in experimental medicine and biology* **892**, 33–68. doi:10.1007/978-3-319-25304-6_3

Kennedy EP (1956). The Biolgical Synthesis of Phospholipids. *Canadian Journal of Biochemistry and Physiology* **34**, 334–348. doi:10.3389/fcell.2020.00337

Khmelinskaia A, Marquês JMT, Bastos AEP, Antunes CAC, Bento-Oliveira A, Scolari S, Lobo GM da S, Malhó R, Herrmann A, Marinho HS, De Almeida RFM (2020). Liquid-Ordered Phase Formation by Mammalian and Yeast Sterols: A Common Feature With Organizational Differences. *Frontiers in Cell and Developmental Biology* **8**, 531452. doi:10.3389/FCELL.2020.00337/BIBTEX

Kinosita K, Kawato S, Ikegami A (1977). A theory of fluorescence polarization decay in membranes. *Biophysical journal* **20**, 289–305. doi:10.1016/S0006-3495(77)85550-1

Klostermeier D, Rudolph MG (2017). 'Biophysical chemistry'. (CRC Press) doi:10.1201/9781315156910

Kuhry JG, Fonteneau P, Duportail G, Maechling C, Laustriat G (1983). TMA-DPH: A suitable fluorescence polarization probe for specific plasma membrane fluidity studies in intact living cells. *Cell Biophysics* **5**, 129–140. doi:10.1007/BF02796139

Lakowicz JR (2006). Principles of fluorescence spectroscopy. *Principles of Fluorescence Spectroscopy*, 1–954. doi:10.1007/978-0-387-46312-4

Langes Y, Swaisgoodllii MH, Ramoss B V, Steckn TL (1989). Plasma Membranes Contain Half the Phospholipid and 90% of the Cholesterol and Sphingomyelin in Cultured Human Fibroblasts. *Journal of Biological Chemistry* **264**, 3786–3793. doi:10.1016/S0021-9258(19)84918-9

Lanze CE, Gandra RM, Foderaro JE, Swenson KA, Douglas LM, Konopka JB (2020). Plasma Membrane MCC/Eisosome Domains Promote Stress Resistance in Fungi. *Microbiology and Molecular Biology Reviews* **84**. doi:10.1128/MMBR.00063-19

Laroche C, Beney L, Marechal PA, Gervais P (2001). The effect of osmotic pressure on the membrane fluidity of Saccharomyces cerevisiae at different physiological temperatures. *Applied Microbiology and Biotechnology* **56**, 249–254. doi:10.1007/S002530000583

Leber A, Fischer P, Schneiter R, Kohlwein SD, Daum G (1997). The yeast mic2 mutant is defective in the formation of mannosyl-diinositolphosphorylceramide. *FEBS Letters* **411**, 211–214. doi:10.1016/S0014-5793(97)00692-3

Lentz BR (1993). Use of fluorescent probes to monitor molecular order and motions within liposome bilayers. *Chemistry and Physics of Lipids* **64**, 99–116. doi:10.1016/0009-3084(93)90060-G

Lentz BR, Barenholz Y, Thompson TE (1976). Fluorescence Depolarization Studies of Phase Transitions and Fluidity in Phospholipid Bilayers. 2. Two-Component Phosphatidylcholine Liposomes. *Biochemistry* **15**, 4529–4537. doi:10.1021/BI00665A030/ASSET/BI00665A030.FP.PNG_V03

Lichtman JW, Conchello JA (2005). Fluorescence microscopy. *Nature Methods* **2**, 910–919. doi:10.1038/nmeth817

Lingwood D, Simons K (2010). Lipid rafts as a membrane-organizing principle. *Science* **327**, 46–50. doi:10.1126/SCIENCE.1174621

Lodish H, Berk A, Matsudaira P, Kaiser CA, Krieger M, Scott MP, Zipursky L, Darnell J (2005). 'Molecular Cell Biology' 5th ed. (W. H. Freeman)

Loew LM (1988). 'Spectroscopic Membrane Probes. Volume 2' 1st ed. (CRC Press - Taylor and Francis Group)

Lombard J (2014). Once upon a time the cell membranes: 175 years of cell boundary research. *Biology Direct* **9**. doi:10.1186/s13062-014-0032-7

Malinsky J, Opekarová M, Grossmann G, Tanner W (2013). Membrane Microdomains, Rafts, and Detergent-Resistant Membranes in Plants and Fungi. *Annual Review of Plant Biology* **64**, 501–529. doi:10.1146/annurev-arplant-050312-120103

Malinsky J, Opekarová M, Tanner W (2010). The lateral compartmentation of the yeast plasma membrane. *Yeast* **27**, 473–478. doi:10.1002/YEA.1772

Mallela SK, Merscher S, Fornoni A (2022). Implications of Sphingolipid Metabolites in Kidney Diseases. *International Journal of Molecular Sciences* **23**. doi:10.3390/IJMS23084244

Marquês JT, Cordeiro AM, Viana AS, Herrmann A, Marinho HS, De Almeida RFM (2015). Formation and Properties of Membrane-Ordered Domains by Phytoceramide: Role of Sphingoid Base Hydroxylation. *Langmuir* **31**, 9410–9421. doi:10.1021/ACS.LANGMUIR.5B02550/SUPPL_FILE/LA5B02550_SI_001.PDF

Marquês JT, Marinho HS, De Almeida RFM (2018). Sphingolipid hydroxylation in mammals, yeast and plants – An integrated view. *Progress in Lipid Research* **71**, 18–42. doi:10.1016/J.PLIPRES.2018.05.001

Martin ML (2011). Role of the regulation of cell lipid composition and membrane structure in the antitumor effect of 2-hydroxyoleic acid. Universitat de les Illes Balears.

Maslanka R, Kwolek-Mirek M, Zadrag-Tecza R (2018). Autofluorescence of yeast Saccharomyces cerevisiae cells caused by glucose metabolism products and its methodological implications. *Journal of Microbiological Methods* **146**, 55–60. doi:10.1016/J.MIMET.2018.01.017

Matmati N, Hannun YA (2008). Thematic Review Series: Sphingolipids. ISC1 (inositol phosphosphingolipid-phospholipase C), the yeast homologue of neutral sphingomyelinases. *Journal of Lipid Research* **49**, 922–928. doi:10.1194/JLR.R800004-JLR200

Van Meer G (1989). Lipid traffic in animal cells. *Annual Review of Cell and Developmental Biology* **5**. doi:10.1146/annurev.cb.05.110189.001335

Van Meer G, Voelker DR, Feigenson GW (2008). Membrane lipids: where they are and how they behave. *Nature Reviews Molecular Cell Biology* **9**, 112–124. doi:10.1038/nrm2330

Megyeri M, Riezman H, Schuldiner M, Futerman AH (2016). Making Sense of the Yeast Sphingolipid Pathway. *Journal of Molecular Biology* **428**, 4765–4775. doi:10.1016/J.JMB.2016.09.010

Mitchell AG, Martin CE (1997). Fah1p, a Saccharomyces cerevisiae cytochrome b5 fusion protein, and its Arabidopsis thaliana homolog that lacks the cytochrome b5 domain both function in the alpha-hydroxylation of sphingolipid-associated very long chain fatty acids. *The Journal of biological chemistry* **272**, 28281–28288. doi:10.1074/JBC.272.45.28281

Mollinedo F (2012). Lipid raft involvement in yeast cell growth and death. *Frontiers in Oncology* **2**, 32450. doi:10.3389/FONC.2012.00140

Morimoto Y, Tani M (2014). Synthesis of mannosylinositol phosphorylceramides is involved in maintenance of cell integrity of yeast Saccharomyces cerevisiae. *Molecular Microbiology* **95**, 706–722. doi:10.1111/MMI.12896/SUPPINFO

Mukhopadhyay K, Kohli A, Prasad R (2002). Drug susceptibilities of yeast cells are affected by membrane lipid composition. *Antimicrobial Agents and Chemotherapy* **46**, 3695–3705. doi:10.1128/AAC.46.12.3695-3705.2002/ASSET/912CE862-E3C3-43D7-8B48-6575630F9715/ASSETS/GRAPHIC/AC1220281007.JPEG

Nelson DL, Cox MM (2005). 'Lehninger Principles of Biochemistry' 4th ed. (W.H. Freeman & Co)

Nicolson GL (2013). The Fluid-Mosaic Model of Membrane Structure: Still relevant to understanding the structure, function and dynamics of biological membranes after more than 40 years. *Biochimica et Biophysica Acta* **1838**, 1451–66. doi:10.1016/j.bbamem.2013.10.019

Odds FC, Brown AJP, Gow NAR (2003). Antifungal agents: Mechanisms of action. *Trends in Microbiology* **11**, 272–279. doi:10.1016/S0966-842X(03)00117-3

Parks LW, Casey WM (1995). Physiological implications of sterol biosynthesis in yeast. *Annual Review of Microbiology* **49**, 95–116. doi:10.1146/ANNUREV.MI.49.100195.000523

Pathak P, London E (2011). Measurement of lipid nanodomain (Raft) formation and size in sphingomyelin/POPC/cholesterol vesicles shows TX-100 and transmembrane helices increase domain size by coalescing preexisting nanodomains but do not induce domain formation. *Biophysical Journal* **101**, 2417–2425. doi:10.1016/j.bpj.2011.08.059

Patton JL, Lester RL (1991). The Phosphoinositol Sphingolipids of Saccharomyces cerevisiae Are Highly Localized in the Plasma Membrane. *Journal of Bacteriology* **173**, 3101–3108. doi:10.1128/jb.173.10.3101-3108.1991

Pedroso N, Matias AC, Cyrne L, Antunes F, Borges C, Malhó R, de Almeida RFM, Herrero E, Marinho HS (2009). Modulation of plasma membrane lipid profile and microdomains by H2O2 in Saccharomyces cerevisiae. *Free Radical Biology and Medicine* **46**, 289–298. doi:10.1016/J.FREERADBIOMED.2008.10.039

Plesofsky NS, Levery SB, Castle SA, Brambl R (2008). Stress-induced cell death is mediated by ceramide synthesis in Neurospora crassa. *Eukaryotic Cell* **7**, 2147–2159. doi:10.1128/EC.00147-08/ASSET/6363B291-7BBA-4D91-8593-3745BDDFD127/ASSETS/GRAPHIC/ZEK0120832530010.JPEG

Poojari C, Wilkosz N, Lira RB, Dimova R, Jurkiewicz P, Petka R, Kepczynski M, Róg T (2019). Behavior of the DPH fluorescence probe in membranes perturbed by drugs. *Chemistry and Physics of Lipids* **223**, 104784. doi:10.1016/J.CHEMPHYSLIP.2019.104784

Präbst K, Engelhardt H, Ringgeler S, Hübner H (2017). Basic Colorimetric Proliferation Assays: MTT, WST, and Resazurin. *Methods in Molecular bBology* **1601**, 1–17. doi:10.1007/978-1-4939-6960-9_1

Prendergast FG, Callahan PJ, Haugland RP (1981). 1-[4-(Trimethylamino)phenyl]-6-phenylhexa-1,3,5-triene: Synthesis, Fluorescence Properties, and Use as a Fluorescence Probe of Lipid Bilayers. *Biochemistry* **20**, 7333–7338. doi:10.1021/BI00529A002/ASSET/BI00529A002.FP.PNG_V03

Rego A, Trindade D, Chaves SR, Manon S, Costa V, Sousa MJ, Côrte-Real M (2014). The yeast model system as a tool towards the understanding of apoptosis regulation by sphingolipids. *FEMS Yeast Research* **14**, 160–178. doi:10.1111/1567-1364.12096

Van Der Rest ME, Kamminga AH, Nakano A, Anraku Y, Poolman B, Konings WN (1995). The Plasma Membrane of Saccharomyces cerevisiae: Structure, Function, and Biogenesis. *Microbiological Reviews* **59**, 304–322. doi:10.1128/mr.59.2.304-322.1995

Revie NM, Iyer KR, Robbins N, Cowen LE (2018). Antifungal Drug Resistance: Evolution, Mechanisms and Impact. *Current Opinion in Microbiology* **45**, 70–76. doi:10.1016/j.mib.2018.02.005

Rodrigues ML (2018). The Multifunctional Fungal Ergosterol. *mBio* **9**. doi:10.1128/mBio.01755-18

Rogawansamy S, Gaskin S, Taylor M, Pisaniello D, Toscano WA, Tchounwou PB (2015). An

Evaluation of Antifungal Agents for the Treatment of Fungal Contamination in Indoor Air Environments. *International Journal of Environmental Research and Public Health* **12**, 6319–6332. doi:10.3390/ijerph120606319

Sankaram MB, Thompson TE (1991). Cholesterol-induced fluid-phase immiscibility in membranes. *Proceedings of the National Academy of Sciences* **88**, 8686–8690. doi:10.1073/PNAS.88.19.8686

Sankaram MB, Thompson TE (1990). Modulation of Phospholipid Acyl Chain Order by Cholesterol. A Solid-State 2H Nuclear Magnetic Resonance Study. *Biochemistry* **29**, 10676–10684. doi:10.1021/BI00499A015/ASSET/BI00499A015.FP.PNG_V03

Sant DG, Tupe SG, Ramana C V, Deshpande M V (2016). Fungal cell membrane-promising drug target for antifungal therapy. *Journal of Applied Microbiology* **121**, 1498–1510. doi:10.1111/jam.13301

Dos Santos AG, Marquês JT, Carreira AC, Castro IR, Viana AS, Mingeot-Leclercq MP, De Almeida RFM, Silva LC (2017). The molecular mechanism of Nystatin action is dependent on the membrane biophysical properties and lipid composition. *Physical Chemistry Chemical Physics* **19**, 30078–30088. doi:10.1039/C7CP05353C

Santos FC, Fernandes AS, Antunes CAC, Moreira FP, Videira A, Marinho HS, De Almeida RFM (2017). Reorganization of plasma membrane lipid domains during conidial germination. *Biochimica et biophysica acta. Molecular and cell biology of lipids* **1862**, 156–166. doi:10.1016/J.BBALIP.2016.10.011

Santos FC, Lobo GM, Fernandes AS, Videira A, De Almeida RFM (2018). Changes in the biophysical properties of the cell membrane are involved in the response of neurospora crassa to staurosporine. *Frontiers in Physiology* **9**, 410343. doi:10.3389/FPHYS.2018.01375/BIBTEX

Santos FC, Marquês JT, Bento-Oliveira A, De Almeida RFM (2020). Sphingolipid-enriched domains in fungi. *FEBS Letters* **594**, 3698–3718. doi:10.1002/1873-3468.13986

Schweizer T, Kubach H, Koch T (2021). Investigations to characterize the interactions of light radiation, engine operating media and fluorescence tracers for the use of qualitative light-induced fluorescence in engine systems. *Automotive and Engine Technology* **6**, 275–287. doi:10.1007/S41104-021-00092-3

Shah A, Chen D, Boda AR, Foster LJ, Davis MJ, Hill MM (2015). RaftProt: mammalian lipid raft proteome database. *Nucleic Acids Research* **43**, D335–D338. doi:10.1093/NAR/GKU1131

Sherman F (2002). Getting started with yeast. *Methods in Enzymology* **350**, 3–41. doi:10.1016/S0076-6879(02)50954-X

Simons K, Ikonen E (1997). Functional rafts in cell membranes. *Nature* **387**. doi:10.1038/42408

Simons K, Van Meer G (1988). Lipid Sorting in Epithelial Cells. *Biochemistry* **27**, 6197–6202. doi:10.1021/BI00417A001/ASSET/BI00417A001.FP.PNG_V03

Singer SJ, Nicolson GL (1972). The Fluid Mosaic Model of the Structure of Cell Membranes. *Science* **175**, 720–731. doi:10.1126/SCIENCE.175.4023.720

Sinha B, Bhattacharya D, Sinha DK, Talwar S, Maharana S, Gupta S, Shivashankar G V (2010). Dynamic Organization of Chromatin Assembly and Transcription Factories in Living Cells. *Methods in Cell Biology* **98**, 57–78. doi:10.1016/S0091-679X(10)98003-5

Sklar LA (1980). The partition of cis-parinaric acid and trans-parinaric acid among aqueous, fluid lipid, and solid lipid phases. *Molecular and Cellular Biochemistry* **32**, 169–177. doi:10.1007/BF00227444/METRICS

Solanko LM, Sullivan DP, Sere YY, Szomek M, Lunding A, Solanko KA, Pizovic A, Stanchev LD, Pomorski TG, Menon AK, Wüstner D (2018). Ergosterol is mainly located in the cytoplasmic leaflet of the yeast plasma membrane. *Traffic* **19**, 198–214. doi:10.1111/TRA.12545

Sousa C, Santos FC, Bento-Oliveira A, Mestre B, Silva LC, De Almeida RFM (2021). Biophysical analysis of lipid domains in mammalian and yeast membranes by fluorescence spectroscopy. *Methods in Molecular Biology* **2187**, 247–269. doi:10.1007/978-1-0716-0814-2_14

Stilwell W (2016). 'An Introduction to Biological Membranes: Composition, Structure and Function' 2nd ed. (Elsevier)

Tada R, Latge J-P, Aimanianda V (2013). Undressing the fungal cell wall/cell membrane - The antifungal drug targets. *Current pharmaceutical design* **19**, 3738–3747. doi:10.2174/1381612811319200012

Tofalo R, Suzzi G (2015). Yeasts. *Encyclopedia of Food and Health*, 593–599. doi:10.1016/B978-0-12-384947-2.00762-5

Tran SL, Puhar A, Ngo-Camus M, Ramarao N (2011). Trypan Blue Dye Enters Viable Cells Incubated with the Pore-Forming Toxin HlyII of Bacillus cereus. *PLoS ONE* **6**. doi:10.1371/JOURNAL.PONE.0022876

Urban K, Chu S, Scheufele C, Giesey RL, Mehrmal S, Uppal P, Delost GR (2021). The global, regional, and national burden of fungal skin diseases in 195 countries and territories: A cross-sectional analysis from the Global Burden of Disease Study 2017. *JAAD International* **2**, 22–27. doi:10.1016/j.jdin.2020.10.003

Valeur B, Berberan-Santos MN (2012). 'Molecular Fluorescence: Principles and Applications' 2nd ed. (Wiley-VCH)

Vist MR, Davis JH (1990). Phase Equilibria of Cholesterol/Dipalmitoylphosphatidylcholine Mixtures: 2H Nuclear Magnetic Resonance and Differential Scanning Calorimetry. *Biochemistry* **29**, 451–464. doi:10.1021/BI00454A021/ASSET/BI00454A021.FP.PNG_V03

Vitiello A, Ferrara F, Boccellino M, Ponzo A, Cimmino C, Comberiati E, Zovi A, Clemente S, Sabbatucci M (2023). Antifungal Drug Resistance: An Emergent Health Threat. *Biomedicines* **11**, 1063. doi:10.3390/BIOMEDICINES11041063

Vrabl P, Schinagl CW, Artmann DJ, Heiss B, Burgstaller W (2019). Fungal Growth in Batch Culture – What We Could Benefit If We Start Looking Closer. *Frontiers in Microbiology* **10**. doi:10.3389/fmicb.2019.02391

Watson H (2015). Biological membranes Structure and organization of membranes. *Essays Biochem* **59**, 43–70. doi:10.1042/BSE0590043

Werner-Washburne M, Braun EL, Crawford ME, Peck VM (1996). Stationary phase in Saccharomyces cerevisiae. *Molecular Microbiology* **19**, 1159–1166. doi:10.1111/J.1365-2958.1996.TB02461.X